SPEED CONTROL OF SINGLE PHASE INDUCTION MOTOR

A Project Report

submitted by

T V JESHMA

in partial fulfilment of the requirements
for the award of the degree of

MASTER OF TECHNOLOGY

DEPARTMENT OF ELECTRICAL ENGINEERING
INDIAN INSTITUTE OF TECHNOLOGY MADRAS

MAY 2013

CERTIFICATE

This is to certify that the project work titled **SPEED CONTROL OF SINGLE PHASE INDUCTION MOTOR**, submitted by **T V Jeshma**, to the Indian Institute of Technology, Madras, for the award of the degree of **Master of Technology**, is a bonafide record of the project work done by her under my supervision. The contents of this report, in full or in part, have not been submitted to any other Institute or University for the award of any degree or diploma.

Prof.Krishna Vasudevan
Project Guide
Professor
Dept. of Electrical Engineering
IIT-Madras, 600 036

Place: Chennai

Date:

ACKNOWLEDGEMENTS

I wish to express my deepest gratitude to Dr. Krishna Vasudevan, Professor, Electrical Engineering Department, IIT Madras, my mentor and guide. He has always been a source of inspiration for me. He inspired me greatly to work in this project. This project would not have been successful without his guidance and encouragement to work.

I would like to thank my evaluators Dr. Srirama Srinivas , Dr. Lakshmi Narasamma and Dr. Kamalesh Hatua for their suggestions about the project which helped me identify and overcome my mistakes and to finish the project in an appropriate manner.

I also appreciate the help from Mrs. Jayasudha and Mr. Kodandaraman for their help with the lab facilities and equipment.

I would also like to thank all my lab-mates who have been supportive throughout the completion of the project.

I am thankful to my family and my friends for their continuous encouragement and support.

Finally, I thank God for enabling me to complete my work without hassles.

ABSTRACT

KEYWORDS: PSC SPIM; Speed Control; ceiling fan.

Single Phase Induction Motors are used in many household appliances like ceiling fans, air conditioners refrigerators etc. Speed control techniques used in ceiling fan motors are being studied in this project. The present day regulators used for speed control in ceiling fans are being analysed in the project. The voltage and current waveforms and the harmonic profiles when these regulators are used are also being studied. The present day household fan speed regulators which are used extensively are listed below.

- Rheostatic Fan Regulators
- Phase Angle Controlled(TRIAC) Regulators
- Capacitive Regulators

The major disadvantage found in all of these regulators is the non-linearity in the speed response, especially in the lower speed ranges. To overcome this difficulty, new topologies for achieving better speed control of the SPIM, have been designed and simulated in simulink as well as in ORCAD. First the modelling of 2-phase induction motor is done to do simulations in ORCAD and simulink.

The following topologies have been designed and simulated for betterment in the fan speed control.

- Bidirectional Switch Stator Voltage Controller
- SPWM Inverter based Speed Controller(without auxiliary winding capacitor)
- SPWM Inverter based Constant V/f Control(without auxiliary winding capacitance)
- SPWM Inverter based Stator Voltage Control(with auxiliary winding capacitance)
- SPWM Inverter based Constant V/f Control(with auxiliary winding capacitance)

TABLE OF CONTENTS

LIST OF TABLES

LIST OF FIGURES

CHAPTER 1

INTRODUCTION

1.1 Introduction

Single phase induction motors are widely used because of their low cost and high reliability. SPIMs have two stator windings which operates on single phase AC supply and have a squirrel cage rotor. They are used in refrigerators, air conditioners, ceiling fans etc. The motor is not self starting when it is connected to ac mains. To provide the necessary starting torque, they are provided with a main and an auxiliary winding which are placed in space quadrature which generates a phase shifted magnetic field and hence the starting torque. A capacitor is connected in series with auxiliary winding to shift the phase of one stator current relative to the other, thereby producing an average starting torque. Connecting a capacitor in series with the auxiliary winding makes the current in the auxiliary winding to have a phase shift of 90° from the main winding current which generates a starting torque. After the motor has attained 75% of the nominal speed, the auxiliary winding and the capacitor may be removed using a centrifugal switch.

In most of the fan motors, the auxiliary winding and the capacitor are permanently connected. These types of motors are called Permanent Split Capacitor(PSC) AC induction motor. In this project, various speed control techniques on PSC SPIM motors are discussed.

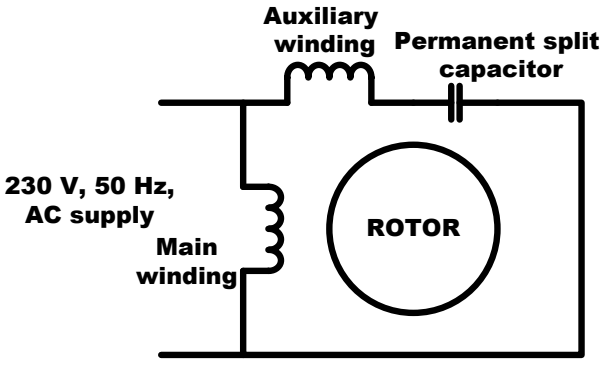

Figure 1.1: PSC Motor

1.2 Fan Speed Regulators

The fan speed regulators which are used presently are being discussed below.

1.2.1 Rheostatic Fan Regulators

A high wattage variable resistor with 3 or 4 tapping is used in series with the fan. By changing the tapping, a different resistor value is connected in series with the motor terminals. This in turn changes the applied voltage across the motor terminals and hence the required speed variation can be achieved.

Advantages

- Cost effective
- Speed range attained is better compared to other regulators used.

Disadvantages

- The major disadvantage of using Conventional(Rheostatic) ceiling fan regulators is the heating in the resistor leading to considerable energy loss.
- At lower speeds, power loss is significant.
- Bulky.
- Very high energy consumption.

1.2.2 Phase Angle Controlled(TRIAC) Regulators

A TRIAC switch is connected between the AC mains supply and the motor terminals aas shown in figure 1.2. The TRIAC is on for a particular time period in each cycle. Depending upon the duration for which the TRIAC is on in a cycle, the rms value of the motor voltage changes. The rms voltage across the motor terminals in turn decides the motor speed. In the figure 1.3, depending upon firing angle γ, the rms applied voltage to the motor varies, which in turn decides the speed.

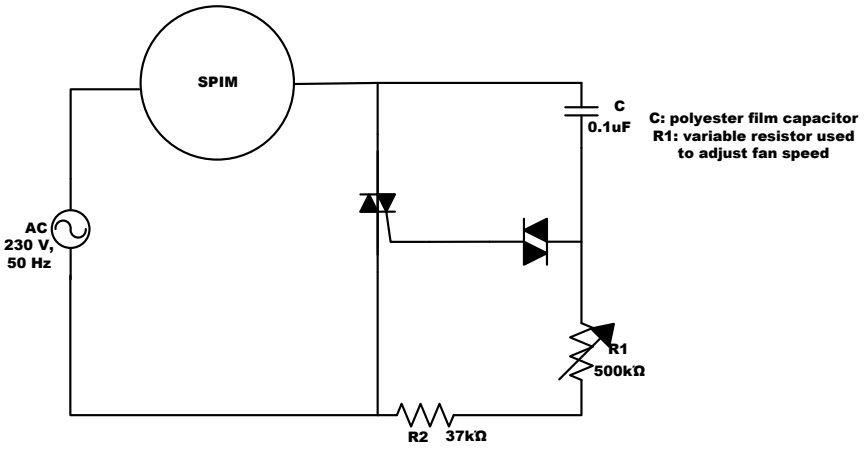

Figure 1.2: TRIAC based speed controller

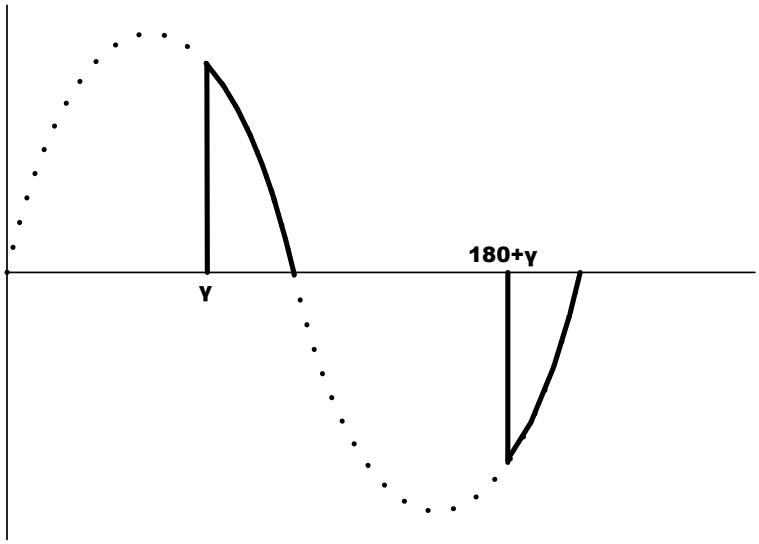

Figure 1.3: Voltage Waveform

Advantages

- Continuous speed control
- Energy saving device. There is a power saving at all speeds.
- Smaller size and weight.

Disadvantages

- Speed control is not linear.
- Higher failure rates as active devices are susceptible to power transients.
- The speed range attained is the worst in these type of regulators.

1.2.3 Capacitive Regulator

In this type of regulators, different capacitor values are attached in series with the fan motor for each regulator knob position. This in turn will change the applied voltage across the motor terminals which thereby changes the speed.

The voltage across the capacitor is given by the formula $V = Q/C$ where Q is the charge across the capacitor and C is the capacitance. According to the formula above,

$$C \, \alpha \, 1/V \tag{1.1}$$

As C increases V decreases. Thus, the voltage across the fan increases. Therefore, the speed increases. So, by increasing the value of capacitor, the speed of the fan can be increased. Thus, by employing suitable combinations of capacitors,the fan speed can be regulated. The schematic for capacitive regulator is shown in figure 1.4.

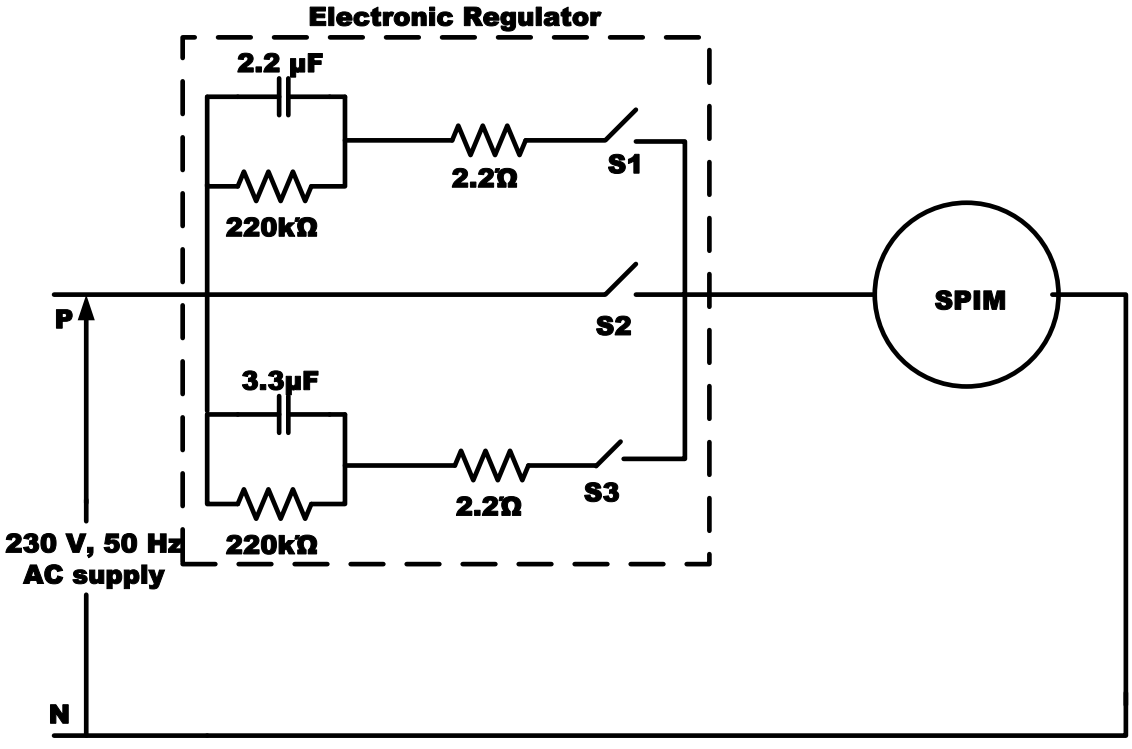

Figure 1.4: Capacitive Regulator

A resistor is put in series with the capacitor in order to limit the current flowing to the capacitor to a safe value. A parallel resistance across the capacitor is put which serves

as a discharging path for the capacitor for each supply cycle.

Table 1.1: Capacitive Regulator: Switching scheme

Knob Position	Switching scheme
1	S1-ON S2,S3-OFF
2	S3-ON S1,S2-OFF
3	S1,S3-ON S2-OFF
4	S2-ON S1,S3-OFF

Table 1.1 gives the switching combination for attaining different speeds using capacitive regulators.

Advantages

- Energy saving device: There is a power saving at all speeds.
- Smaller size and weight.
- The speed range attained is better compared to the TRIAC regulator.
- High reliability as compared to electronic type regulator.

Disadvantages

- non linearity in the speed response achieved.

1.3 Scope of the project

The major disadvantage in the present day speed control techniques available for fan motors is the non linearity in the speed response especially in the lower speed ranges. For betterment in the speed response of fans, various topologies have been designed and simulated. First, modelling of single phase induction motors was done to do simulations in simulink as well as in ORCAD. Then some improved topologies were simulated to see the speed response characteristics. The following topologies were simulated for betterment in the fan speed control.

- Bidirectional Switch Stator Voltage Controller: This is a stator voltage control method. The input ac voltage to the fan is switched on and off at a frequency

of $10kHz$ using a pair of bidirectional switches.The fundamental stator voltage magnitude can be changed by the variation in the duty ratio of the pulses applied to the switches.One of the bidirectional switches is placed in series with the supply and another across the motor terminals.

- SPWM Inverter based Speed Controller(without auxiliary winding capacitor): The motor is run as 2 phase induction motor wherein the auxiliary winding capacitor is removed. A 90° phase shift is introduced between the main and auxiliary winding fundamental voltages by using 90° phase shifted sine waves as modulating waves in SPWM switching schemes for the two legs. The amplitude of the modulating sine wave alone was varied thereby changing the magnitude of the applied stator voltage to the motor.

- SPWM Inverter based Constant V/f Control(without auxiliary winding capacitance): The amplitude as well as the frequency of the modulating sine wave was varied in such a way that the ratio of voltage of sine wave to the frequency of the sine wave(V/f) was maintained a constant.

- SPWM Inverter based Stator Voltage Control(with auxiliary winding capacitance): Here the motor model(with the auxiliary winding capacitor) is connected across the inverter legs and stator voltage control scheme is implemented.

- SPWM Inverter based Constant V/f Control(with auxiliary winding capacitance): Here, constant volts per hertz scheme is implemented.

The speed response characteristics as well as voltage and current waveforms of some of the present day regulators were taken down.

Hardware implementation of the constant volts per hertz schemes was designed and tested.

1.4 Organization of the Project

First, the modelling of the 2-phase induction motor is done to do simulation in ORCAD as well as in Simulink.

The simulations of the designed topologies are done and the speed range achieved are compared among the simulated topologies. The harmonic profiles of the main and auxiliary winding voltages and currents are also studied.

The present day regulators are analysed and the speed control characteristics of these various types of regulators are plotted. The harmonic profile of motor current and voltages when these regulators are used are also studied.

The hardware implementation of the feasible topologies among the designed ones were tried out and the obtained results are given.

CHAPTER 2

MODELLING OF SINGLE PHASE INDUCTION MOTOR

The modelling of single phase induction motors used in ceiling fans is being done to do simulations in Simulink and ORCAD.

The single phase induction motors used in ceiling fans have two stator windings which are non-identical. Such motors are called unsymmetrical 2-phase induction motors. They can be modelled as a 2 phase induction machine. The stator windings are non-identical windings that are arranged in space quadrature with each other. The main winding is assumed to have N_m equivalent turns with resistance r_{1m}. The auxiliary winding is assumed to have N_a equivalent turns with resistance r_{1a}. The rotor is considered as two identical sinusoidally distributed windings arranged in space quadrature with N_r equivalent turns with resistance r_r.

Here, modelling of an unsymmetrical 2-phase induction motor has been done in stationary reference frame(ω=0). All quantities are referred to the stator windings. All q variables are referred to the main winding with N_m effective turns and all d variables are referred to the auxiliary winding with N_a effective turns.

The notations representing machine parameters are listed in the table 2.1. The notation is used for the parameter after being referred to the respective stator winding.

Table 2.1: Machine Parameters

Machine Parameter	Notation
Main winding stator resistance	r_{1m}
Main winding rotor resistance	r_{2m}
Auxiliary winding stator resistance	r_{1a}
Auxiliary winding rotor resistance	r_{2a}
Main winding stator leakage inductance	L_{slm}
Main winding rotor leakage inductance	L_{rlm}
Auxiliary winding stator leakage inductance	L_{sla}
Auxiliary winding rotor leakage inductance	L_{rla}
Main winding magnetising inductance	L_{mm}
Auxiliary winding magnetising inductance	L_{ma}
Moment of Inertia	J
Aux.Capacitor Impedance	C
Turns ratio(aux/main)	Na/Nm

Voltage and electromagnetic torque equations in stationary reference frame variables($\omega = 0$) for unsymmetrical 2-phase induation motors are as given below.

$$V_{qs} = r_{1m} i_{qs} + \frac{p}{\omega_b} \psi_{qs} \tag{2.1}$$

$$V_{ds} = r_{1a} i_{ds} + \frac{p}{\omega_b} \psi_{ds} \tag{2.2}$$

$$V_{qr}^{'} = r_{2m} i_{qr}^{'} - \frac{1}{n} \frac{\omega_r}{\omega_b} \psi_{dr}^{'} + \frac{p}{\omega_b} \psi_{qr} \tag{2.3}$$

$$V_{dr}^{'} = r_{2a} i_{dr}^{'} + n \frac{\omega_r}{\omega_b} \psi_{qr}^{'} + \frac{p}{\omega_b} \psi_{dr} \tag{2.4}$$

where ω_b is the base electrical angular velocity used to calculate the inductive reac-

tances. The flux linkages per second terms are given as follows:

$$\psi_{qs} = X_{slm} i_{qs} + X_{mm}(i_{qs} + i_{qr}^{'}) \tag{2.5}$$

$$\psi_{ds} = X_{sla} i_{ds} + X_{ma}(i_{ds} + i_{dr}^{'}) \tag{2.6}$$

$$\psi_{qr} = X_{rlm} i_{qr} + X_{mm}(i_{qs} + i_{qr}^{'}) \tag{2.7}$$

$$\psi_{dr} = X_{rla} i_{dr} + X_{ma}(i_{ds} + i_{dr}^{'}) \tag{2.8}$$

In matrix form, the equations become

$$\begin{bmatrix} V_{qs} \\ V_{ds} \\ V_{qr}^{'} \\ V_{dr}^{'} \end{bmatrix} = \begin{bmatrix} r_{1m} + \frac{p}{\omega_b} X_{1m} & 0 & \frac{p}{\omega_b} X_{mm} & 0 \\ 0 & r_{1a} + \frac{p}{\omega_b} X_{1a} & 0 & \frac{p}{\omega_b} X_{ma} \\ \frac{p}{\omega_b} X_{mm} & \frac{-1}{n}\frac{\omega_r}{\omega_b} X_{ma} & r_{2m} + \frac{p}{\omega_b} X_{2m} & \frac{-1}{n}\frac{\omega_r}{\omega_b} X_{2a} \\ n\frac{\omega_r}{\omega_b} X_{mm} & \frac{p}{\omega_b} X_{ma} & n\frac{\omega_r}{\omega_b} X_{2m} & r_{2a} + \frac{p}{\omega_b} X_{2a} \end{bmatrix} \begin{bmatrix} i_{qs} \\ i_{ds} \\ i_{qr}^{'} \\ i_{dr}^{'} \end{bmatrix} \tag{2.9}$$

where turns ratio, n= $\frac{N_a}{N_m}$ and

$$X_{1m} = X_{slm} + X_{mm} \tag{2.10}$$

$$X_{1a} = X_{sla} + X_{ma} \tag{2.11}$$

$$X_{2m} = X_{rlm} + X_{mm} \tag{2.12}$$

$$X_{2a} = X_{rla} + X_{ma} \tag{2.13}$$

$$\tag{2.14}$$

Since, rotor of the machine is squirrel cage, the rotor voltages are set equal to zero. Hence the equations reduces to:

$$\begin{bmatrix} V_{qs} \\ V_{ds} \\ 0 \\ 0 \end{bmatrix} = \begin{bmatrix} r_{1m} + \frac{p}{\omega_b} X_{1m} & 0 & \frac{p}{\omega_b} X_{mm} & 0 \\ 0 & r_{1a} + \frac{p}{\omega_b} X_{1a} & 0 & \frac{p}{\omega_b} X_{ma} \\ \frac{p}{\omega_b} X_{mm} & \frac{-1}{n}\frac{\omega_r}{\omega_b} X_{ma} & r_{2m} + \frac{p}{\omega_b} X_{2m} & \frac{-1}{n}\frac{\omega_r}{\omega_b} X_{2a} \\ n\frac{\omega_r}{\omega_b} X_{mm} & \frac{p}{\omega_b} X_{ma} & n\frac{\omega_r}{\omega_b} X_{2m} & r_{2a} + \frac{p}{\omega_b} X_{2a} \end{bmatrix} \begin{bmatrix} i_{qs} \\ i_{ds} \\ i_{qr}^{'} \\ i_{dr}^{'} \end{bmatrix} \tag{2.15}$$

The instantaneous electromagnetic torque equation is given as:

$$\tau = \frac{P}{2}\frac{N_a}{N_m}L_{mm}(i_{qs} * i'_{dr} - i_{ds} * i'_{qr}) \tag{2.16}$$

The d-q model of two phase induction motor which is being used in simulations in this project is as given in figure 2.1.

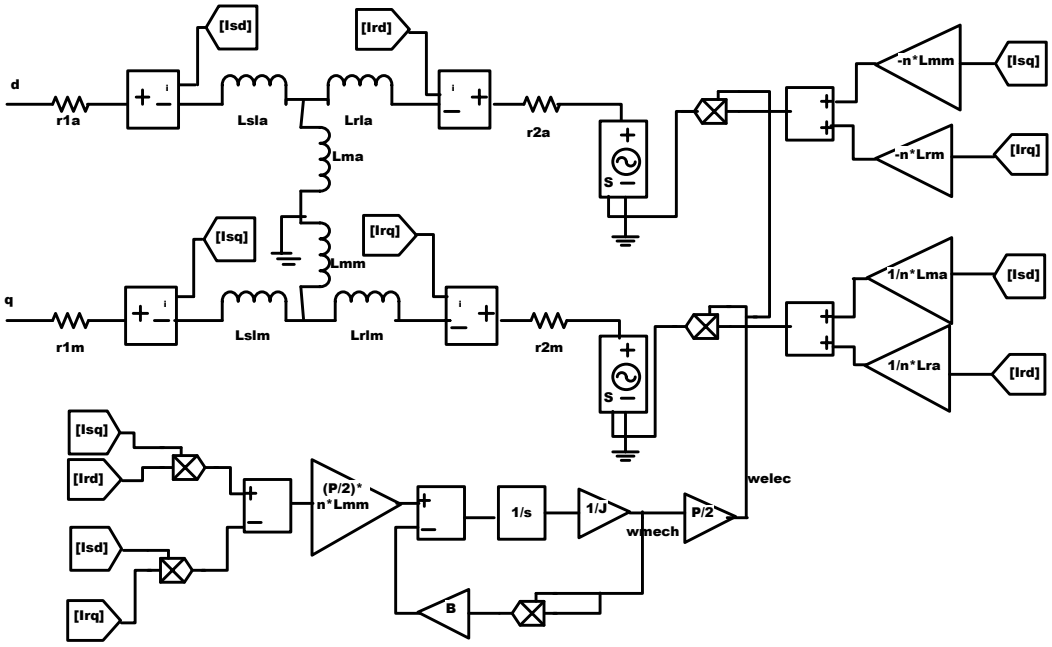

Figure 2.1: Machine Model

The modelling was done to test various designed topologies for betterment in fan speed control by doing simulations in Simulink and ORCAD. The simulation study of the designed topologies in simulink is being presented in the following chapter.

CHAPTER 3

SIMULATION RESULTS

The simulation results of various topologies designed for betterment in the fan speed control are being presented in this chapter.

3.1 Machine Data

The unsymmetrical 2-phase induction machine, which is used to demonstrate the different schemes of speed control, is a 4-pole, $\frac{1}{4}hp$,$230V$,$50Hz$ machine with the parameters as given in table 3.1.

Table 3.1: Machine Data

Machine Parameter	Notation	Value
Main winding stator resistance	r_{1m}	$2.02\ \Omega$
Main winding rotor resistance	r_{2m}	$4.12\ \Omega$
Auxiliary winding stator resistance	r_{1a}	$7.14\ \Omega$
Auxiliary winding rotor resistance	r_{2a}	$5.74\ \Omega$
Main winding stator leakage inductance	L_{slm}	$0.0148\ H$
Main winding rotor leakage inductance	L_{rlm}	$0.0112\ H$
Auxiliary winding stator leakage inductance	L_{sla}	$0.0171\ H$
Auxiliary winding rotor leakage inductance	L_{rla}	$0.0156\ H$
Main winding magnetising inductance	L_{mm}	$0.3543\ H$
Auxiliary winding magnetising inductance	L_{ma}	$0.4928\ H$
Moment of Inertia	J	$0.0146\ kgm^{-2}$
Aux.Capacitor Impedance	C	$6 - j206.4\ \Omega$
Turns ratio(aux/main)	Na/Nm	1.18

It is assumed that the motor load is $B\omega^2$ and at rated speed, the load power is rated motor power. The motor was assumed to rotate at 4% (i.e. $\omega = 1440rpm$) slip condition when

it delivers rated power.

$\Rightarrow B\omega^3 = 186.5$, where $\omega = 150.8 rad/s$

$\Rightarrow B = 5.45 * 10^{-5}$

3.2 Machine Model: Simulation Results

The machine model is run as a PSC SPIM using 230 V, 50 Hz ac supply and the simulation results are as shown below.

The only load torque given in the model is the air friction load Bω^2. The constant frictional load which exists in any machine is not incorporated in the machine model here.

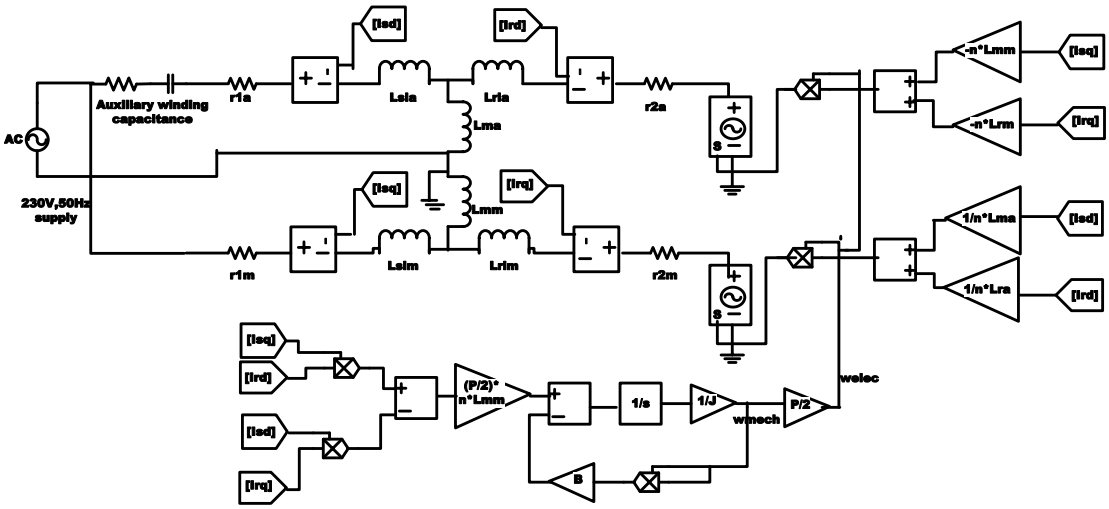

Figure 3.1: PSC SPIM run from $230V, 50Hz$ ac supply

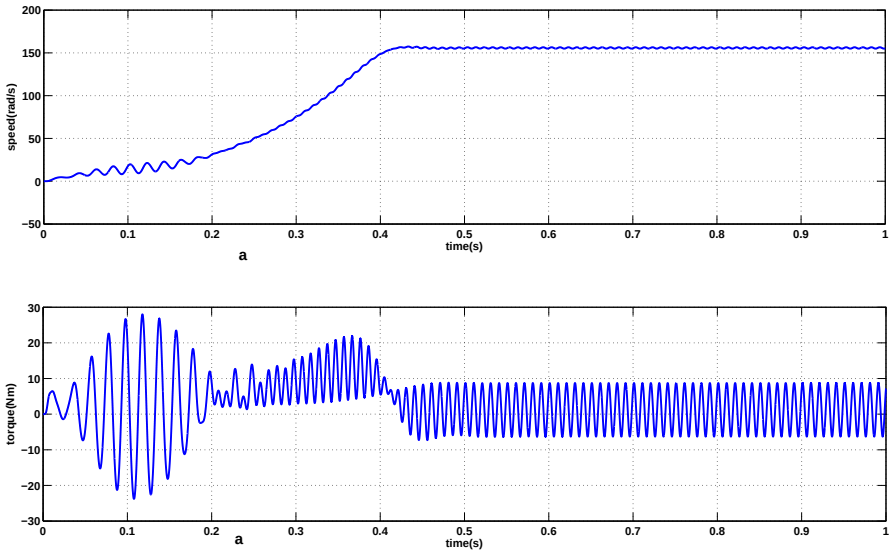

Figure 3.2: Speed and torque variation wrt time

Figure 3.2 shows the speed and torque variation of the motor wrt time. The speed is found to settle at 155.5 rad/s at a time of 0.43s. The ripple in the torque waveform at steady state is due to the imbalance in the stator winding currents. The torque ripple is of frequency 100Hz. The mean value of this torque is equal to the load torque.

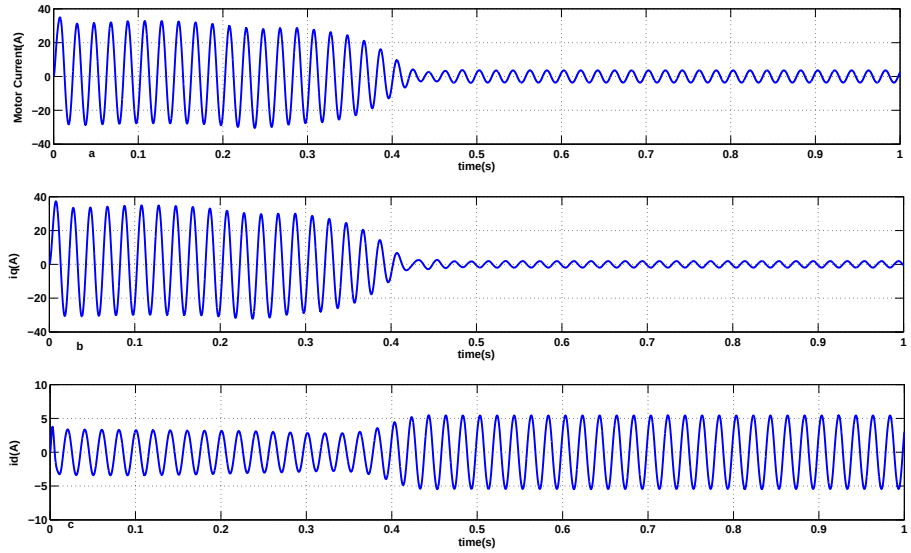

Figure 3.3: (a) motor input current (b) main winding current (c) auxiliary winding current

Figure 3.3 shows the various current waveforms of the motor. All are found to be sinusoids. The transient part of motor input current shows the inrush current phenomenon.

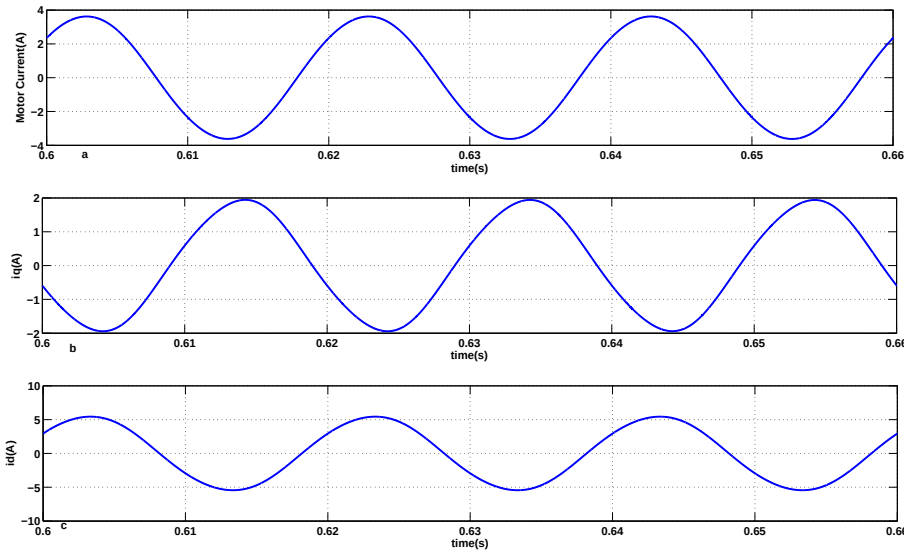

Figure 3.4: (a) motor input current (b) main winding current (c) auxiliary winding current

Figure 3.4 shows the various current waveforms of the motor in the steady state .

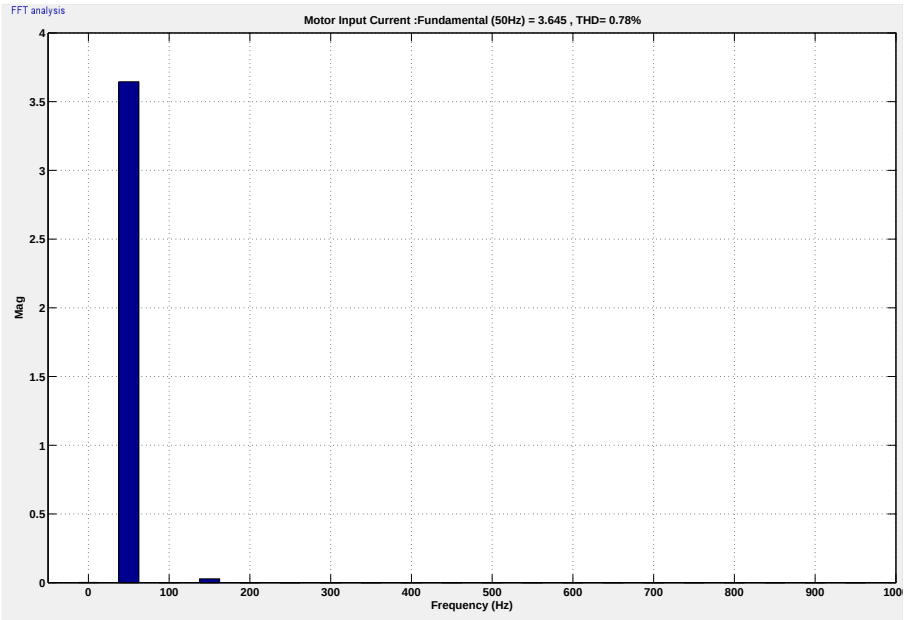

Figure 3.5: Harmonic Spectrum : Total motor current

Figure 3.5 shows the harmonic profile of the motor current. The $\%$ THD is found to be 0.78%. The fundamental current component is found to have a peak of 3.6 A.

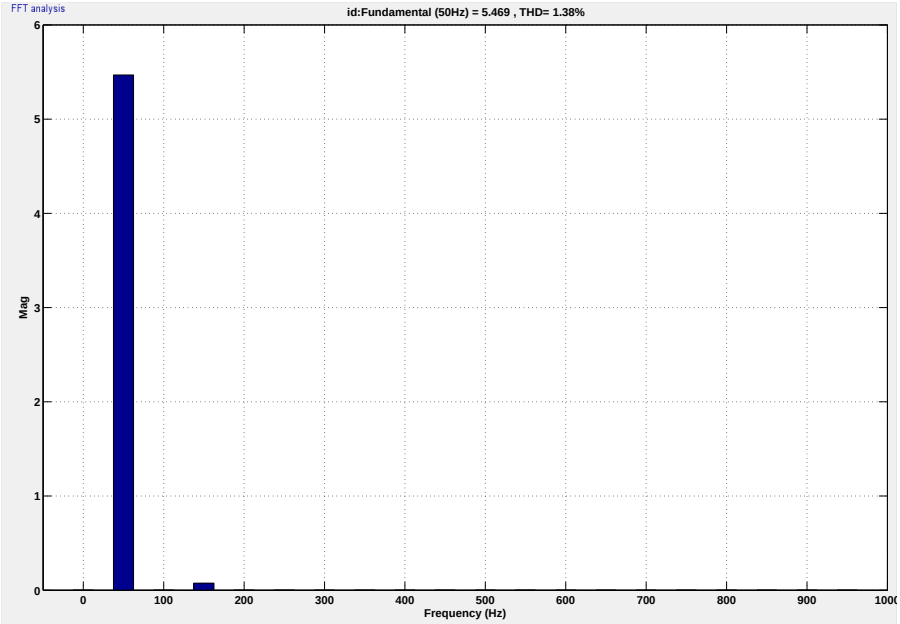

Figure 3.6: Harmonic Spectrum: auxiliary winding current

Figure 3.6 shows the harmonic profile of the auxiliary winding current. The $\%$ THD is found to be 1.4%. The fundamental current component is found to have a peak of 5.5 A.

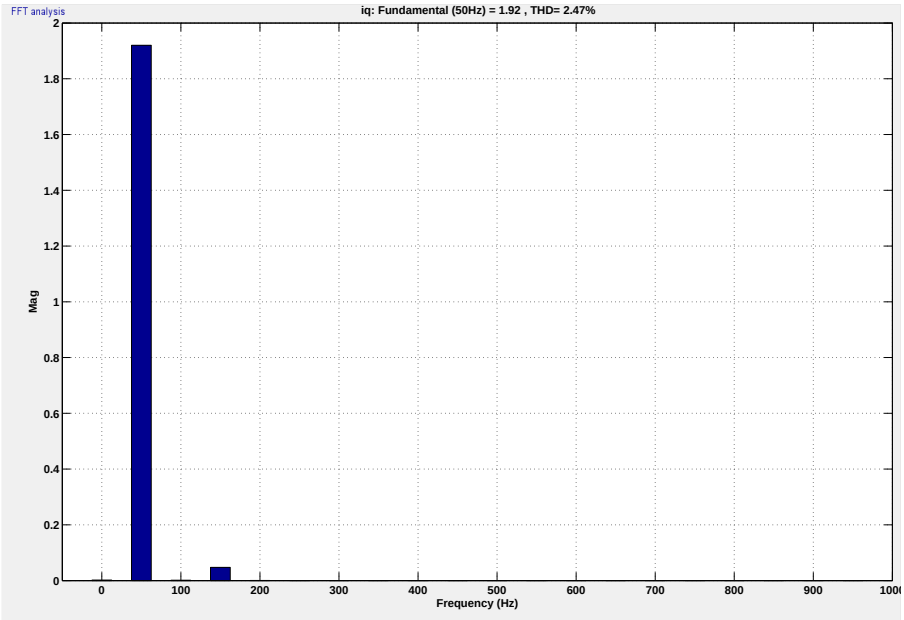

Figure 3.7: Harmonic Spectrum: main winding current

Figure 3.7 shows the harmonic profile of the main winding current respectively.The $\%$ THD is found to be 2.47%. The fundamental current component is found to have a peak of 2 A.

It is seen that there is a double frequency pulsating torque component over an average torque in the steady state. The pulsating torque is due to the unbalanced flow of stator currents. The reduction in pulsating torque occurs as a result of minimizing the unbalancing of the stator currents. This leads to the reduction of rotor circuit losses due to the negatively rotating magnetic field established by unbalanced stator currents. Selecting the value of capacitor to improve starting torque as well as minimizing the pulsating torque during normal operation are objectives involved in the design of singe phase induction motor capacitor.

The following topologies were simulated for betterment in the fan speed control.

- Bidirectional Switch Stator Voltage Controller
- SPWM Inverter based Speed Controller(without auxiliary winding capacitor)
- SPWM Inverter based Constant V/f Control(without auxiliary winding capacitance)
- SPWM Inverter based Stator Voltage Control(with auxiliary winding capacitance)
- SPWM Inverter based Constant V/f Control(with auxiliary winding capacitance)

The simulation results for these topologies mentioned above are given in the following pages.

3.3 Bidirectional Switch: Stator Voltage Control Scheme

The input ac voltage to the fan is switched on and off at a frequency of 10 kHz using a pair of bidirectional switches. The fundamental stator voltage magnitude can be changed by the variation in the duty ratio of the pulses applied to the switches. One of the bidirectional switches is placed in series with the supply and another across the motor terminals. The bidirectional switch across the fan terminals is provided so as to maintain a continuous flow of current in the motor as the motor windings are inductive in nature.

When the switch S1 in figure 3.8 is on, the input AC voltage reaches the motor terminals and when it is off, the motor input voltage is 0. The instantaneous part of sine wave when S1 is on, is applied to the motor terminals in each switching cycle. So depending upon the duty cycle at which S1 is operated, the rms value of the applied voltage to

the motor terminals is varied which is responsible for the speed variation. When S1 is off, S2 is turned on simultaneously and this way, the current in the motor is not discontinuous.

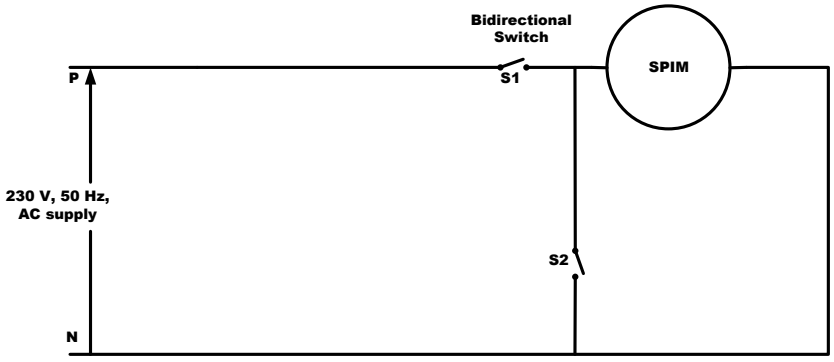

Figure 3.8: Bidirectional Switch Voltage Control:Circuit Diagram

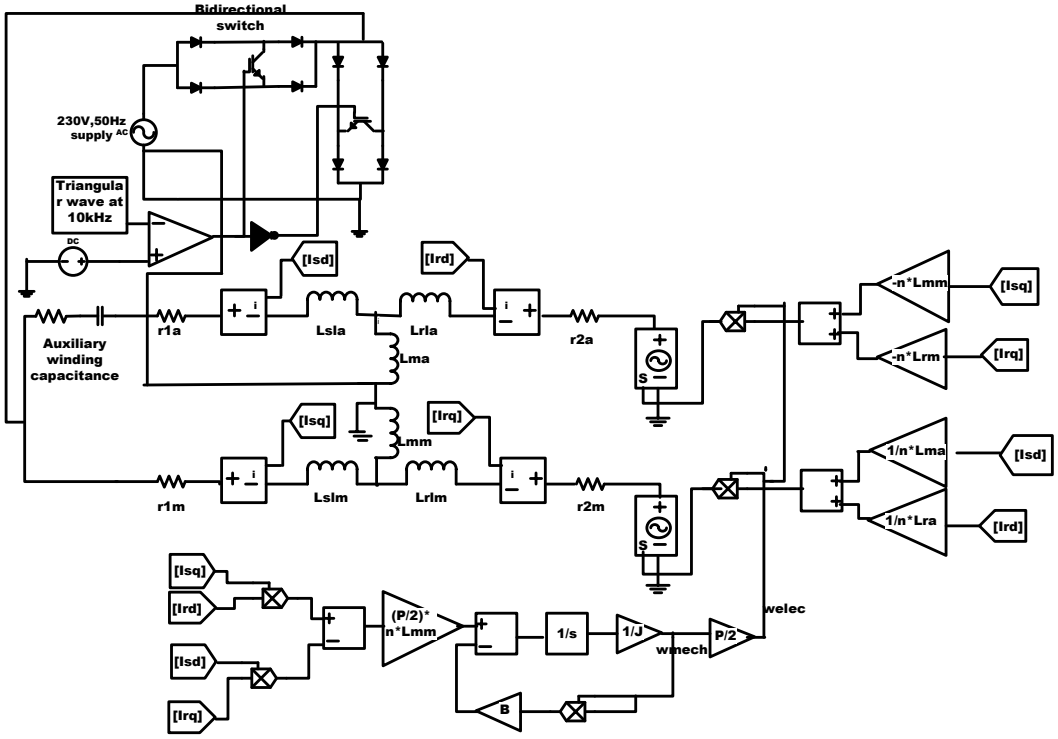

Figure 3.9: Bidirectional Switch Voltage Control schematic

In figure 3.9, the motor is represented as the motor model which is used in simulations.

Table 3.2: Bidirectional Switch: Stator Voltage Control Scheme Results

Duty Ratio(D)	Speed (rpm)	Torque (Nm)	Input rms current(A)	Active Power(W)	Settling Time(s)
0.95	1486	1.32	2.43	430	0.48
0.9	1484	1.316	2.3	405	0.52
0.85	1483	1.314	2.18	380	0.56
0.8	1480	1.309	2.1	357	0.62
0.75	1478	1.306	1.965	336	0.7
0.7	1475	1.301	1.866	316	0.8
0.65	1471	1.29	1.78	295	0.95
0.6	1467	1.286	1.7	280	1.1
0.55	1460	1.275	1.64	264	1.3
0.5	1451	1.26	1.52	249	1.6
0.45	1438	1.236	1.4	220	2

Table 3.2 shows the steady state values of speed attained by the motor, electromagnetic torque, input line current drawn, active power input and the settling time to attain steady state for various operating conditions. It is clear from these observations that a considerable speed range could not be achieved with this topology. The steady state value of electromagnetic torque is equal to the load torque which is $B\omega^2$

The simulation results obtained for an operating condition of duty ratio, $D = 0.9$ is as given below.

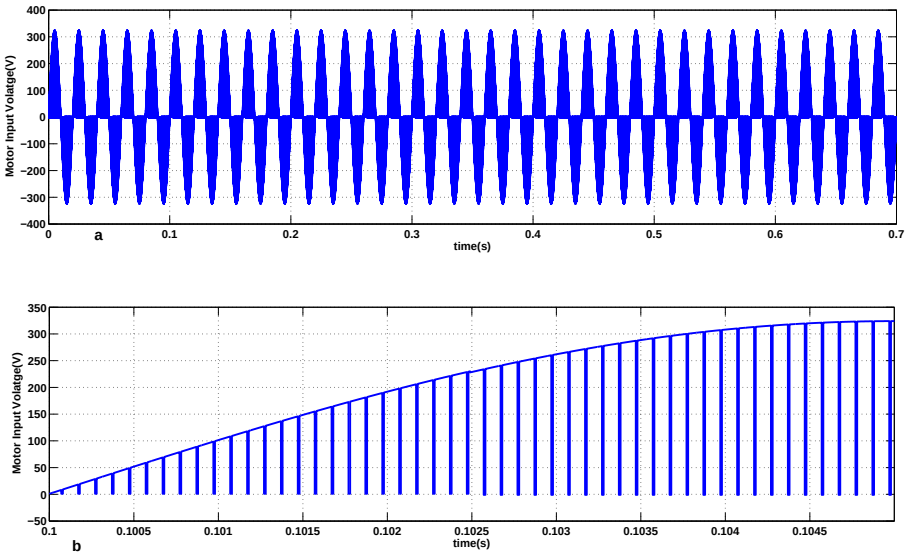

Figure 3.10: Stator voltage wrt time

Figure 3.10 shows the applied voltage to the motor stator terminals. The voltage is found to be switching on and off at a switching frequency of 10 kHz with the applied duty ratio of 0.9. That is, for 90% of the cycle the instantaneous value of sine wave is applied to the motor terminals and for 10% of the cycle, the motor input voltage is 0.

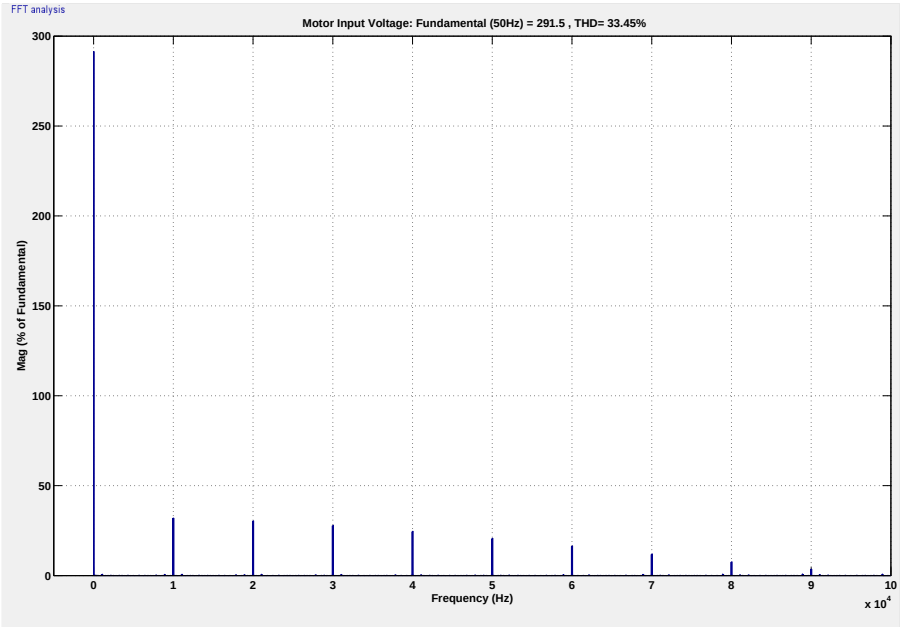

Figure 3.11: Harmonic Spectrum Analysis of the motor input voltage

Figure 3.11 shows the harmonic profile of applied voltage to the motor stator terminals. The % THD is found to be 33.5%. The fundamental motor voltage is found to have a peak of $292V$. THD is found to be high because of the discontinuities in the volt-

age waveform. The harmonic components at multiples of switching frequencies have eminent magnitudes.

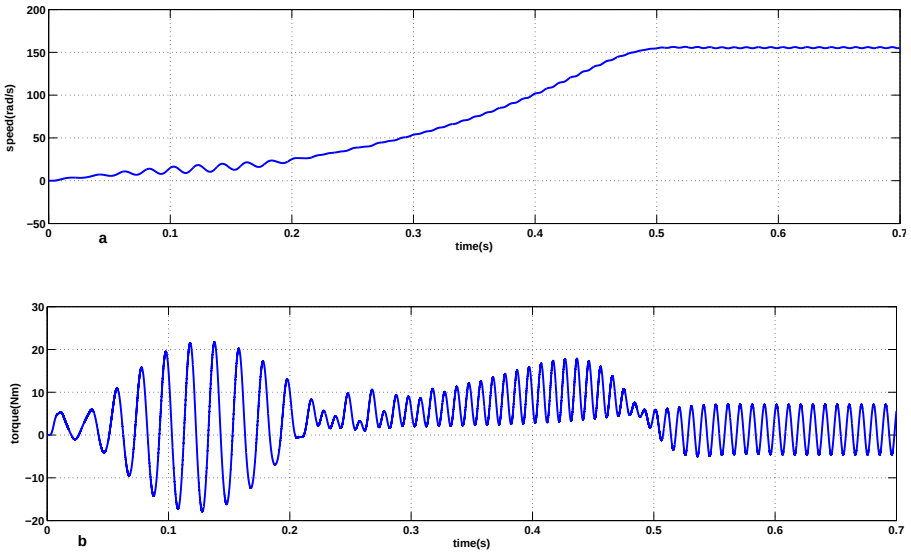

Figure 3.12: Speed and torque variation wrt time

Figure 3.12 shows the speed and torque variation of the motor wrt time. The speed was found to settle down at 155.4 rad/s at 0.52s from start. There was a torque ripple observed at steady state which is due to the imbalance in the stator winding currents(this could be seen from the current waveforms in figure 3.13). The mean value of torque at steady state was found to be equal to the load torque.

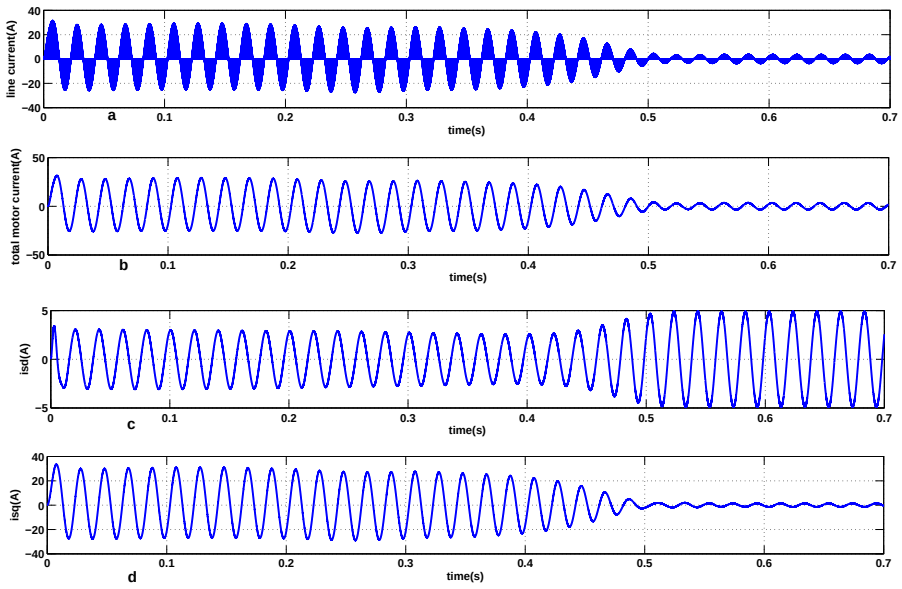

Figure 3.13: (a)line current (b)total motor current (b)auxiliary winding current (b)main winding current

Figure 3.13 shows the various current waveforms. The stator winding current imbalance at steady state is very much evident from the graphs. This current imbalance leads to the torque ripple which is explained in the previous graph.

The total motor current input is very high in the starting(inrush phenomenon). This is reflected in the line current waveform also.

The harmonic analysis of these current waveforms are given in the following pages.

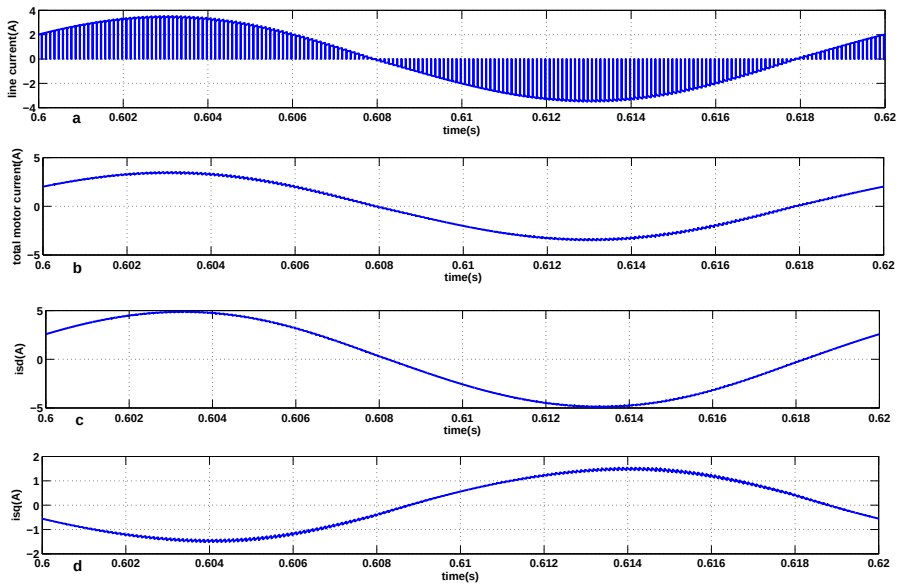

Figure 3.14: (a)line current (b)total motor current (b)auxiliary winding current (b)main winding current

Figure 3.14 shows the expanded view of current waveforms in steady state.

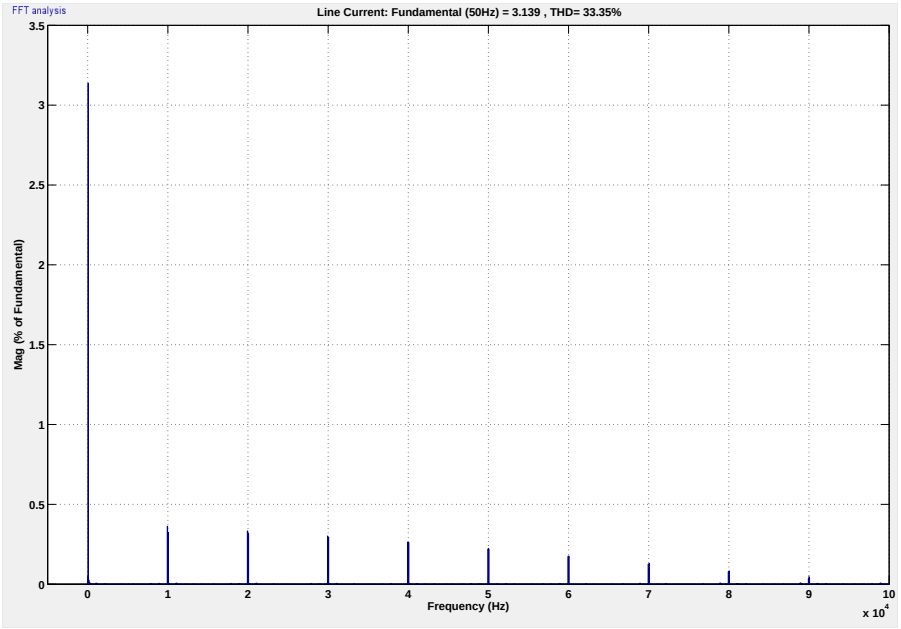

Figure 3.15: Harmonic Spectrum Analysis of the line current

Figure 3.15 shows the harmonic profile of input line current. The $\%$ THD is found to be 33.3%. The fundamental line current component is found to have a peak of 3.1 A. The line current THD is very high which is not good for the supply side.

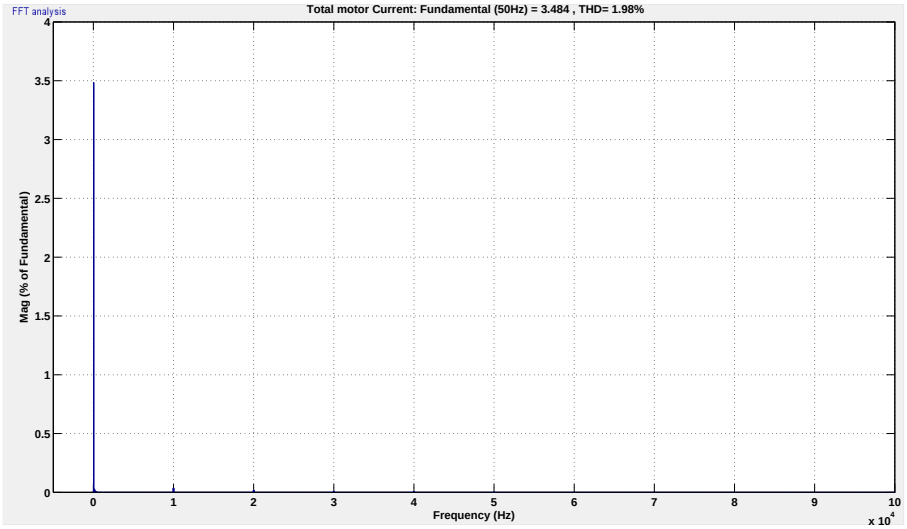

Figure 3.16: Harmonic Spectrum Analysis of the total motor input current

Figure 3.16 shows the harmonic profile of total motor input current. The $\%$ THD is found to be 2%. The fundamental current component is found to have a peak of 3.5 A. The THD is found to be very less. This is preferred as the motor losses will be less.

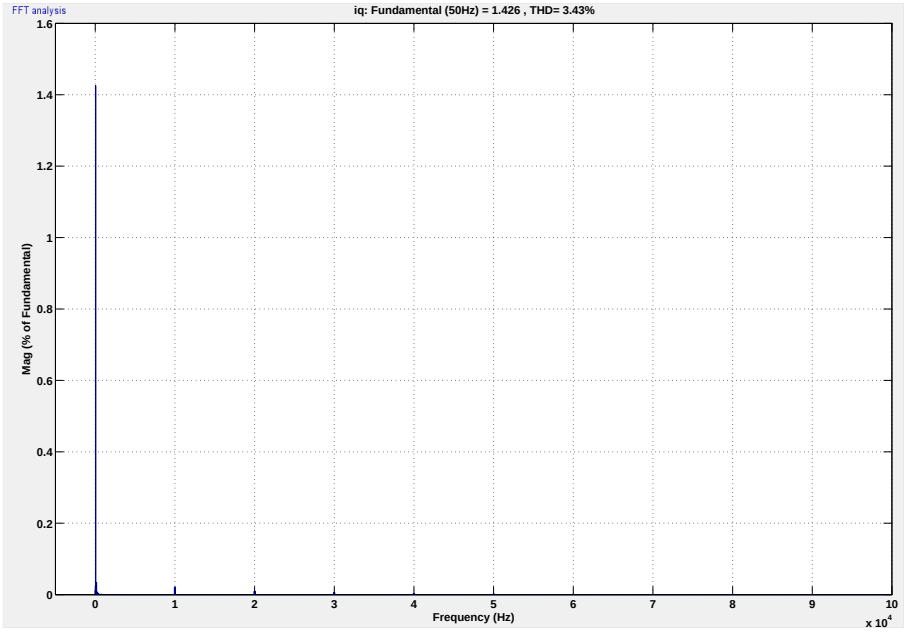

Figure 3.17: Harmonic Spectrum Analysis of the main winding current

Figure 3.17 shows the harmonic profile of the main winding current. The $\%$ THD is found to be 3.4%. The fundamental current component is found to have a peak of 1.4 A. THD is again less here.

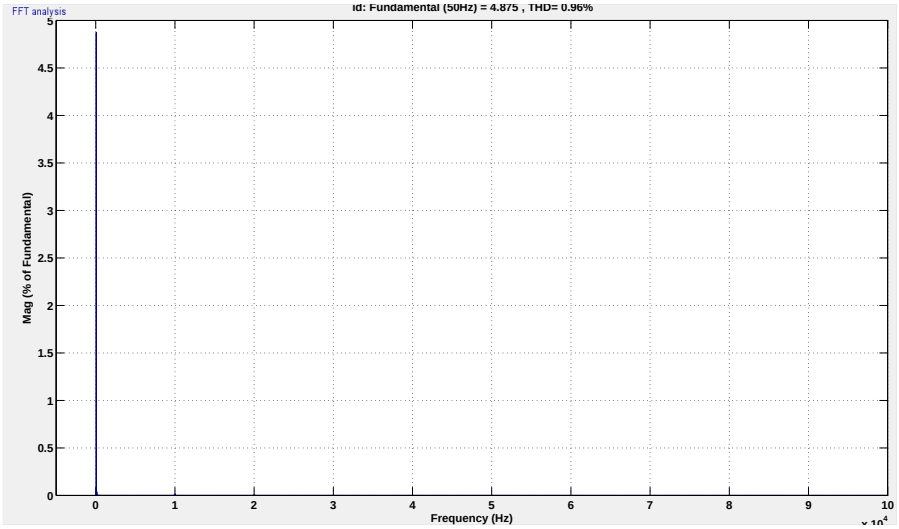

Figure 3.18: Harmonic Spectrum Analysis of the auxiliary winding current

Figure 3.18 shows the harmonic profile of the auxiliary winding current. The $\%$ THD is found to be 0.96%. The fundamental current component is found to have a peak of 4.9 A.THD is very less leading to reduced motor losses.

3.4 SPWM Inverter based Speed Controller without Auxiliary Winding Capacitor

The split phase capacitor in the auxiliary winding of the fan is removed and the fan is run as a 2-phase induction motor. The main and auxiliary windings of the motor are connected to two half bridge inverter legs, employing sinusoidal pulse width modulation technique for pulse generation.

A 90° phase shift is introduced between the main and auxiliary winding fundamental voltages by using 90° phase shifted sine waves as modulating waves in SPWM switching schemes for the two legs. This way the capacitor in the auxiliary winding of the fan can be removed.

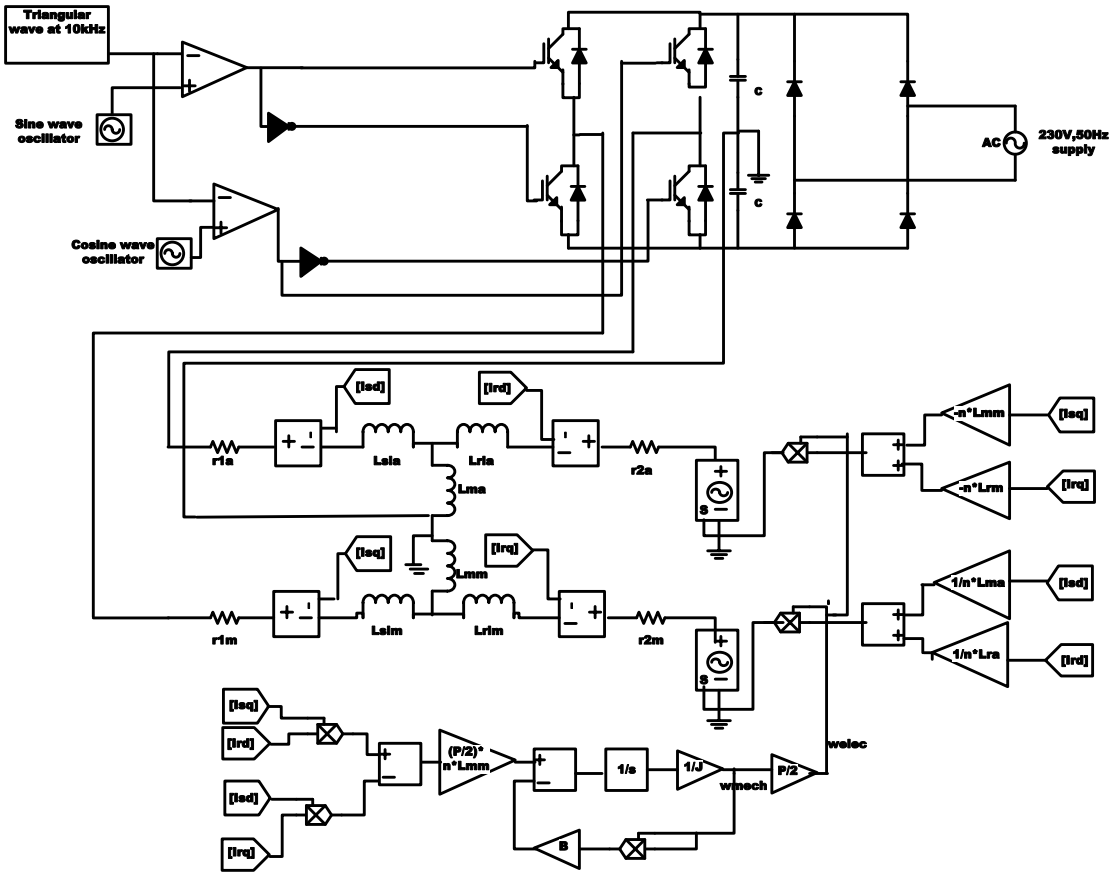

Figure 3.19: SPWM Inverter based Speed Controller without Auxiliary Winding Capacitor

The amplitude of the fundamental voltage applied to each phase is given by

$$V_p = \frac{m_a V_{dc}}{2} \tag{3.1}$$

where m_a is the modulation index given by $m_a = \frac{V_{sin}}{V_{tri}}$
This means that by changing the magnitude of the modulating sine wave, the magnitude of the fundamental applied voltage can be changed.

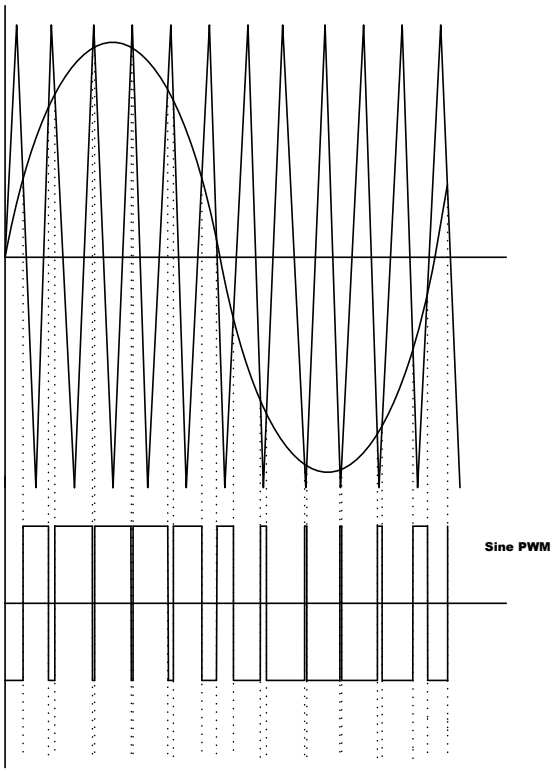

Figure 3.20: Sine PWM

3.4.1 DC Bus Capacitor Calculation

The motor load is approximated as a resistive load of $250W$. The allowable ripple in the bus voltage is 10%. So, the average voltage across the load is $0.95 * V_p$, where V_p is the sine wave peak . Equating the power across the load,

$$\frac{(0.95 * V_p)^2}{R} = 250 \tag{3.2}$$

$$Here, V_p = 230 * \sqrt{2} \tag{3.3}$$

$$= 325.26 \tag{3.4}$$

$$\Rightarrow R = 381.3\Omega \tag{3.5}$$

Capacitor discharges from V_p to $0.9V_p$ in a time of $\frac{T}{2}$ approximately.
At $t = \frac{T}{2}$, capacitor voltage $V_c = 0.9 * V_p$

$$0.9 * V_p = V_p * [e^{-\frac{T}{2RC}}] \tag{3.6}$$

From this, we get C=0.25 mF.

The simulations were done using a capacitor of 0.5 mF to have the dc bus voltage ripples within desired limits.

3.4.2 Simulation Results

The following two methods were implemented in this configuration.

SPWM Inverter based Stator Voltage Control: The amplitude of the modulating sine wave alone is varied thereby changing the magnitude of the applied stator voltage to the motor. The simulation results obtained are tabulated in table 3.3

SPWM Inverter based Constant V/f Control: The amplitude as well as the frequency of the modulating sine wave are varied in such a way that the ratio of voltage of sine wave to the frequency of the sine wave(V/f) is maintained a constant. The simulation results obtained are tabulated in table 3.4

DC Bus capacitor=0.5 mF

Initially the calculated value of bus capacitance, $0.5mF$ is used in the simulations. With this value the bus voltage ripple was found to be within limits.

Table 3.3: SPWM Inverter based Stator Voltage Control(without auxiliary winding capacitance) dc bus capacitor $= 0.5mF$):Results

Sine amp. (V)	Speed (rpm)	Torque (Nm)	input current (rms)(A)	dc bus current(avg)(A)	Active Power input(W)	Settling Time(s)
9.8	1432	1.22	2.6	0.69	220	0.7
9	1420	1.2	2.55	0.68	215	0.8
8	1400	1.17	2.5	0.67	210	1.1
7	1370	1.12	2.45	0.65	205	1.4
6	1327	1.1	2.4	0.62	200	1.8

Table 3.3 shows the steady state values of speed attained by the motor, electromagnetic torque, input line current drawn, dc bus current, active power input and the settling time to attain steady state for various operating conditions. In this scheme, the stator voltage fundamental magnitude is varied. Hence the speed range attained will be lim-

ited. It is clear from the observation table that a considerable speed range could not be achieved with this topology. The settling time is found to increase as the modulation index decreases.

Table 3.4: SPWM Inverter based Constant V/f Control(without auxiliary winding capacitance) dc bus capacitor=0.5 mF: Results

Modulating sine		Speed	Torque	input current	dc bus current	Active Power	Settling
amp.(V)	freq.(Hz)	(rpm)	(Nm)	(rms)(A)	(avg)(A)	input(W)	Time(s)
9.8	49	1408	1.18	2.5	0.65	210	0.7
9	45	1298	1	2.1	0.5	160	0.6
8	40	1160	0.8	1.7	0.4	120	0.6
7	35	1017	0.62	1.5	0.3	90	0.6
6	30	869	0.45	1.25	0.25	80	0.6
5	25	726	0.3	0.8	0.1	60	0.6
4	20	592	0.2	0.7	0.1	40	0.6
3	15	440	0.1	0.6	0.08	30	0.6
2	10	296	0.05	0.4	0.06	15	0.6

Table 3.4 shows the steady state values of speed attained by the motor, torque, input line current drawn, dc bus current, active power input and the settling time to attain steady state for various operating conditions. It is clear from these observations that a considerable speed range could be achieved with this topology. It is also found that the steady state of speed is attained in almost the same time for all the operating conditions.

The simulation results for constant volts per hertz scheme when the modulating sine wave amplitude is 9.8 V and the frequency is 49Hz are given below. The dc capacitor used is 0.5 mF.

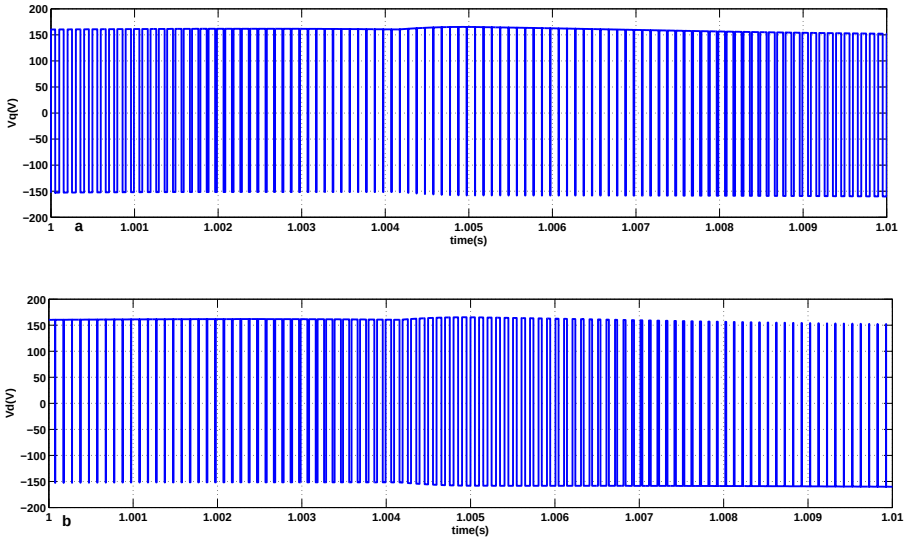

Figure 3.21: Applied Stator Voltage wrt time: (a) Main winding voltage (b) Auxiliary winding voltage

Figure 3.21 shows the main winding and auxiliary winding voltage. The dc bus voltage is switched on and off at 10 kHz. The 90° phase shift between main and auxiliary winding voltages can be easily seen in the figure. The dc bus ripple can be seen as the varying pulse amplitude in the voltage waveforms.

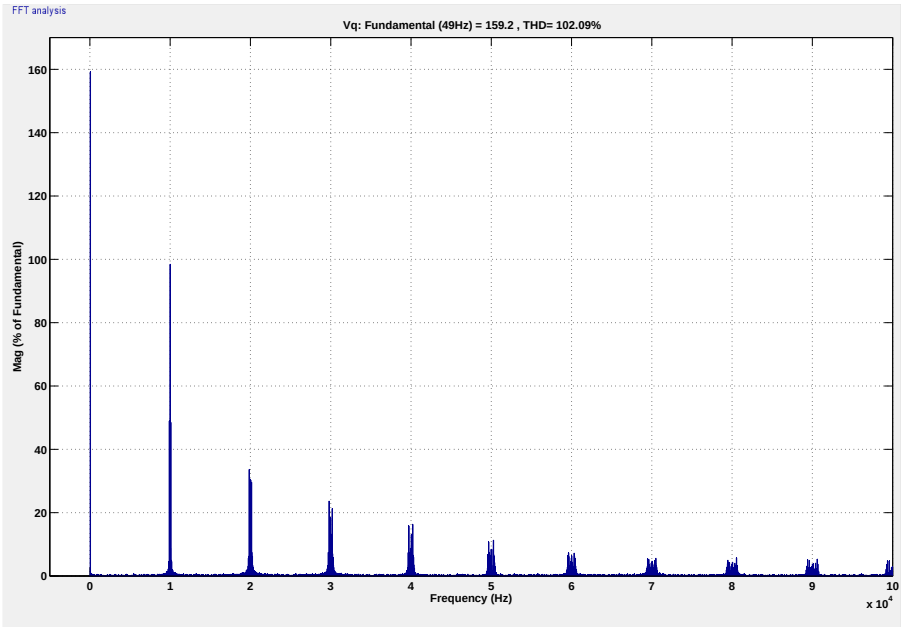

Figure 3.22: harmonic spectrum analysis: Motor Input Voltage

Figure 3.22 shows the harmonic profile of the main winding voltage(auxiliary winding voltage also has the same harmonic profile). The $\%$ THD is found to be 102%. The

fundamental main winding voltage is found to have a peak of $159V$ at 49 Hz. The harmonic voltage at 10 kHz is found to be 66% of fundamental. They can overheat the machine due to the effects of harmonic currents(depending on their frequency). This is because of additional rotating magnetic fields in the motor. It can produce high frequency currents in rotor circuits.

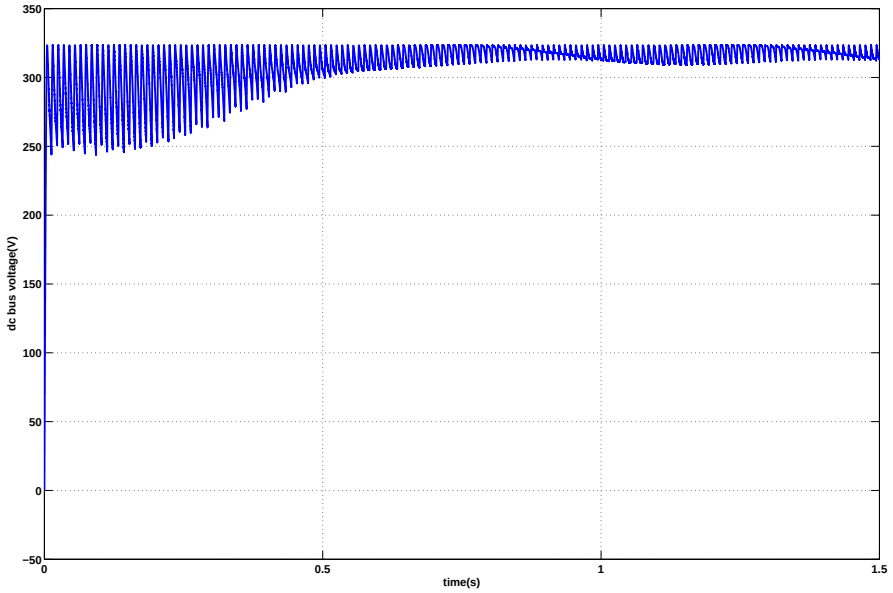

Figure 3.23: DC Bus Voltage wrt time

Figure 3.23 shows the dc bus voltage when the bus capacitor used is 0.5 mF. The ripple in the dc bus voltage is within the design limits. Initially, in the transient state, because of inrush currents, this ripple is higher than the specified limits as the current drawn is more.

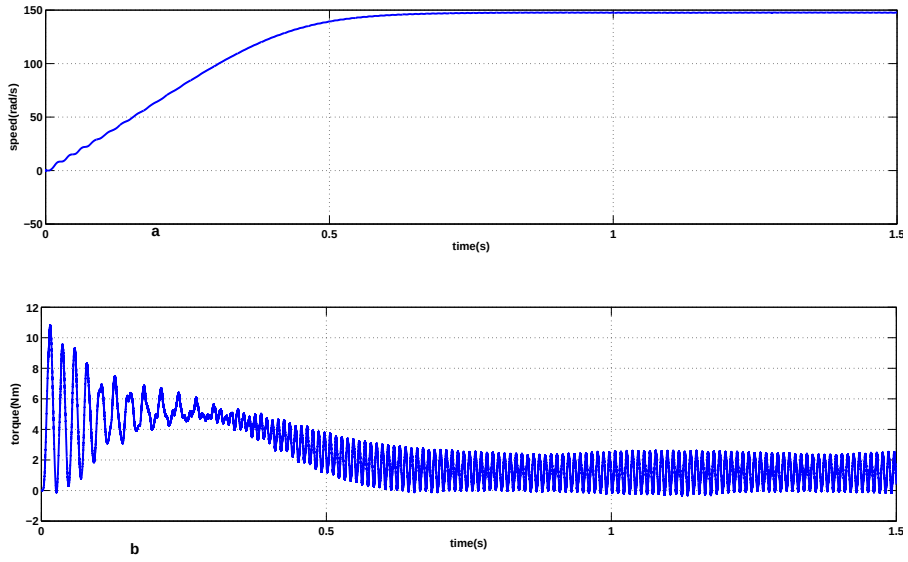

Figure 3.24: Speed and torque variation wrt time

Figure 3.24 shows the speed and torque variation wrt time. The speed is found to settle at a value of 147.5 rad/s at 0.7s. The torque ripple observed is due to stator current imbalance. Also there is a slight variation of torque ripple magnitude which is of lesser frequency(when the dc bus capacitor used is 0.5 mF).

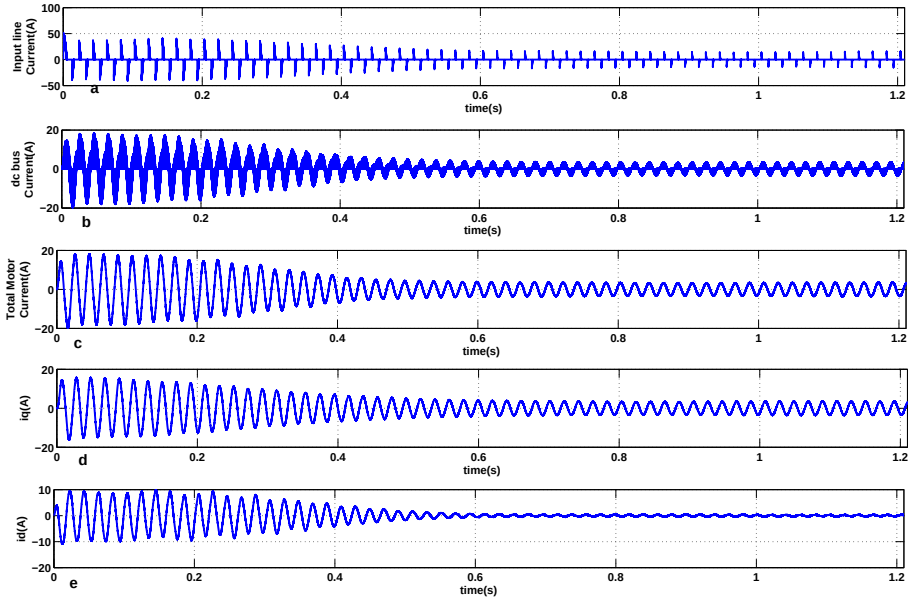

Figure 3.25: Current Waveforms: (a) Line Current (b) DC bus current (c) Total Motor current (d) Main Winding current (e) Auxiliary Winding Current

Figure 3.25 shows the various current waveforms. The inrush current phenomenon is observed in the transient state in the total motor current and the dc bus current. The

imbalance in the stator winding currents at steady state leading to torque ripple can also be seen.

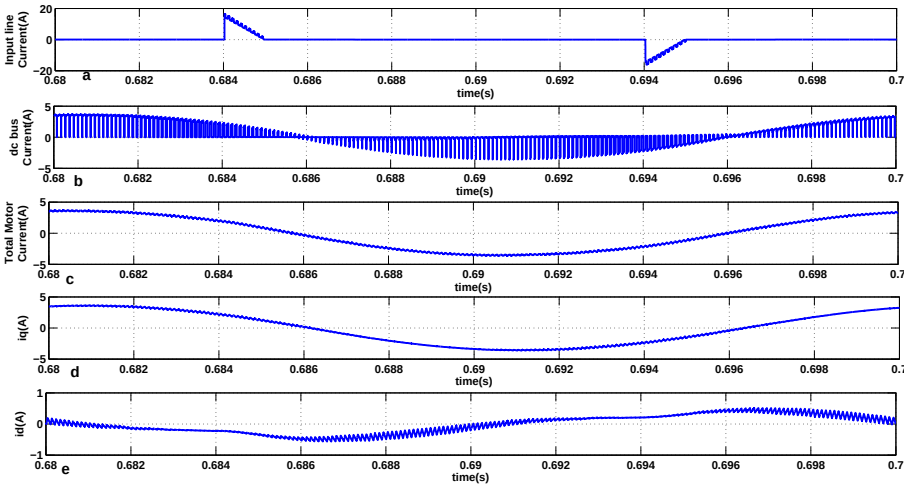

Figure 3.26: Current Waveforms: (a) Line Current (b) DC bus current (c) Total Motor current (d) Main Winding current (e) Auxiliary Winding Current

Figure 3.26 shows the various current waveforms in steady state on an expanded scale. The auxiliary winding current is found to be distorted.

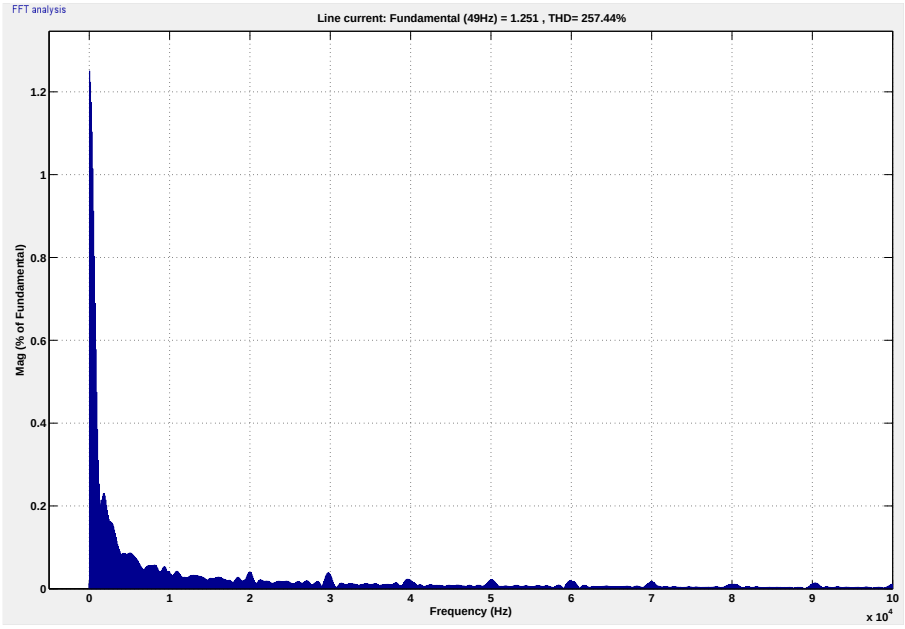

Figure 3.27: Current Harmonic Spectrum: Line Current

Figure 3.27 shows the harmonic profile of the line current. The $\%$ THD is found to be very high at 257%. The fundamental line current is found to have a peak of $1.25A$. The line current is found to be highly polluted which is not desirable.

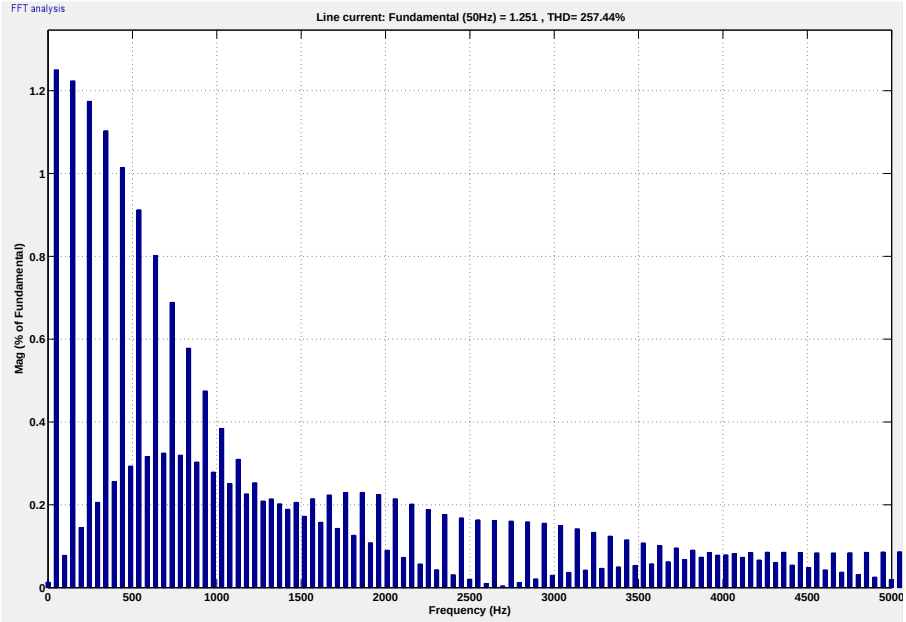

Figure 3.28: Current Harmonic Spectrum: Line Current

Figure 3.28 shows the harmonic profile of the line current on an expanded scale.

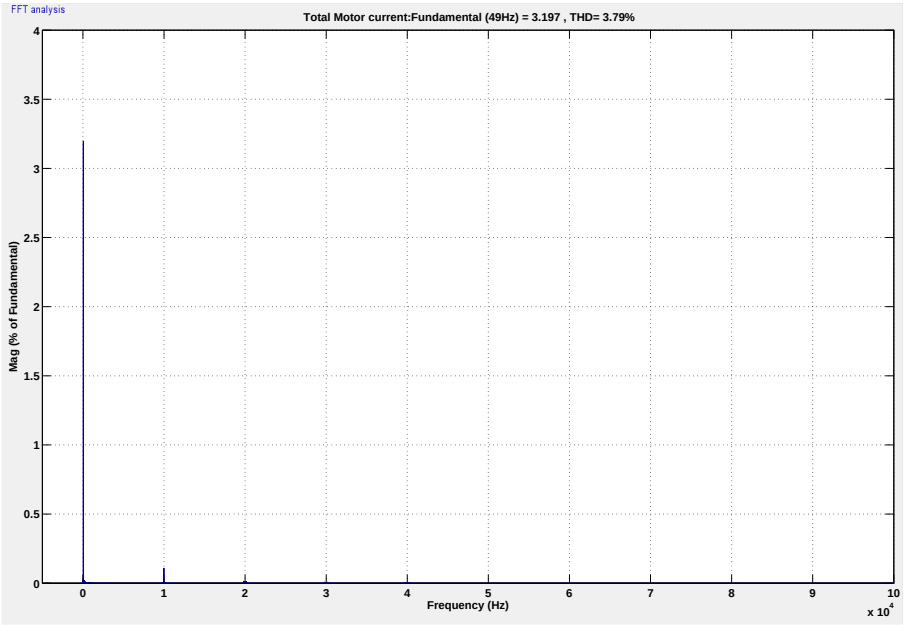

Figure 3.29: Current Harmonic Spectrum: Total Motor current

Figure 3.29 shows the harmonic profile of the total motor current. The $\%$ THD is found to be 3.8%. The fundamental motor current is found to have a peak of 3.2 A. The THD is lesser here.

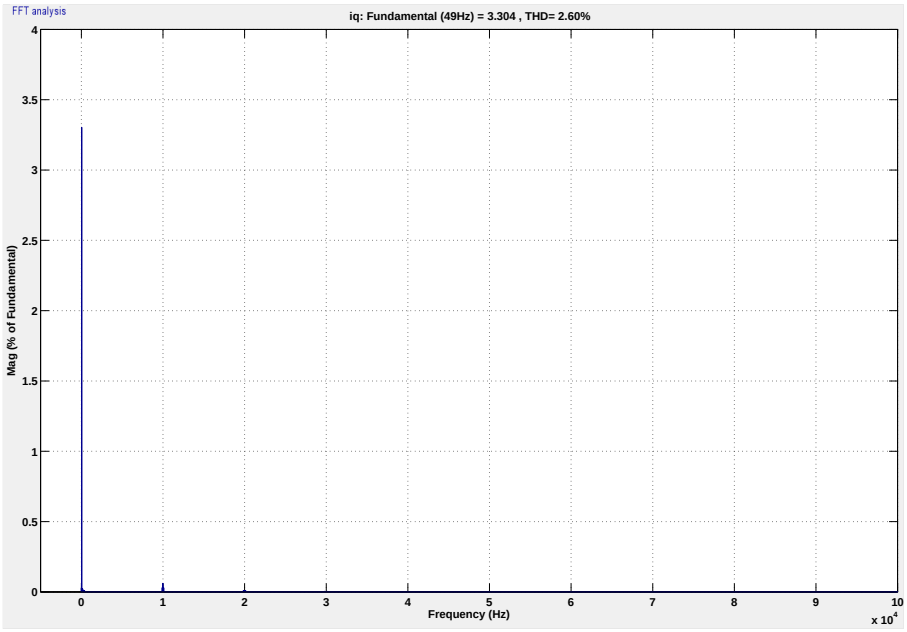

Figure 3.30: Current Harmonic Spectrum: Main Winding current

Figure 3.30 shows the harmonic profile of the main winding current. The $\%$ THD is found to be 2.6%. The fundamental main winding current is found to have a peak of 3.3 A. The THD is again less here.

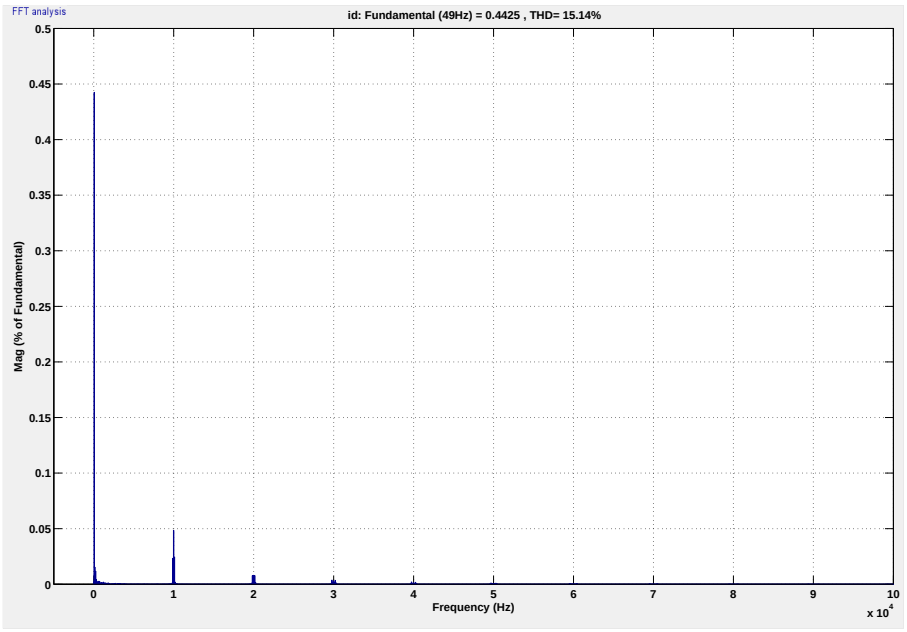

Figure 3.31: Current Harmonic Spectrum: Auxiliary Winding Current

Figure 3.31 shows the harmonic profile of the auxiliary winding current. The $\%$ THD is found to be 15.1%. The fundamental auxiliary winding current is found to have a peak of 0.44 A. The THD is higher as the auxiliary winding current is a bit distorted which can be seen in its wave shape.

DC Bus capacitor=22 mF

A dc bus capacitance of 22mF is then used for the simulations. When this is done, the dc bus voltage is found to have minimum ripple. This is done to analyze the machine performance under ideal conditions of ripple free bus voltage. The results obtained for the following schemes are as given below.

SPWM Inverter based Stator Voltage Control: The amplitude of the modulating sine wave alone is varied thereby changing the magnitude of the applied stator voltage to the motor. The simulation results obtained are tabulated in table 3.5

SPWM Inverter based Constant V/f Control: The amplitude as well as the frequency of the modulating sine wave are varied in such a way that the ratio of voltage of sine wave to the frequency of the sine wave(V/f) is maintained a constant. The simulation results obtained are tabulated in table 3.6

Table 3.5: SPWM Inverter based Stator Voltage Control(without auxiliary winding capacitance)dc bus capacitor=22 mF):Results

Sine amp. (V)	Speed (rpm)	Torque (Nm)	input current (rms)(A)	dc bus current(avg)(A)	Active Power input(W)	Settling Time(s)
9.8	1432	1.22	5.5	0.68	220	0.7
9	1423	1.21	5.45	0.66	217	0.8
8	1400	1.17	5.3	0.64	210	1.1
7	1370	1.12	5.1	0.62	203	1.45
6	1327	1	5	0.59	195	2
5	1250	0.9	4.6	0.57	180	3

Table 3.5 shows the steady state values of speed attained by the motor, electromagnetic torque, input line current drawn, dc bus current, active power input and the settling time to attain steady state for various operating conditions. It is clear from these observations that a considerable speed range could not be achieved with this topology as this is a stator voltage control scheme. The time taken to attain steady state is found to increase with decrease in modulation index.

Table 3.6: SPWM Inverter based Constant V/f Control(without auxiliary winding capacitance) dc bus capacitor=22 mF: Results

Modulating sine		Speed	Torque	input current	dc bus current	Active Power	Settling
amp.(V)	freq.(Hz)	(rpm)	(Nm)	(rms)(A)	(avg)(A)	input(W)	Time(s)
9.8	49	1404	1.25	5.24	0.64	200	0.7
9	45	1297	1	4.5	0.5	170	0.6
8	40	1158	0.75	3.5	0.38	120	0.6
7	35	1018	0.62	2.5	0.27	80	0.6
6	30	879	0.5	2	0.17	60	0.6
5	25	735	0.3	1.5	0.12	40	0.6
4	20	592	0.2	1	0.1	25	0.6
3	15	440	0.1	0.5	0.05	15	0.6
2	10	296	0.05	0.4	0.02	10	0.6

Table 3.6 shows the steady state values of speed attained by the motor, electromagnetic torque, input line current drawn, dc bus current, active power input and the settling time to attain steady state for various operating conditions. It is clear from these observations that a considerable speed range could be achieved. It is also found that the steady state of speed is attained in almost the same time for all the operating conditions.

At lower values of modulation indices, the applied stator voltage will be very less. In real life situation, every motor has a frictional load(which is not incorporated in the machine model used in the simulations here). At these low levels of motor input voltage, the motor may stall. The motor may not be able to pick up speed. For this, required modification has to be done in hardware implementation of the topology.

The various simulation results obtained for constant volts-per-hertz scheme when the modulating sine wave is of amplitude 9.8 V and frequency 49 Hz is given below. The dc bus capacitor used is 22 mF.

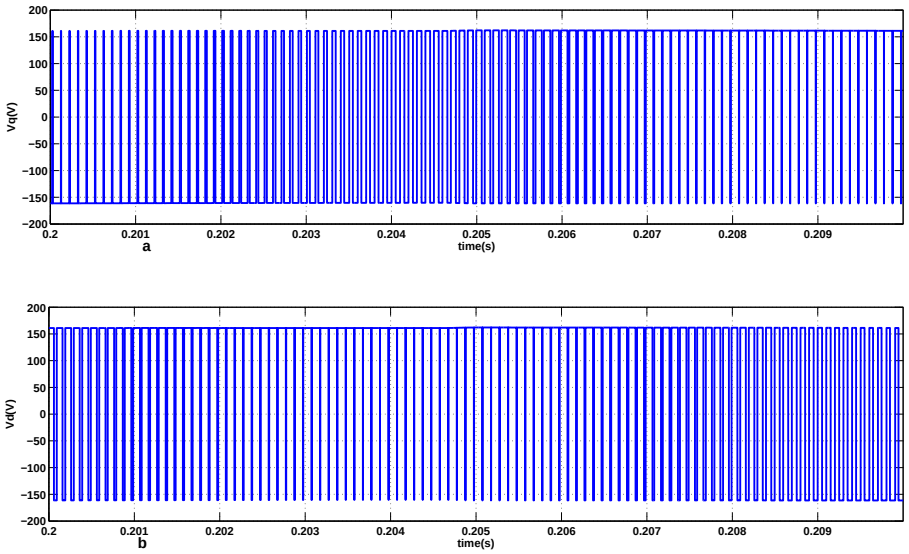

Figure 3.32: Applied Stator Voltage wrt time: (a)Main winding voltage (b) Auxiliary winding voltage

Figure 3.32 shows the main winding and auxiliary winding voltages. The dc bus voltage is switched on and off at 10 kHz. The 90° phase shift between main and auxiliary winding voltages can be easily seen in the figure. The pulse amplitudes are found to be almost fixed with time as the dc bus ripple is very minimum.

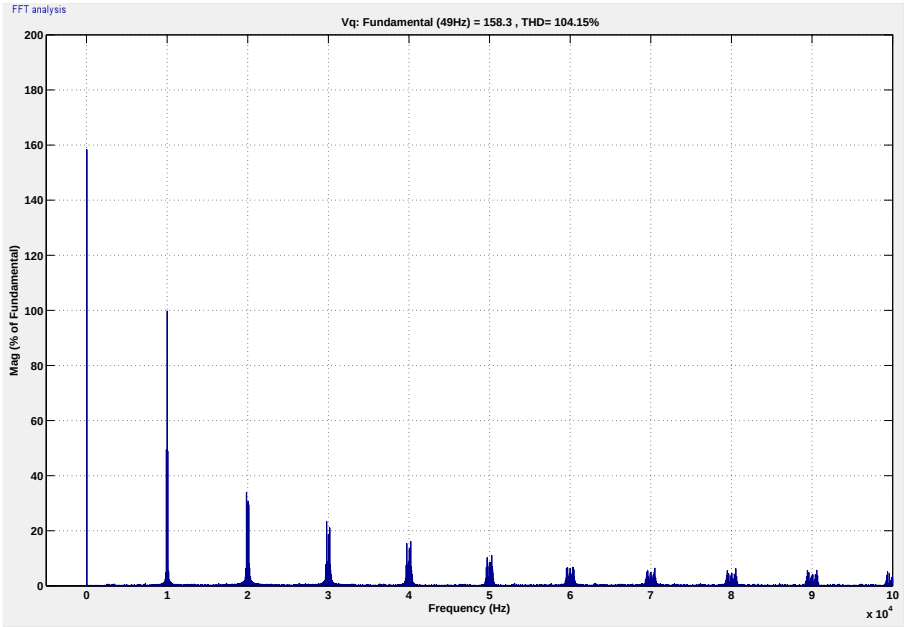

Figure 3.33: harmonic spectrum analysis: Motor Input Voltage

Figure 3.33 shows the harmonic profile of the main winding voltage(auxiliary winding voltage also has the same harmonic profile). The $\%$ THD is found to be 104%. The fun-

damental main winding voltage is found to have a peak of $158V$ at 49 Hz.The harmonic voltage at 10 kHz is found to be 66% of fundamental. They can overheat the machine due to the effects of harmonic currents(depending on their frequency).

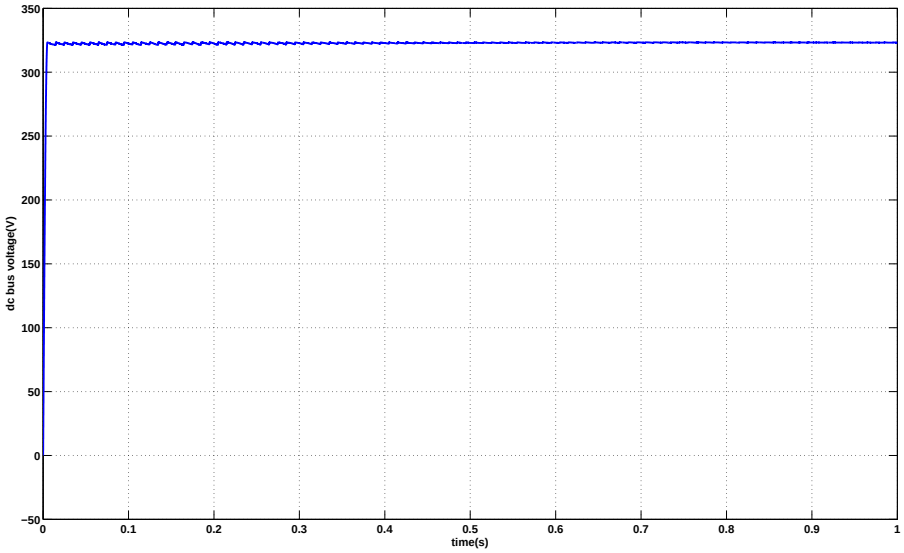

Figure 3.34: DC Bus Voltage wrt time

Figure 3.34 shows the dc bus voltage when the bus capacitor used is 22 mF. The ripple in the dc bus voltage is very less in this case.

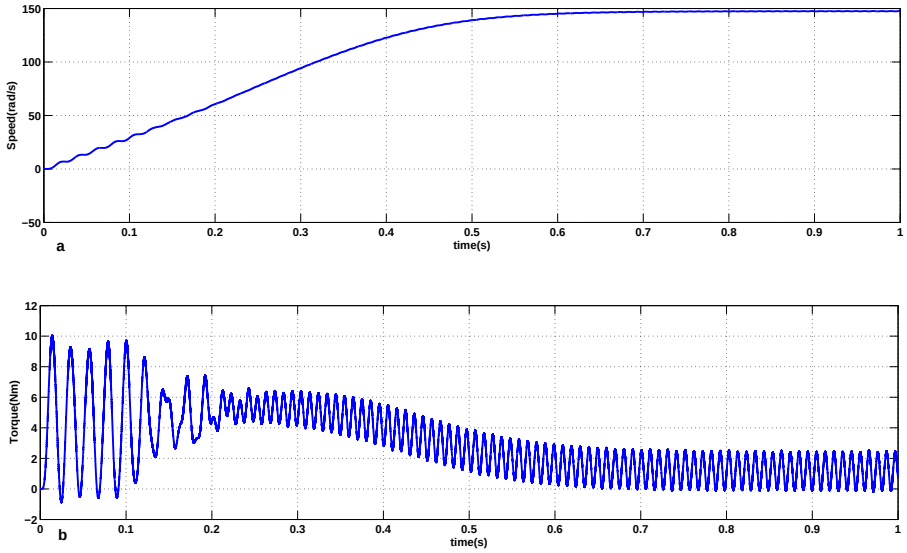

Figure 3.35: Speed and torque variation wrt time

Figure 3.35 shows the speed and torque variation wrt time. The speed is found to settle at a value of 147 rad/s at 0.7s. The torque ripple observed is due to stator current

imbalance. Here the mean value of torque was found to be a constant at steady state equal to the load torque of $B\omega^2$. The slight variation of torque ripple magnitude with a low frequency which was observed when dc capacitor of 0.5 mF was used is not observed here.

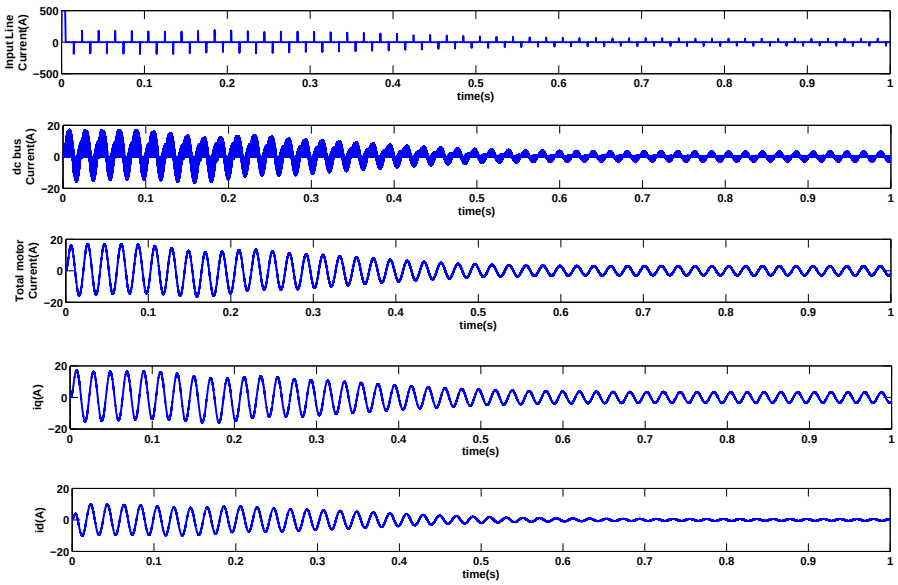

Figure 3.36: Current Waveforms: (a)Line Current (b)DC bus current (c)Total Motor current (d)Main Winding current (e)Auxiliary Winding Current

Figure 3.36 shows various current waveforms. The inrush current phenomenon and the stator current imbalance is also observed as in previous case. The input line current peaks are found to be lesser here.

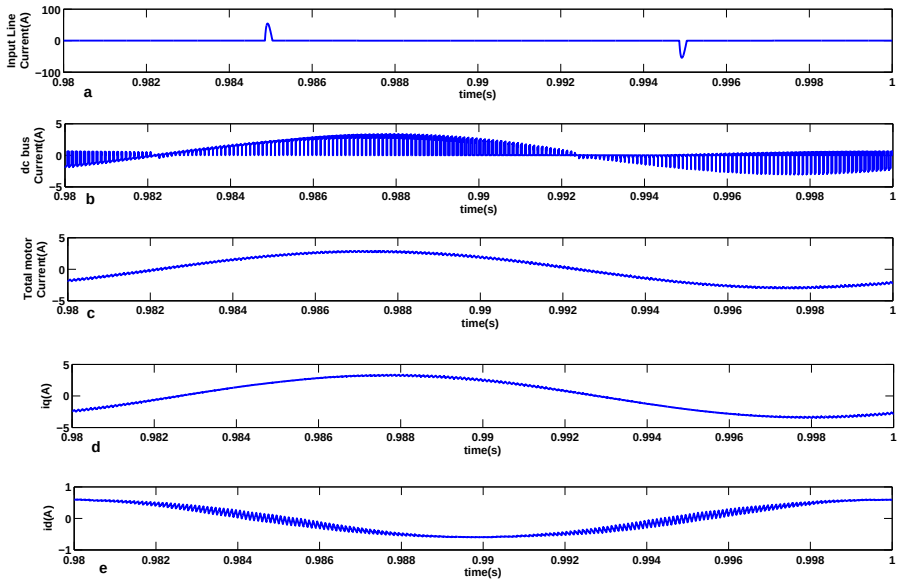

Figure 3.37: Current Waveforms: (a)Line Current (b)DC bus current (c)Total Motor current (d)Main Winding current (e)Auxiliary Winding Current

Figure 3.37 shows various current waveforms at steady state on an expanded scale. The distortion in auxiliary winding current is reduced here from previous case.

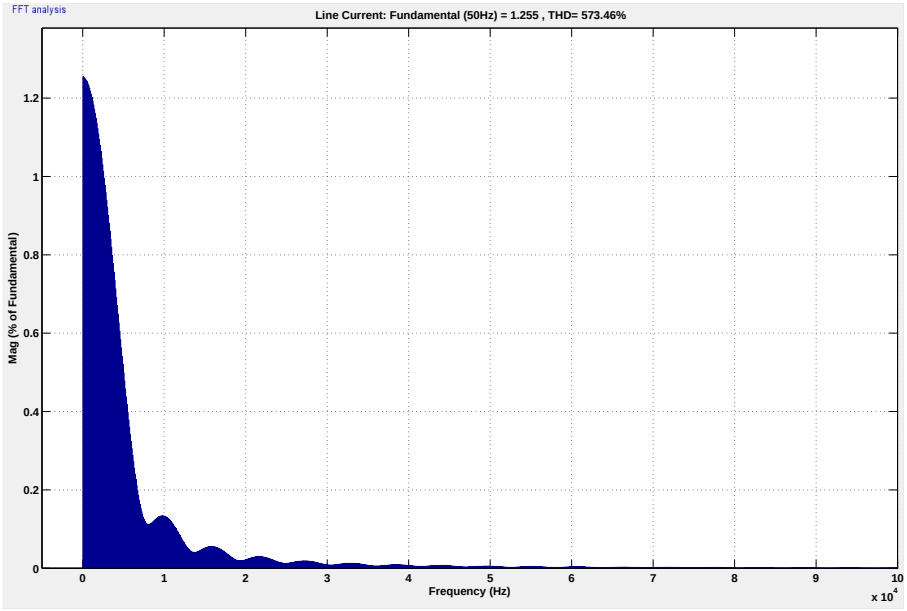

Figure 3.38: Current Harmonic Spectrum: Line Current

Figure 3.38 shows the harmonic profile of the line current. The $\%$ THD is found to be 573%. The fundamental line current is found to have a peak of 1.25 A. The line current is found to be highly polluted.

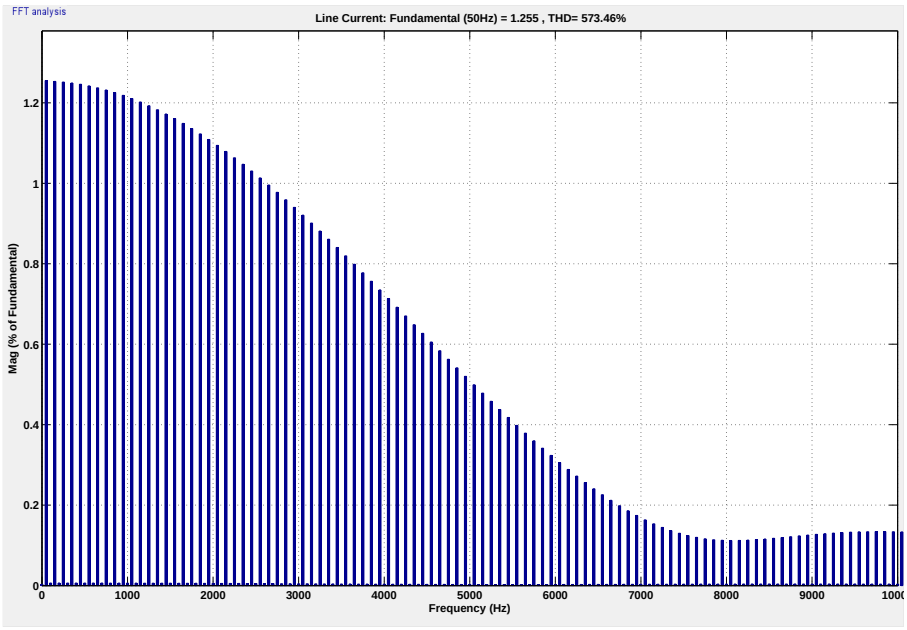

Figure 3.39: Current Harmonic Spectrum: Line Current

Figure 3.39 shows the harmonic profile of the line current on an expanded scale. The THD is more compared to the previous case of dc capacitor of 0.5 mF.

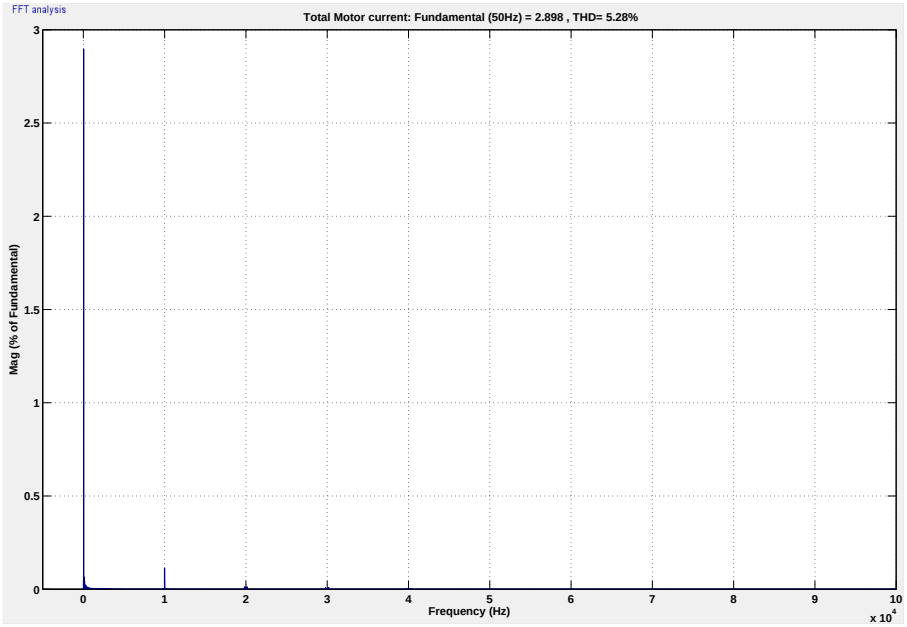

Figure 3.40: Current Harmonic Spectrum: Total Motor current

Figure 3.40 shows the harmonic profile of the total motor input current. The $\%$ THD is found to be 5.28%. The fundamental line current is found to have a peak of 3 A. The THD is more compared to the previous case of dc capacitor of 0.5 mF.

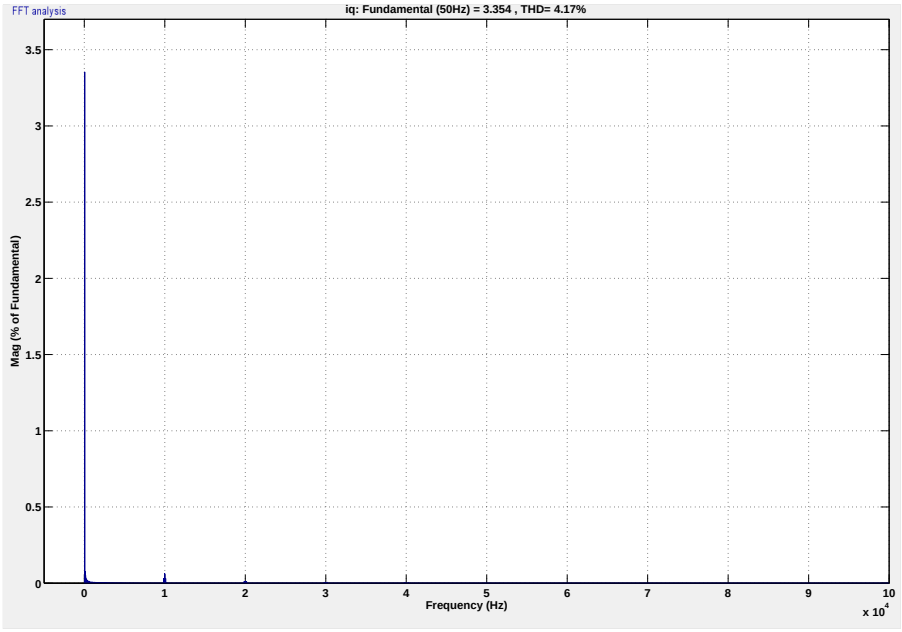

Figure 3.41: Current Harmonic Spectrum: Main Winding current

Figure 3.41 shows the harmonic profile of the main winding current. The $\%$ THD is found to be 4.2%. The fundamental line current is found to have a peak of 3.4 A. The THD is more compared to the previous case of dc capacitor of 0.5 mF.

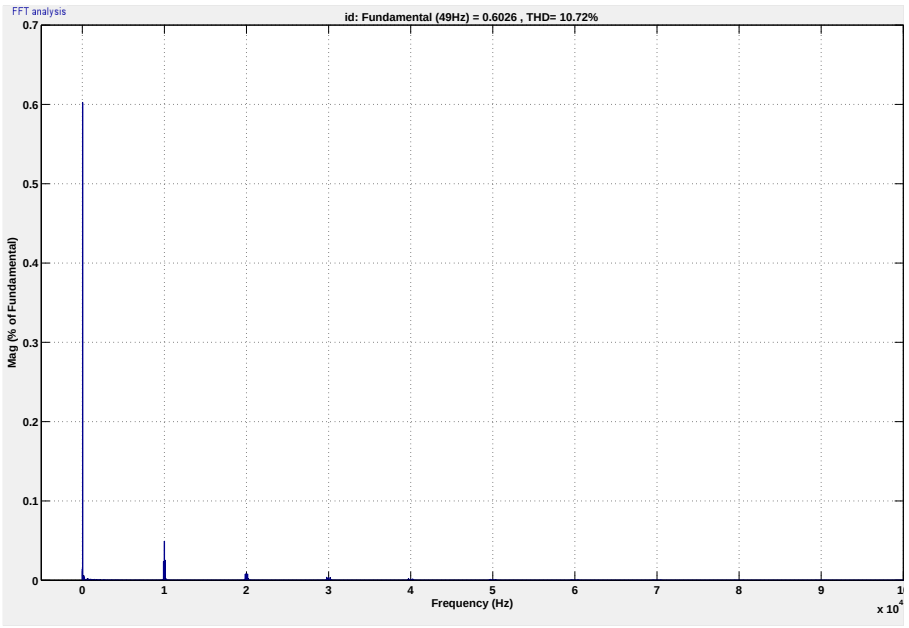

Figure 3.42: Current Harmonic Spectrum: Auxiliary Winding Current

Figure 3.42 shows the harmonic profile of the auxiliary winding current. The $\%$ THD is found to be 10.72%. The fundamental line current is found to have a peak of 0.6 A. The THD is lesser here compared to the previous case of dc capacitor of 0.5 mF.

The input rms line current drawn from mains is found to be higher when the dc capacitor used is 22 mF. Also, at 49Hz of operation, there is a variation in the magnitude of torque ripple at a low frequency at steady state when the dc capacitor is 0.5mF unlike when the dc capacitor used is 22mF.

At lower frequencies of operation, there is a speed ripple observed in the steady state when a dc bus capacitor of 0.5 mF is used. This is because the applied motor voltage rms value changes in every cycle due to the dc bus ripple which is at 100 Hz. When the modulating sine is at 30 Hz, the mean value of dc bus voltage coming in each cycle of modulating sine wave is different which in turn varies the applied stator voltage in each cycle. This in turn changes the current in each cycle and hence the torque. This is the reason for the current waveforms being non uniform sinusoids in steady state in figure 3.45. When the operating frequency is close to 50 Hz, this speed ripple wont be observed.

For an operating condition of $6V, 30Hz$ modulating sine, the speed torque characteristics for the two dc bus capacitor values are shown in figures 3.43 and 3.44. The speed ripple is found to be $4rad/s$, when the dc bus capacitance is $0.5mF$. The speed ripple is very minimum when the dc bus capacitor used is 22mF.

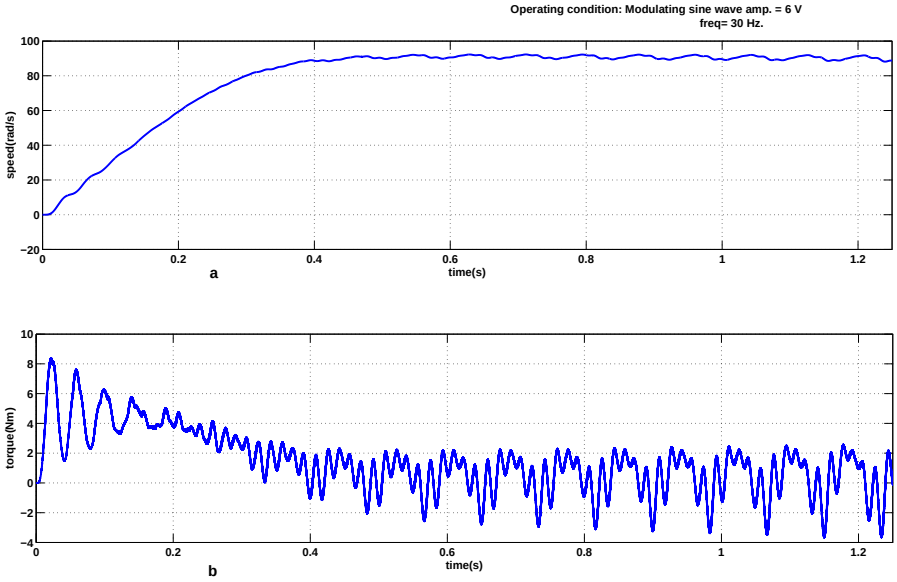

Figure 3.43: Speed and torque variation wrt time: dc capacitor= $0.5mF$

Figure 3.43 shows the speed and torque variation w.r.t time when the dc capacitor used is 0.5 mF. The modulating wave used is 6 V, 30 Hz. The speed is found to settle down

at 91 rad/s at 0.5s with a ripple of 4 rad/s.

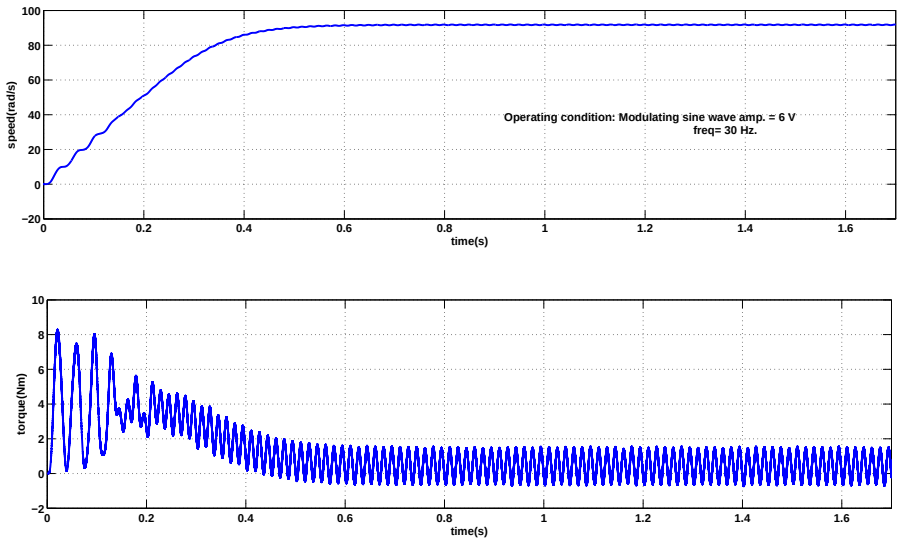

Figure 3.44: Speed and torque variation wrt time: dc capacitor= $22mF$

Figure 3.43 shows the speed torque variation w.r.t time when the dc capacitor used is 22 mF. The modulating wave used is 6 V, 30 Hz. The speed is found to settle down at 92 rad/s at 0.6s. The speed ripple is very minimum here. Torque is found to have a constant mean value of load torque at steady state

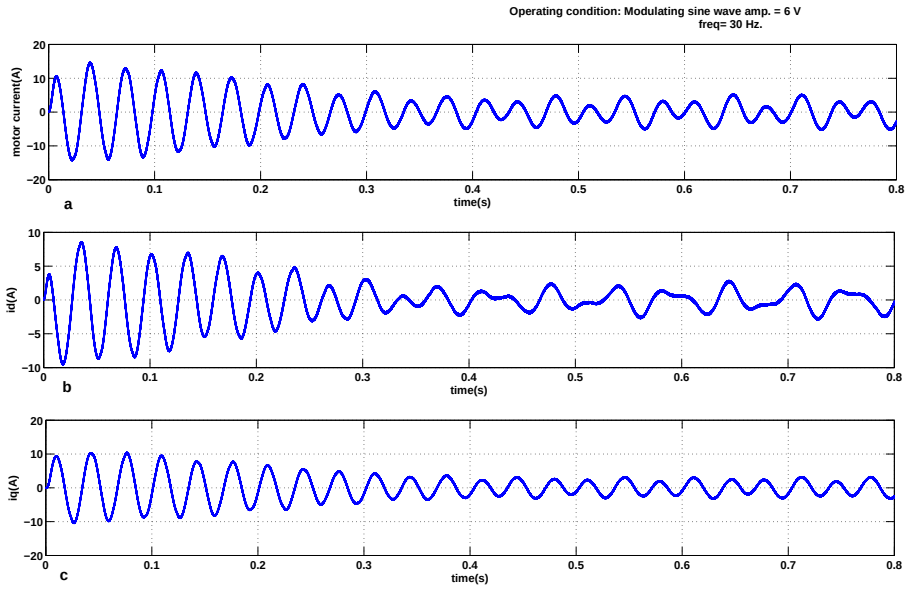

Figure 3.45: Current waveforms wrt time: dc capacitor= $0.5mF$

Figure 3.45 shows the current waveforms when the dc capacitor used is 0.5 mF. It is found to be highly distorted.

3.4.3 Driver Circuit Implementation

The major difficulty in implementing this topology in analog domain is to get a frequency independant sine wave to cosine wave converter. A circuit for the same was designed making use of PI controllers and simulated and the simulation results are given in figures 3.46 and 3.47

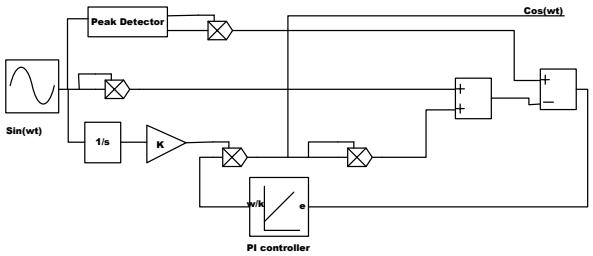

Figure 3.46: Frequency independant sine-cosine converter

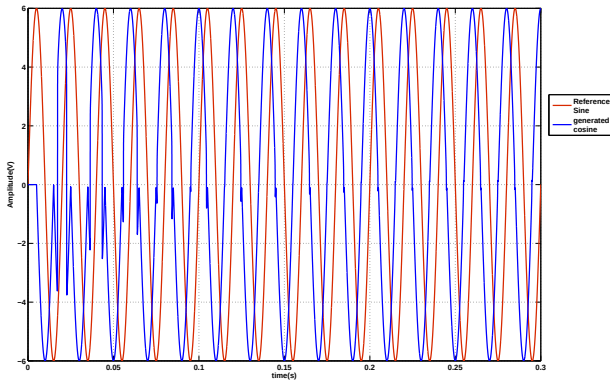

Figure 3.47: Frequency independant sine-cosine converter waveforms

Figure 3.47 shows the reference sine wave and the cosine wave generated from the circuit. The reference wave is shown in red an the generated cosine is shown in blue. The major disadvanage in implementing this circuit in analog domain is the need of four analog multipliers which makes the configuration implementation costly. So this configuration is not used in hardware.

3.5 SPWM Inverter based Speed Controller with Auxilliary Winding Capacitor

In this configuration, the motor model is connected between the inverter legs with the auxiliary winding capacitor connected as shown in figure 3.48.

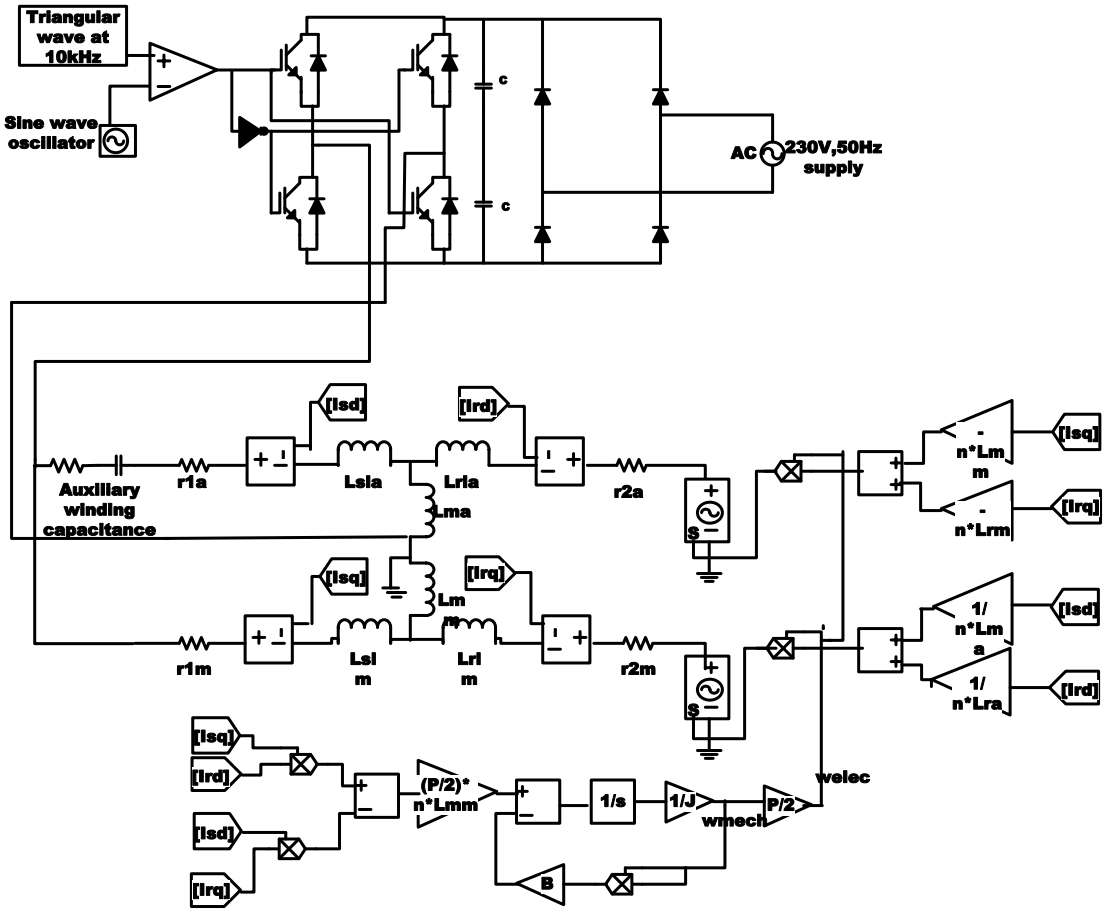

Figure 3.48: SPWM Inverter based Constant V/f Control(with auxiliary winding capacitance)

3.6 Simulation Results

The following two methods were implemented in this configuration.

SPWM Inverter based Stator Voltage Control: The amplitude of the modulating sine wave alone is varied thereby changing the magnitude of the applied stator voltage to the motor.

SPWM Inverter based Constant V/f Control: The amplitude as well as the frequency of the modulating sine wave are varied in such a way that the ratio of voltage of sine wave to the frequency of the sine wave(V/f) is maintained a constant.

DC Bus capacitor=0.5 mF

Initially the calculated value of dc bus capacitance of $0.5mF$ was used and the simulation results obtained are as given below.

Table 3.7: SPWM Inverter based Stator Voltage Control(with auxiliary winding capacitance)dc bus capacitor= $0.5mF$):Results

Sine amp. (V)	Speed (rpm)	Torque (Nm)	input current (rms)(A)	dc bus current(avg)(A)	Active Power input(W)	Settling Time(s)
9.8	1487	1.32	4.35	1.37	432	0.55
9	1483	1.31	4.1	1.25	395	0.6
8	1480	1.31	3.74	1.1	350	0.72
7	1474	1.3	3.43	0.98	312	0.9
6	1466	1.28	3.16	0.87	278	1.2
5	1450	1.26	2.94	0.78	250	1.7

Table 3.7 shows the steady state values of speed attained by the motor, electromagnetic torque, input line current drawn, dc bus current, active power input and the settling time to attain steady state for various operating conditions. It is clear from these observations that a considerable speed range could not be achieved with this topology as this is a stator voltage control scheme. The time taken to attain steady state is found to increase with decrease in modulation index.

Table 3.8: SPWM Inverter based Constant V/f Control(with auxiliary winding capacitance) dc bus capacitor= $0.5mF$: Results

Modulating sine amp.(V)	Modulating sine freq.(Hz)	Speed (rpm)	Torque (Nm)	input current (rms)(A)	dc bus current (avg)(A)	Active Power input(W)	Settling Time(s)
9.8	49	1456	1.27	4.1	1.28	400	0.45
9	45	1337	1.07	3.2	0.92	290	0.5
8	40	1188	0.84	2.4	0.6	200	0.5
7	35	1040	0.65	1.8	0.4	140	0.5
6	30	894	0.5	1.5	0.25	100	0.45
5	25	745	0.3	1.25	0.21	70	0.42
4	20	592	0.2	1	0.17	50	0.43
3	15	449	0.12	0.85	0.16	40	0.43

Table 3.9 shows the steady state values of speed attained by the motor, torque, input line current drawn, dc bus current, active power input and the settling time to attain steady state for various operating conditions. It is clear from these observations that a considerable speed range could be achieved with this topology. It is also found that the steady state of speed is attained in almost the same time for all the operating conditions

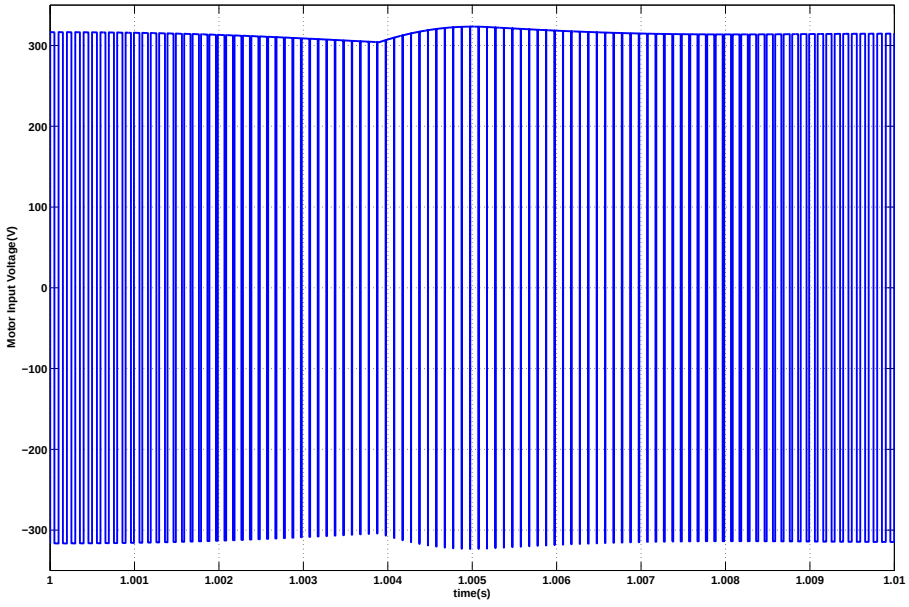

Figure 3.49: Applied Stator Voltage wrt time

Figure 3.49 gives the applied voltage across the motor terminals when connected across the inverter legs. The dc bus ripple can be seen as the varying pulse amplitude in the voltage waveforms.

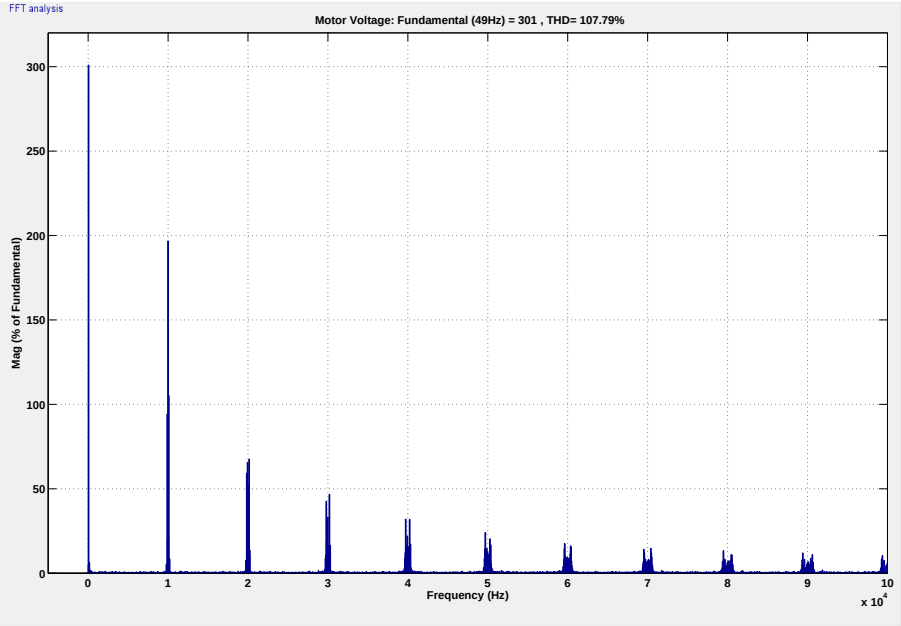

Figure 3.50: harmonic spectrum analysis: Motor Input Voltage

Figure 3.50 shows the harmonic profile of the motor input voltage. The $\%$ THD is found to be 108%. The fundamental motor voltage is found to have a peak of $301V$. The harmonic voltage at 10 kHz is found to be 66% of fundamental. They can overheat the machine due to the effects of harmonic currents. This is because of additional rotating magnetic fields in the motor. It can produce high frequency currents in rotor circuits.

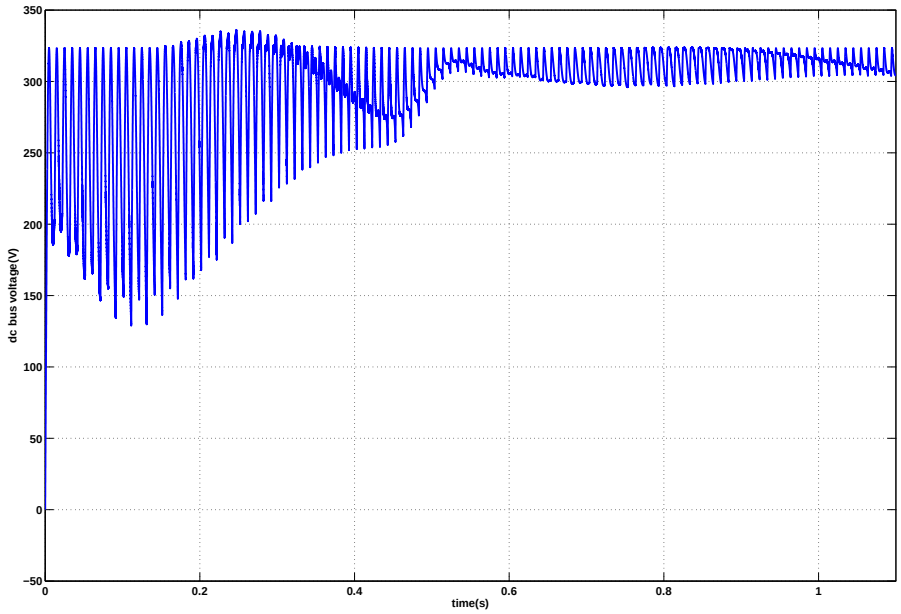

Figure 3.51: DC Bus Voltage wrt time

Figure 3.51 shows the dc bus voltage. As the dc bus capacitor used is a lesser value of 0.5 mF(according to the design), there is a noticeable ripple in the dc bus voltage at steady state which is within the design limits. Initially, in the transient state, because of inrush currents, this ripple is higher than the specified limits as the current drawn is more.

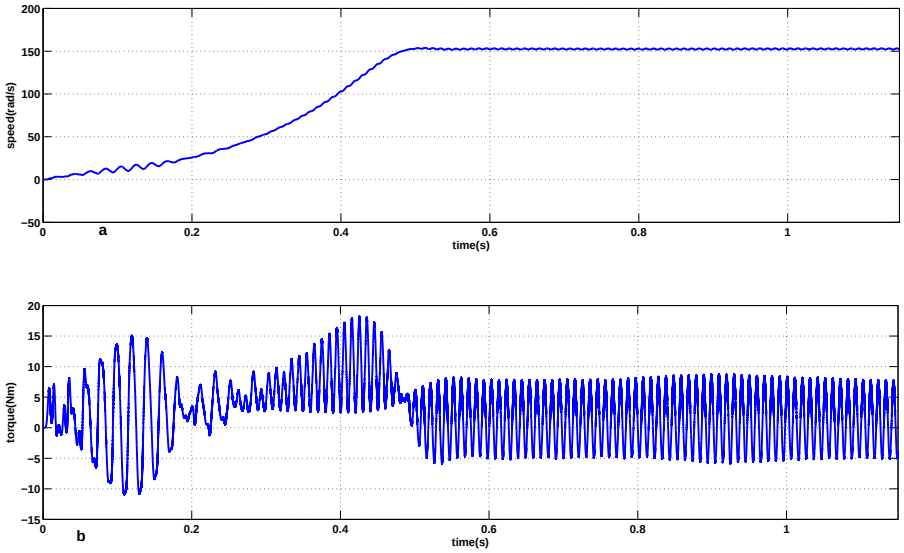

Figure 3.52: Speed and torque variation wrt time

Figure 3.52 shows the speed and torque variation w.r.t time. The speed is found to settle at a value of 152.5 rad/s in a time of 0.5s. The torque is found to have a ripple due to

imbalance in the stator currents. The torque ripple magnitude is found to be varying at a lower frequency.Here the mean value of torque was found to be a constant at steady state equal to the load torque of $B\omega^2$.

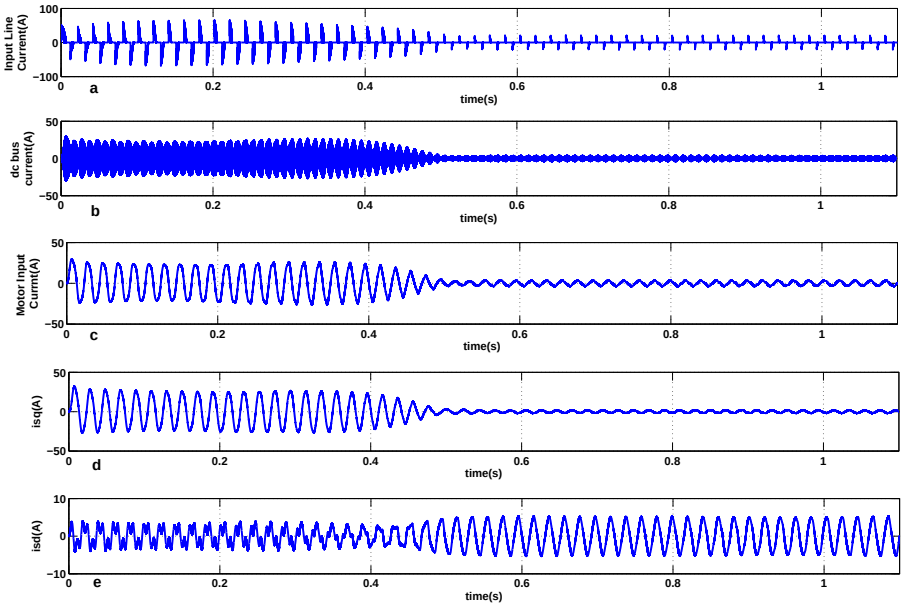

Figure 3.53: Current Waveforms: (a)Line Current (b)DC bus current (c) Motor current (d)Main Winding current (e)Auxiliary Winding Current

Figure 3.53 shows the various current waveforms. The inrush current phenomenon of the motor is evident from the motor current and the line current waveforms.The stator current imbalance is easily observable which leads to torque ripple. The auxiliary winding current in transient state is found to be highly distorted.

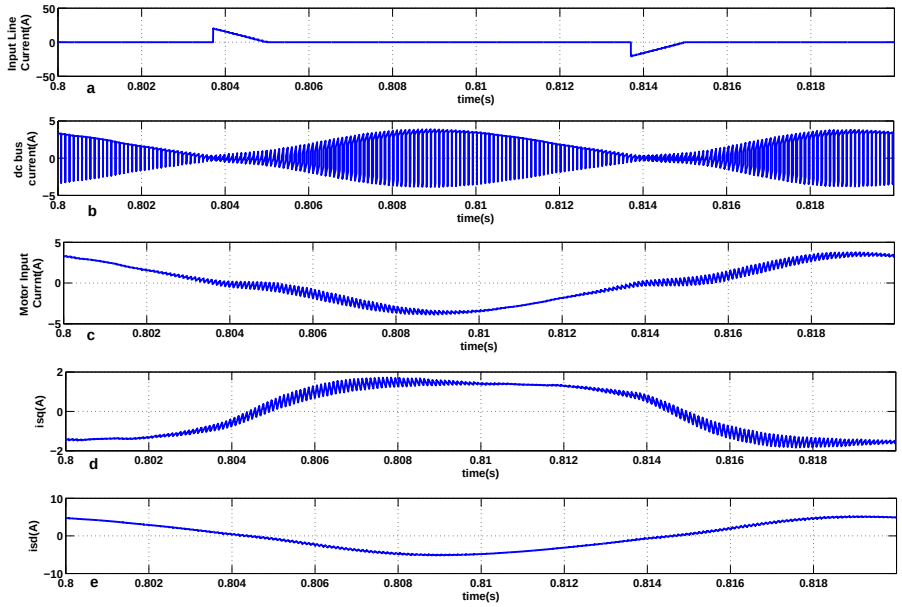

Figure 3.54: Current Waveforms: (a)Line Current (b)DC bus current (c) Motor current (d)Main Winding current (e)Auxiliary Winding Current

Figure 3.54 shows the current waveforms at steady state on an expanded scale. The motor current. auxiliary and main winding currents are found to be distorted.

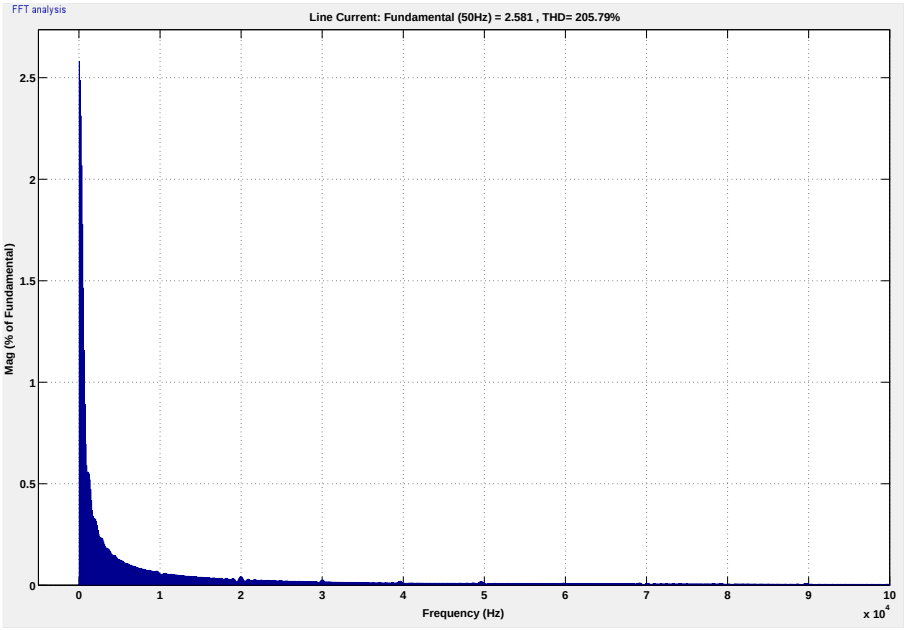

Figure 3.55: Current Harmonic Spectrum: Line Current

Figure 3.55 shows the harmonic profile of the input line current from the mains. The % THD is found to be 205.8%. The fundamental line current is found to have a peak of 2.6 A. The line current is found to be highly distorted which is not desirable.

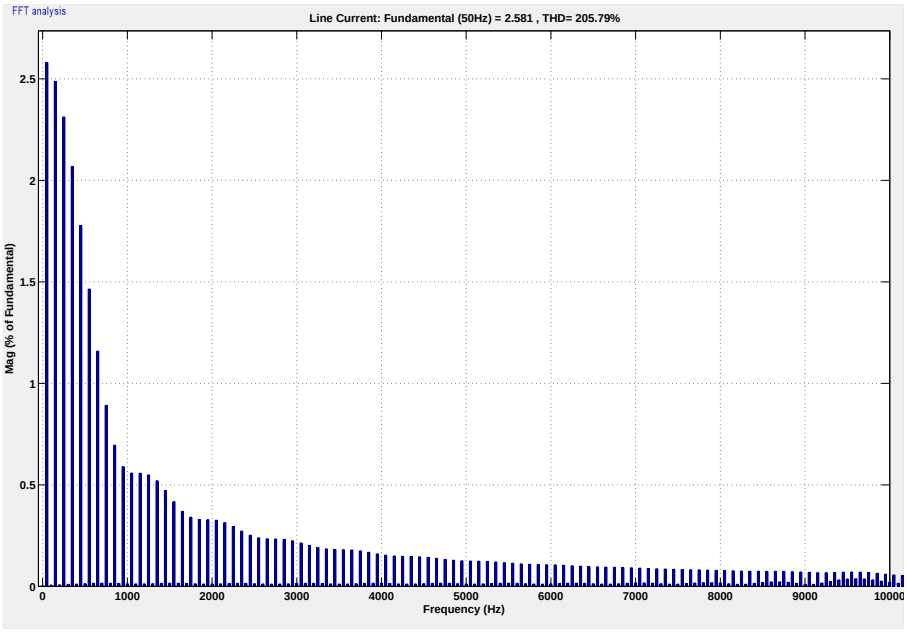

Figure 3.56: Current Harmonic Spectrum: Line Current

Figure 3.56 shows the harmonic profile of the input line current from the mains on an expanded scale.

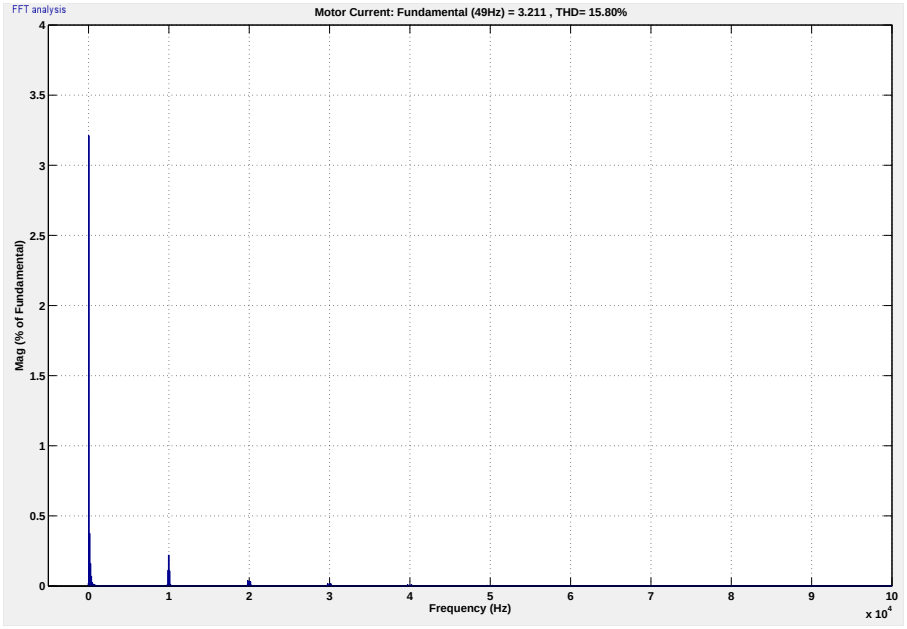

Figure 3.57: Current Harmonic Spectrum: Total Motor current

Figure 3.57 shows the harmonic profile of the total motor current. The $\%$ THD is found to be 15.8%. The fundamental motor input current is found to have a peak of 3.2 A. The wave shape of motor input current is found to be distorted as given in figure 3.54.

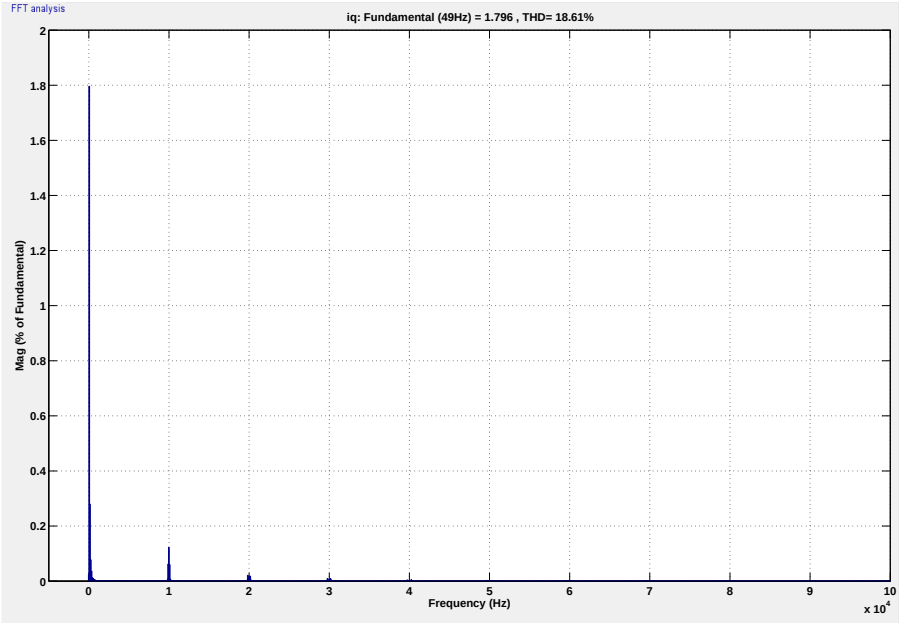

Figure 3.58: Current Harmonic Spectrum: Main Winding current

Figure 3.58 shows the harmonic profile of the main winding current. The $\%$ THD is found to be 18.6%. The fundamental main winding current is found to have a peak of 1.8 A. The high THD is evident from the distortions seen in the current as given in figure 3.54.

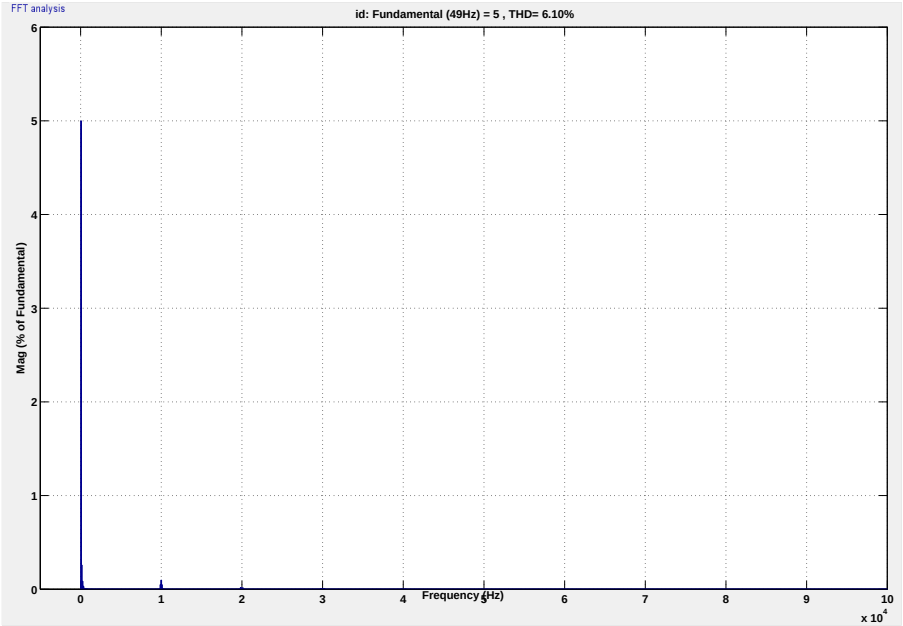

Figure 3.59: Current Harmonic Spectrum: Auxiliary Winding Current

Figure 3.59 shows the harmonic profile of the auxiliary winding current. The $\%$ THD is found to be 6.1%. The fundamental auxiliary winding current is found to have a peak of $5A$. The high THD is evident from the distortions seen in the current as in figure 3.54.

Dc Bus capacitor=22 mF

A dc bus capacitance of 22mF is then used for the simulations. When this is done, the dc bus voltage is found to have minimum ripple. The machine performance under ideal conditions of ripple free bus voltage can be compared with the actual performance with calculated dc capacitor. The results obtained for the following schemes are described.

SPWM Inverter based Stator Voltage Control: The amplitude of the modulating sine wave alone is varied thereby changing the magnitude of the applied stator voltage to the motor.

SPWM Inverter based Constant V/f Control: The amplitude as well as the frequency of the modulating sine wave are varied in such a way that the ratio of voltage of sine wave to the frequency of the sine wave(V/f) is maintained a constant.

Table 3.9: SPWM Inverter based Stator Voltage Control(with auxiliary winding capacitance) dc bus capacitor$= 22mF$):Results

Sine amp. (V)	Speed (rpm)	Torque (Nm)	input current (rms)(A)	dc bus current(avg)(A)	Active Power input(W)	Settling Time(s)
9.8	1490	1.33	10	1.37	450	0.42
9	1480	1.31	9	1.25	400	0.5
8	1478	1.31	8	1.1	360	0.6
7	1475	1.3	7.4	0.98	325	0.75
6	1467	1.3	6.75	0.87	280	1.1
5	1452	1.27	6.25	0.77	260	1.5

Table 3.9 shows the steady state values of speed attained by the motor, electromagnetic torque, input line current drawn, dc bus current, active power input and the settling time to attain steady state for various operating conditions. It is clear from these observations that a considerable speed range could not be achieved with this topology. The time taken to attain steady state is found to increase with decrease in modulation index.

Table 3.10: SPWM Inverter based Constant V/f Control(with auxiliary winding capacitance) dc bus capacitor= $22mF$: Results

Modulating sine amp.(V)	Modulating sine freq.(Hz)	Speed (rpm)	Torque (Nm)	input current (rms)(A)	dc bus current (avg)(A)	Active Power input(W)	Settling Time(s)
9.8	49	1451	1.26	9	1.3	400	0.4
9	45	1337	1.07	7	0.95	300	0.4
8	40	1194	0.9	5	0.6	200	0.38
7	35	1041	0.6	3.8	0.4	145	0.37
6	30	897	0.5	3	0.28	100	0.36
5	25	745	0.3	2.4	0.21	70	0.36
4	20	592	0.2	2	0.18	40	0.35
3	15	449	0.1	1.7	0.16	30	0.4

Table 3.10 shows the steady state values of speed attained by the motor, electromagnetic torque, input line current drawn, dc bus current, active power input and the settling time to attain steady state for various operating conditions. It is clear from these observations that a considerable speed range could be achieved with this topology. It is also found that the steady state of speed is attained in almost the same time for all the operating conditions.

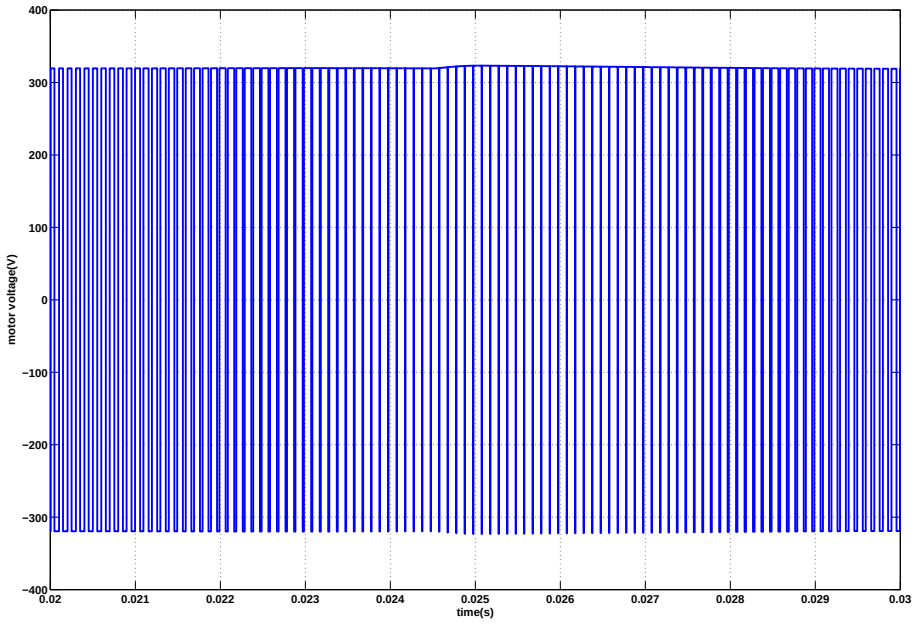

Figure 3.60: Applied Stator Voltage wrt time

Figure 3.60 gives the applied voltage across the motor terminals when connected across the inverter legs. The dc bus capacitance used here is 22 mF. The pulse amplitudes are found to be almost fixed with time as the dc bus ripple is very minimum.

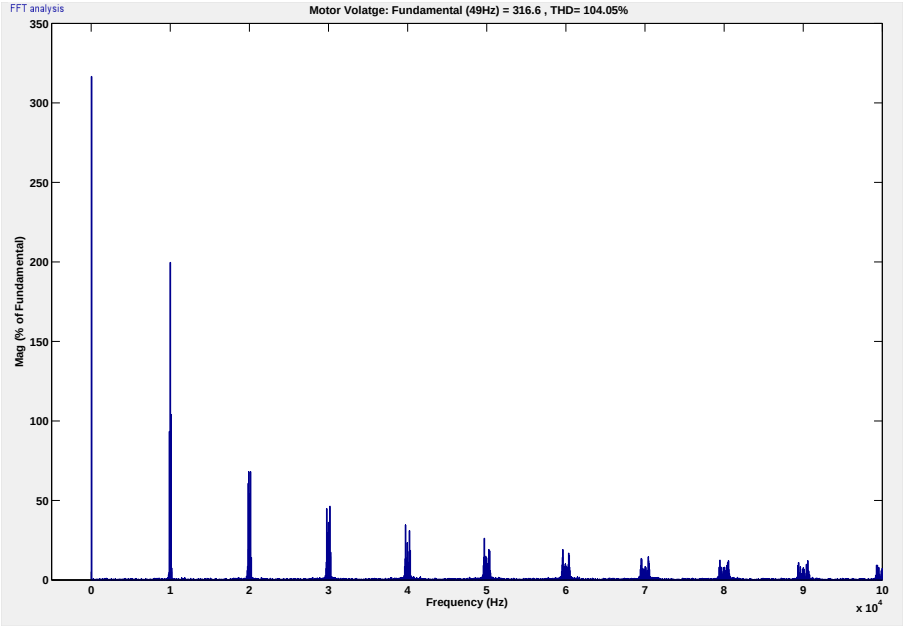

Figure 3.61: harmonic spectrum analysis: Motor Input Voltage

Figure 3.61 shows the harmonic profile of the motor voltage. The $\%$ THD is found to be large with a value of 104%. The fundamental motor voltage is found to have a peak of 317 V. The harmonic voltage at 10 kHz is found to be 66% of fundamental. They can overheat the machine due to the effects of harmonic currents. This is because of additional rotating magnetic fields in the motor. It can produce high frequency currents in rotor circuits.

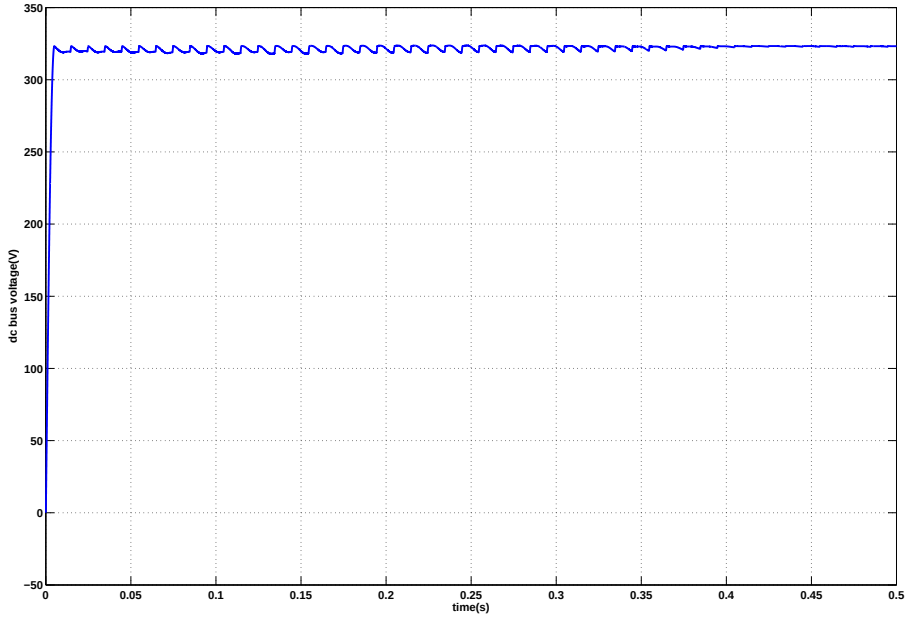

Figure 3.62: DC Bus Voltage wrt time

Figure 3.62 shows the dc bus voltage. Here, the dc bus capacitance used is 22mF. The ripple is found to be very less here compared to the earlier case when a dc bus capacitance of 0.5mF was used.

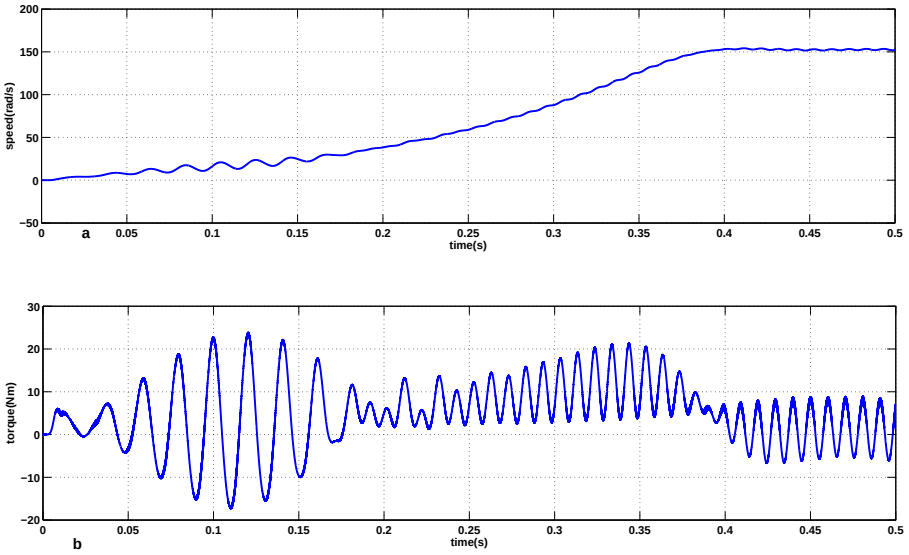

Figure 3.63: Speed and torque variation wrt time

Figure 3.63 shows the speed and electromagnetic torque variation w.r.t time.The speed is found to settle at 152 rad/s at 0.4s. The speed ripple at steady state is observed to be very minimum. The torque ripple observed is due to the imbalance in stator currents.

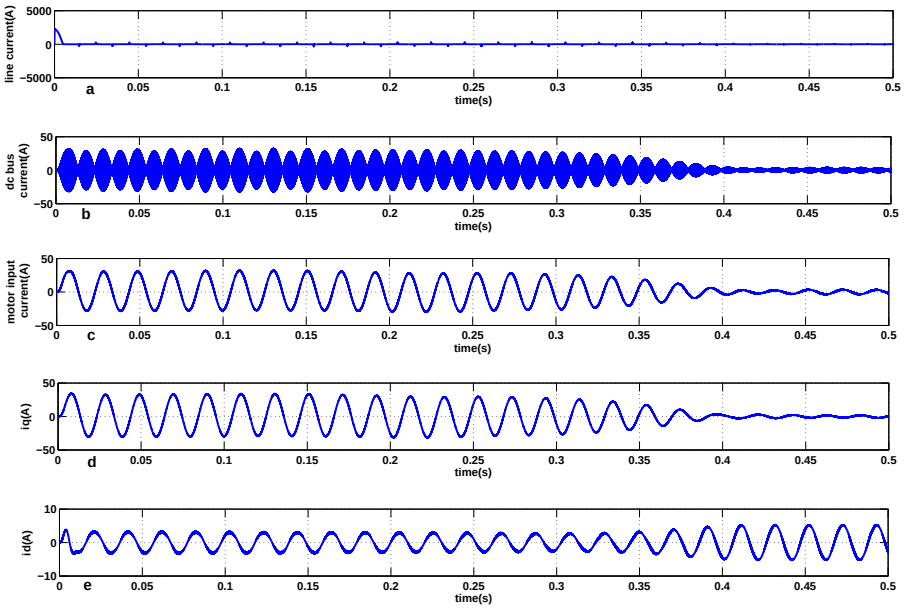

Figure 3.64: Current Waveforms: (a)Line Current (b)DC bus current (c) Motor current (d)Main Winding current (e)Auxiliary Winding Current

Figure 3.64 shows the various current waveforms w.r.t time. The inrush current phenomenon of the motor is evident from the motor current and the line current waveforms. The stator current imbalance is easily observable which leads to torque ripple. The auxiliary winding current in transient state is found to be sinusoidal(it is found to be distorted for dc capacitor of 0.5 mF).

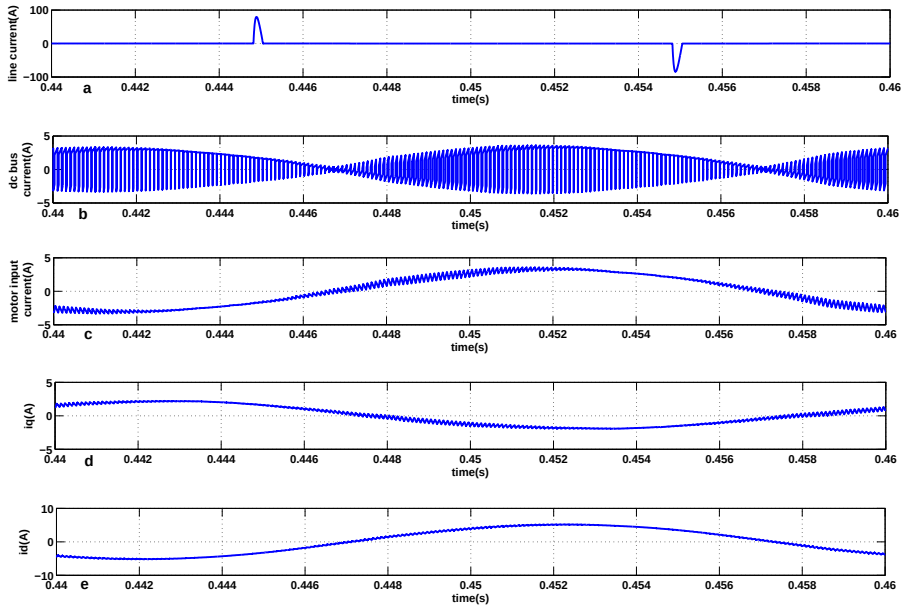

Figure 3.65: Current Waveforms: (a)Line Current (b)DC bus current (c) Motor current (d)Main Winding current (e)Auxiliary Winding Current

Figure 3.65 shows the current waveforms for a cycle at steady state. The input line current peaks are less in magnitude because of the very minimum dc bus ripple. The distortions in motor input current, main and auxiliary winding currents are not observed here as in the case when dc capacitor of 0.5 mF was used.

The harmonic spectrum of the current waveforms are also studied. The results obtained are given below.

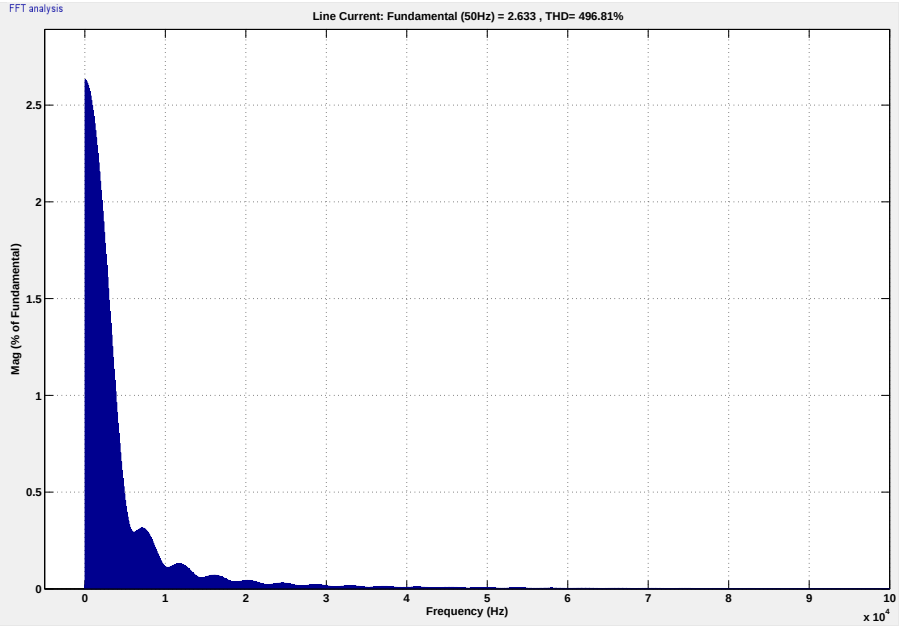

Figure 3.66: Current Harmonic Spectrum: Line Current

Figure 3.66 shows the harmonic profile of the input line current from the mains. The $\%$ THD is found to be very large of the value of 497%. The fundamental line current is found to have a peak of 2.63 A. The THD in line current is found to be very high as compared to the case when a dc capacitor of 0.5 mF is used.

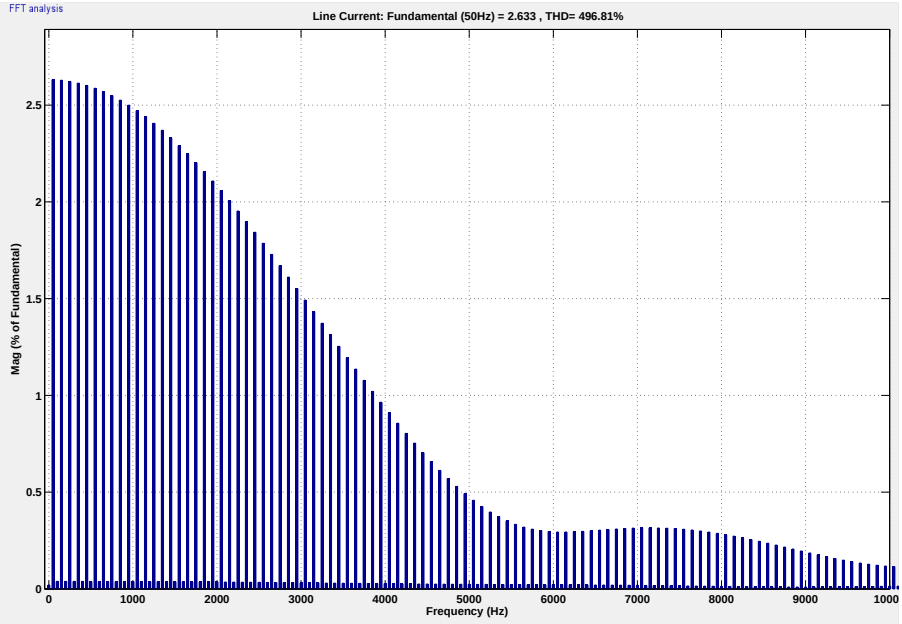

Figure 3.67: Current Harmonic Spectrum: Line Current

Figure 3.67 shows the harmonic profile of the input line current from the mains on an expanded scale.

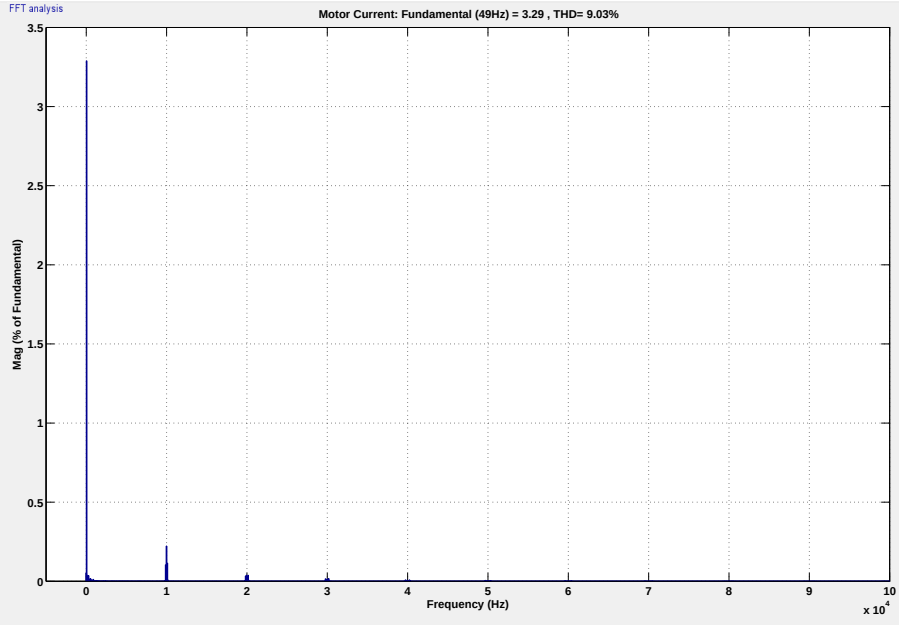

Figure 3.68: Current Harmonic Spectrum: Total Motor current

Figure 3.68 shows the harmonic profile of the total current drawn by the motor. The $\%$ THD is found to be 9.1%. The fundamental motor input current is found to have a peak of 3.3 A. The THD here is lesser as compared to the case when a dc capacitor of 0.5 mF is used.

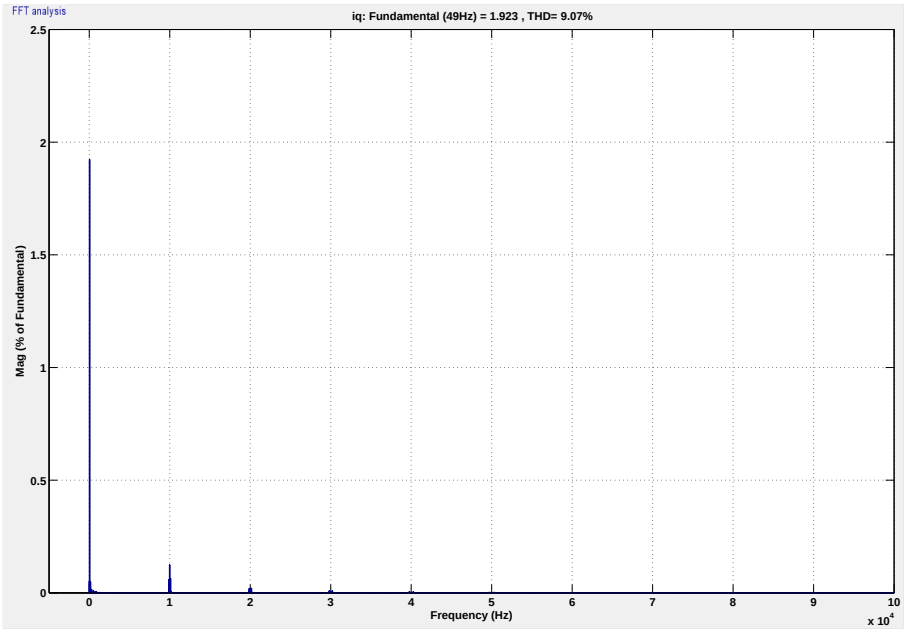

Figure 3.69: Current Harmonic Spectrum: Main Winding current

Figure 3.69 shows the harmonic profile of the main winding current of the motor. The $\%$ THD is found to be 9%. The fundamental main winding current is found to have a peak of 1.9 A. The THD here is lesser as compared to the case when a dc capacitor of 0.5 mF is used.

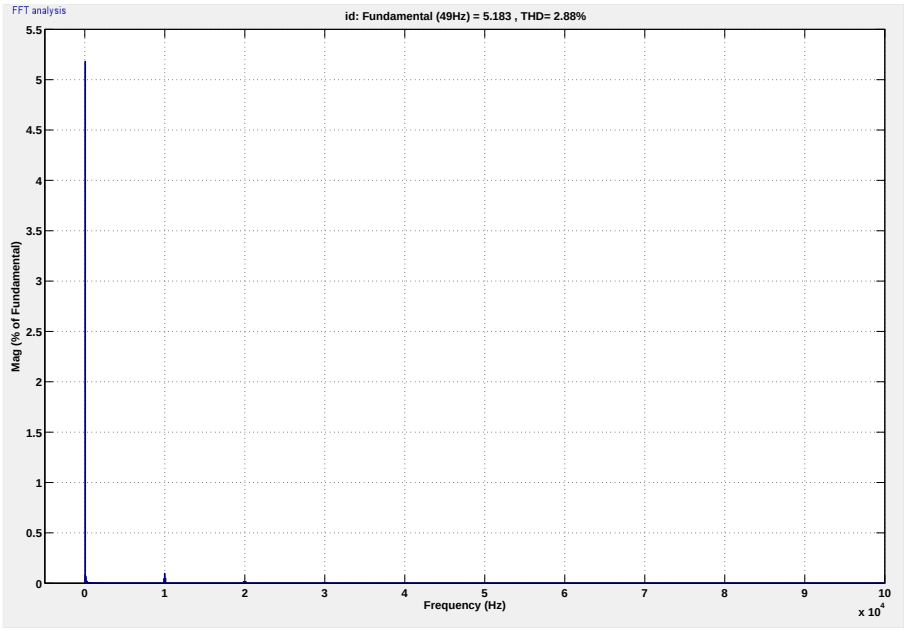

Figure 3.70: Current Harmonic Spectrum: Auxiliary Winding Current

Figure 3.70 shows the harmonic profile of the auxiliary winding current of the motor. The $\%$ THD is found to be 2.88%. The fundamental auxiliary winding current is found to have a peak of 5.18 A. The THD here is lesser as compared to the case when a dc

capacitor of 0.5 mF was used.

3.7 Comparison of topologies

- The Bidirectional Switch Stator Voltage Controller Scheme and SPWM Inverter based Stator Voltage Control(with and without auxiliary capacitance) are basically stator voltage control schemes. The major drawback of voltage control method in SPIM is the limited speed range achievable. This is very evident from the observation tables of these schemes.

- The constant V/f control scheme gives a better speed range and the steady state is attained in a very short duration compared to the stator voltage control schemes.

- There is a speed ripple observed at lower frequencies of modulating sine wave for SPWM based constant volts per hertz control when the motor is run as 2-phase induction motor without auxiliary winding capacitor, when there is a ripple in dc bus voltage(for C=$0.5mF$). When the auxiliary winding capacitor is connected, then the speed ripple is not observed much.

- The active power input drawn at rated speed for the scheme where the auxiliary winding capacitor is connected is almost twice as compared to the topologies where the motor is run without the auxiliary winding capacitor.

The simulation study of the two constant V/f control schemes(with and without auxiliary winding capacitor) have given better results with regards to the speed control. There is definitely an improvised linearity in the speed range achievable. The hardware implementation of these two schemes have to be carried out.

CHAPTER 4

HARDWARE RESULTS

In this chapter, the various hardware results obtained for the project are given. First, the hardware results obtained for various contemporary fan speed regulators are given. The speed characteristics of various regulators are plotted to compare the effectiveness of speed control of the regulators.

The motor voltage waveform and motor current waveform variation w.r.t regulator knob position of these regulators are studied. The harmonic analysis of these waveforms are also studied.

The hardware realization of the constant volts per hertz scheme is explained. The driver circuit realization is also explained.

4.1 Fan Motor directly connected to mains

The ceiling fan motor is directly connected to the 230 V, 50 Hz mains supply and the motor voltage and current waveforms are recorded.

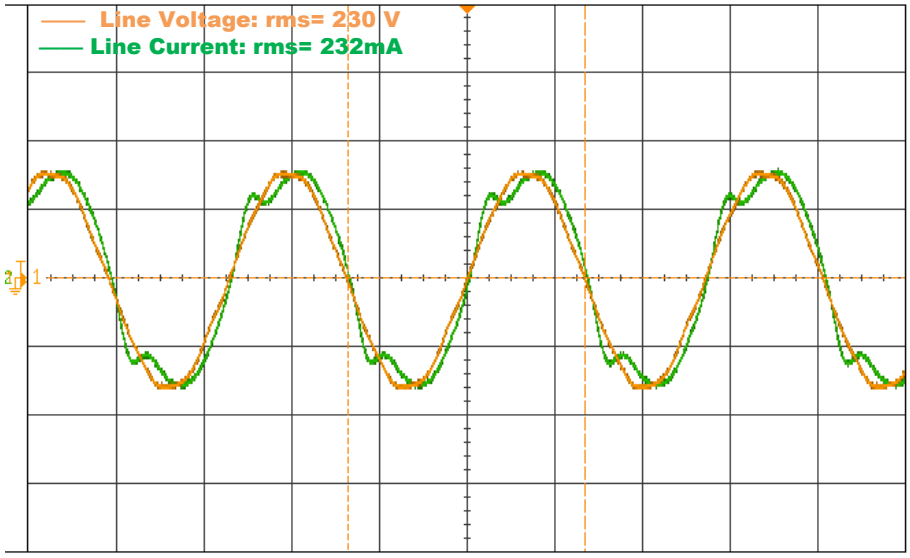

Figure 4.1: Motor Connected to the mains: Line Voltage and Line Current

Figure 4.1 shows the line voltage and the line current when the fan motor is directly connected to the mains supply. It is found that the phase difference between motor voltage and current is 0°. Also, the current waveform is found to saturate. The fan is found to be operating under saturation.

4.2 Speed Control by Contemporary Fan Regulators

The speed variation of the fan for various speed positions using rheostatic regulators and electronic regulators have been found out. This is done to analyze the non linearity in speed response with respect to the regulator knob positions for various regulators.

4.2.1 Rheostatic Regulator

The speed variation of two fans employing rheostatic speed regulators have been found out.

Table 4.1: Rheostatic Regulator: Speed Variation

FAN 1		FAN 2	
Knob Position	Speed(rpm)	Knob Position	Speed(rpm)
1	115	1	141
2	157	2	186
3	194	3	214
4	244	4	271
5	289	5	305

Table 4.1 shows the speed variation w.r.t knob position of two fans employing rheostatic regulator.

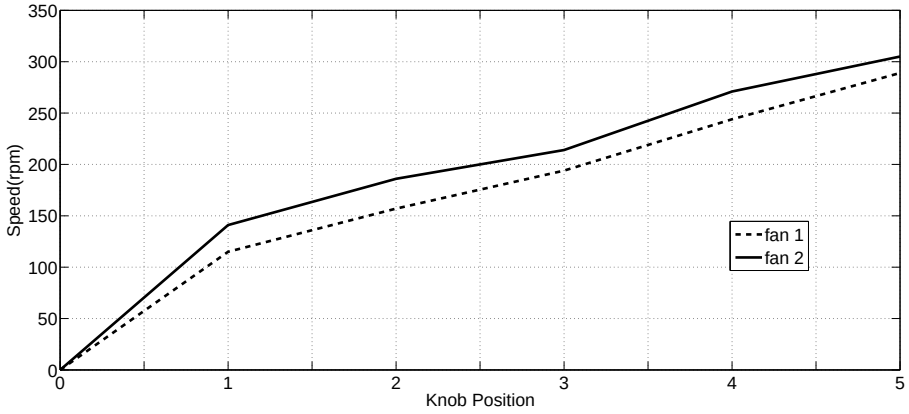

Figure 4.2: Rheostatic Regulator: Speed vs knob position plot

Figure 4.2 shows the speed variation w.r.t knob position of two fans employing rheostatic regulator. The speed response characteristic is found to be good in this type of regulators. It is found to give more or less a linear speed response characteristics.

4.2.2 Phase Angle Controlled(TRIAC) Regulators

The speed variation of a fan employing TRIAC fan speed regulator has been found out.

Table 4.2: TRIAC Regulator: Speed Variation

Angle of Rotation of Regulator Knob(°)	Speed (rpm)
45	26
90	51
135	160
180	250
225	284
270	284
315	284

Table 4.2 shows the speed variation w.r.t angular knob position of a fan employing TRIAC regulator.

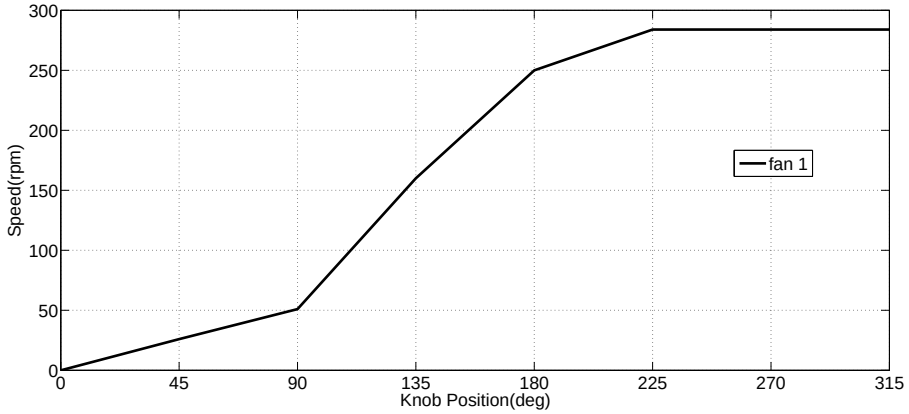

Figure 4.3: TRIAC Regulator: Speed vs knob position plot

Figure 4.3 shows the speed variation w.r.t knob position of a fan employing TRIAC regulator. It is found that the useful range of operation is between 90° and 225°.

4.2.3 Capacitive Regulator

The speed variation of three fans employing 4-step capacitive fan speed regulators have been found out.

Table 4.3: 4-Step Capacitive Regulator: Speed Variation

FAN 1		FAN 2		FAN 3	
Knob Position	Speed(rpm)	Knob Position	Speed(rpm)	Knob Position	Speed(rpm)
1	121	1	97	1	94
2	237	2	198	2	112
3	285	3	250	3	238
4	315	4	314	4	333

Table 4.3 shows the speed variation w.r.t knob position of three fans employing 4-step capacitive regulator.

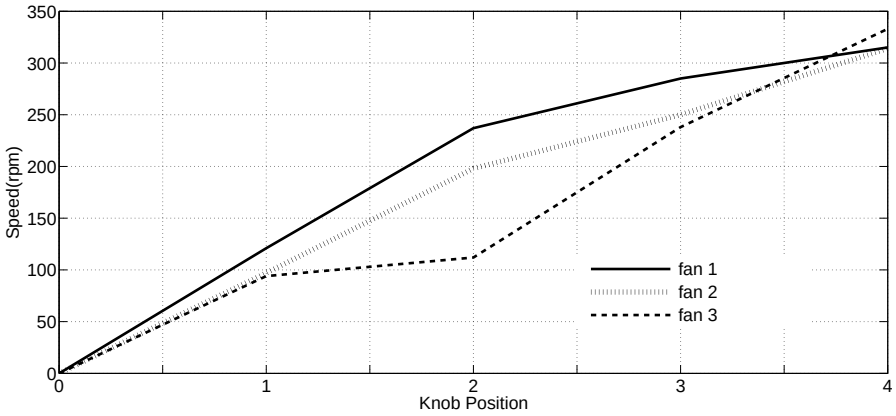

Figure 4.4: 4-step Capacitive Regulator: Speed vs knob position plot

Figure 4.4 shows the speed variation w.r.t knob position of three fans employing 4-step capacitive regulator. Fan 2 capacitive regulator is found to give the most linear speed response among the three 4-step capacitor regulators.
The speed response characteristics is found to be the best in capacitive regulators among the three types of regulators discussed, in terms of linearity in speed response. .

The speed variation of two fans employing 5-step capacitive fan speed regulators has been found out.

Table 4.4: 5-Step Capacitive Regulator: Speed Variation

FAN 1		FAN 2	
Knob Position	Speed(rpm)	Knob Position	Speed(rpm)
1	50	1	74
2	95	2	140
3	111	3	180
4	133	4	210
5	290	5	300

Table 4.4 shows the speed variation w.r.t knob position of two fans employing 5-step capacitive regulators.

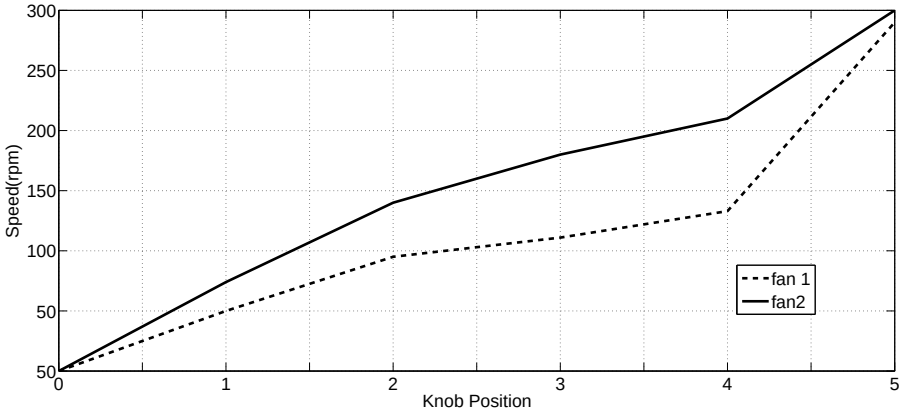

Figure 4.5: 5-step Capacitive Regulator: Speed vs knob position plot

Figure 4.5 shows the speed variation w.r.t knob position of two fans employing 5-step capacitive regulator. The speed response characteristic of fan 2 is more linear compared to fan1.

4.3 Fan Characteristics using Contemporary Fan Regulators

The fan motor alone, without the blades are run from $230V, 50Hz$ mains supply employing TRIAC regulator as well as 4-step capacitive regulator. The various results obtained here are tabulated in tables 4.5 and 4.6.

As the fan is run without the blades (no air friction), the fan motor is under no load. As the regulator knob position is changed, the applied motor voltage is changed. When the motor voltage is changed, the torque slip characteristics of motor and the load troque characteristics(which is 0 here) always intersect at (slip=0) point. Hence the motor speed is found to be fixed at 420 rpm at every regulator knob positions.

4.3.1 TRIAC Regulator: Hardware Results

The hardware results obtained when the fan is connected to the mains supply through a TRIAC regulator are given in the following pages. The results were obtained at various angular positions of the regulator knob.

Table 4.5: TRIAC Regulator: Hardware Results

Regulator Angle(°)	Motor rms Voltage(V)	Motor rms current(A)	Motor Voltage THD(%)	Motor current THD(%)	Motor power(W)	Line power(W)	pf of operation
45	134	0.13	65.87	86.9	10.5	12.75	0.42
90	147.4	0.138	60.7	84	12.5	16	0.49
135	164	0.166	50.3	75.6	21	22	0.57
180	182	0.18	40.3	64.7	25.5	30	0.7
225	204	0.21	31.5	50	36	39.5	0.83
270	218	0.22	21.4	31	45	49	0.96
315	229.5	0.23	6.9	12.9	52	52.5	0.98

Table 4.5 shows the motor rms voltage, motor rms current,motor voltage THD, motor current THD, motor input power, line power and power factor for different knob position of a TRIAC regulator.

For lower knob position angles, the THD in the motor voltage as well as the motor current is found to be very high which is not preferred. As the knob position angle increases, these values are found to come down. The power factor of operation is also found to be higher at higher knob position angles. The regulator loss is also very less

The motor voltage and line current waveforms for various knob angle positions are also shown.

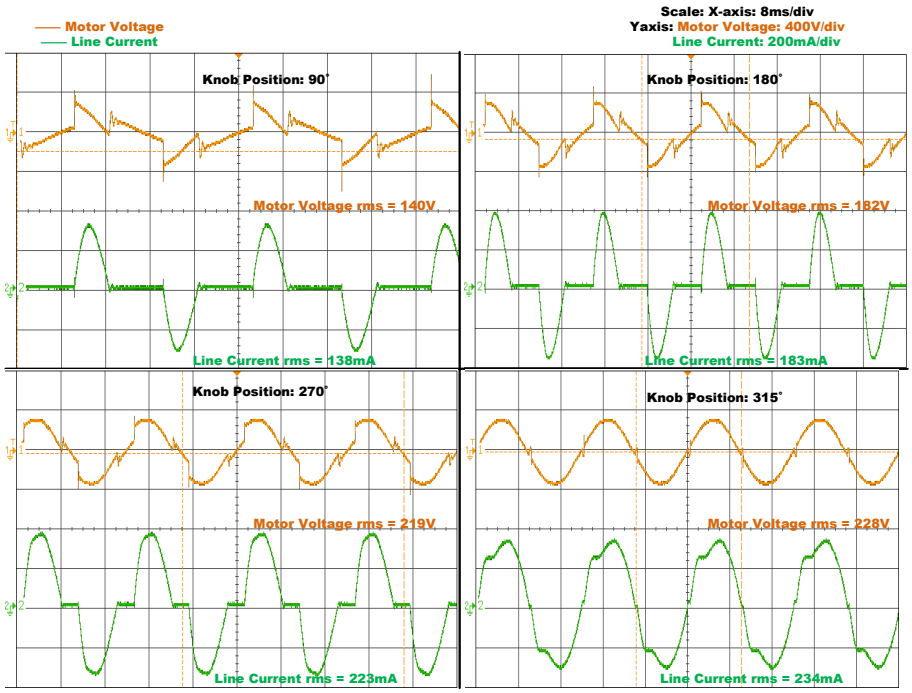

Figure 4.6: TRIAC regulator: Line Current and Motor Voltage Waveforms

Figure 4.6 shows the line current and motor voltage waveforms for different knob position of a TRIAC regulator. It can be clearly seen that the motor voltage at lower angular positions are highly distorted(and hence high THD)

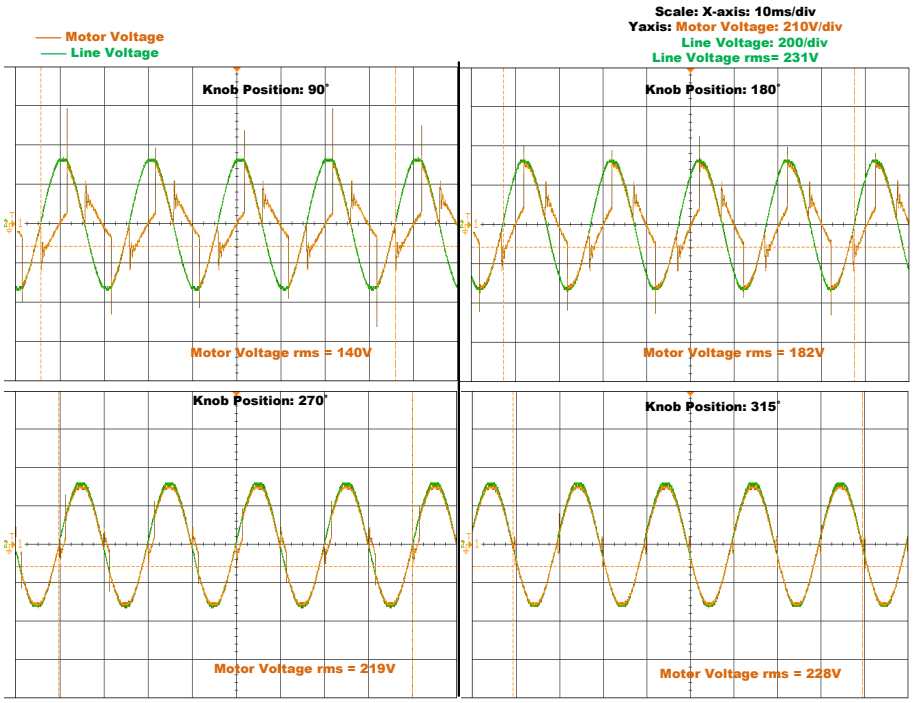

Figure 4.7: TRIAC regulator: Line Voltage and Motor Voltage Waveforms

Figure 4.7 shows the line voltage and motor voltage waveforms for different knob posi-

tion of a TRIAC regulator. At the maximum knob position angle, the entire line voltage is fed to the motor as it is seen from the fourth graph.

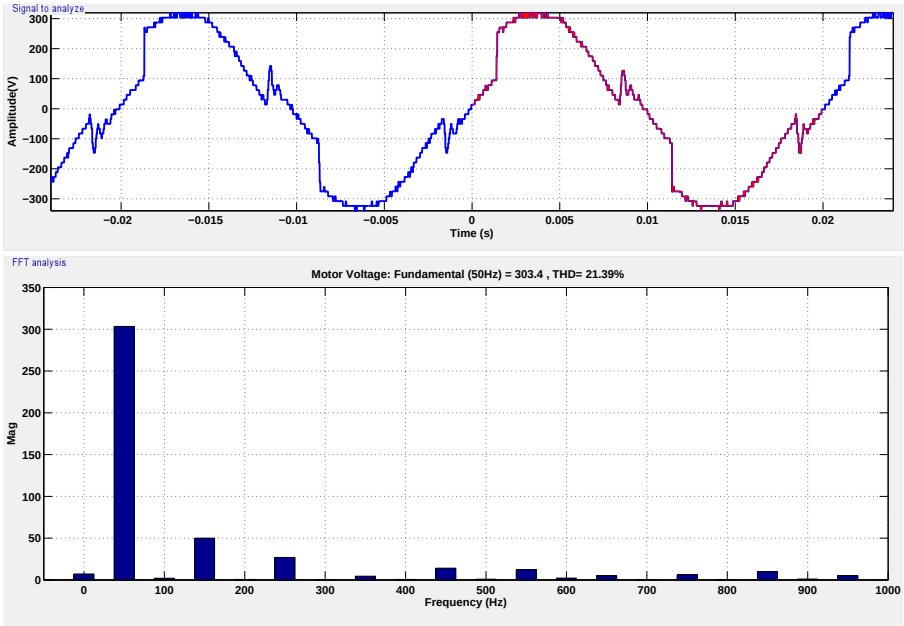

Figure 4.8: TRIAC regulator: Motor Voltage Harmonic spectrum(Knob Position= $270°$)

Figure 4.8 shows the harmonic spectrum of the motor input voltage for a knob position of $270°$ of a TRIAC regulator. The $\%$ THD is found to be 21.4%. The fundamental motor voltage is found to have a peak of 303 V. The third harmonic is found to have a peak value of 50 V which is $\frac{1}{6}^{th}$ of fundamental. The motor voltage harmonics increases the motor copper loss. Also, at lower knob position angles, the THD in motor input voltage is high. This is the bad for the motor as harmonic losses will be very high which causes heating in the motor.

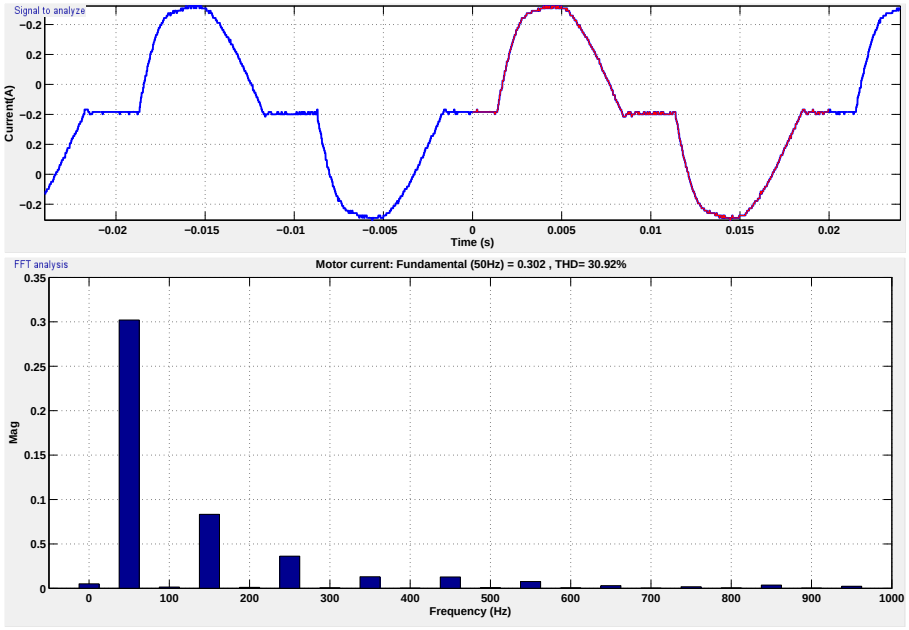

Figure 4.9: TRIAC regulator: Motor Current Harmonic spectrum(Knob Position= $270°$

Figure 4.9 shows the harmonic spectrum of the motor current for a knob position of $270°$ of a TRIAC regulator. The $\%$ THD is found to be 31%. The fundamental motor current is found to have a peak of 0.3 A. The third harmonic is found to have a peak of 0.08 A which is around $\frac{1}{3}^{rd}$ of the fundamental. This not only reduce motor efficiency but also increases line current distortions.

4.3.2 4-step Capacitive Regulator: Hardware Results

Table 4.6: 4-step Capacitive Regulator: Hardware Results

Regulator Position	Motor rms Voltage(V)	Motor rms current(A)	Motor Voltage THD(%)	Motor current THD(%)	Motor power(W)	Line power(W)	pf of operation
1	126	0.11	5.76	14.08	14.1	14.6	0.56
2	161.4	0.1468	5.6	19.7	24	24.5	0.72
3	200	0.195	4.3	23.25	38.7	39.1	0.86
4	230	0.226	1.82	17.5	50	50.35	0.97

Table 4.6 shows the motor rms voltage, motor rms current,motor voltage THD, motor current THD, motor input power, line power and power factor for different knob position of a 4-step Capacitive Regulator.

The THD in the motor voltage as well as the motor current is found to be lesser as compared to the TRIAC regulator. As the motor voltage here is basically lower amplitude sine waves for various knob positions, the motor voltage harmonic is found to be less. The power factor of operation is also found to be higher at higher knob positions.

The motor voltage and line current waveforms for various knob positions are also shown.

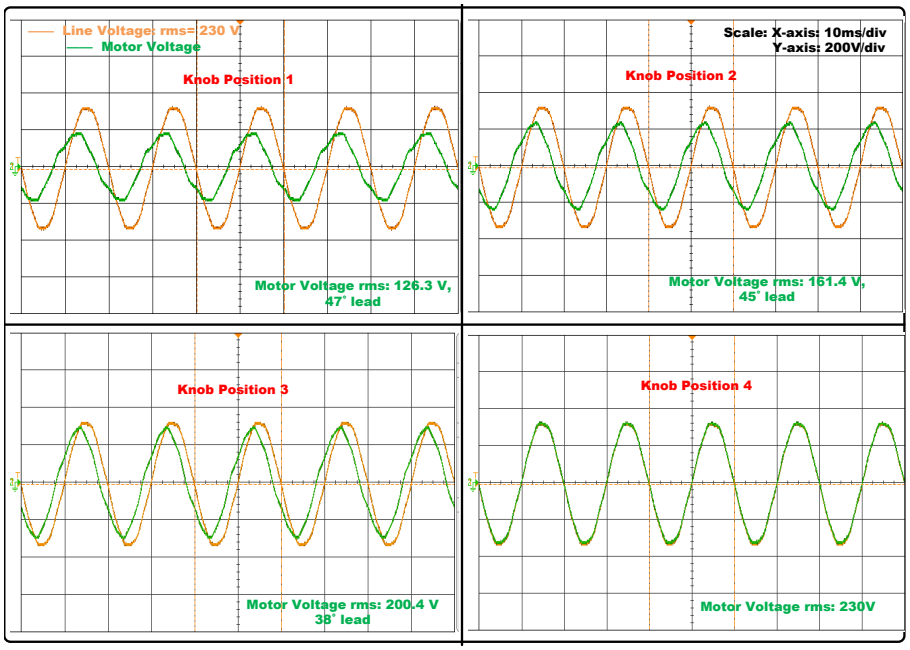

Figure 4.10: 4-step Capacitive Regulator: Line Voltage and Motor Voltage Waveforms

Figure 4.10 shows the line voltage and motor voltage waveforms for different knob position of a 4-step Capacitive regulator. The motor voltage is found to lead the line voltage. This is due to the capacitor in the regulator. This is because from figure 4.1, it is clear that there is no phase lag between motor voltage and motor current of the fan. At knob position 4, the entire line voltage appears across the motor terminals without any phase delay between line and motor voltages. In this position, the regulator knob directly shorts the supply to the motor terminals.

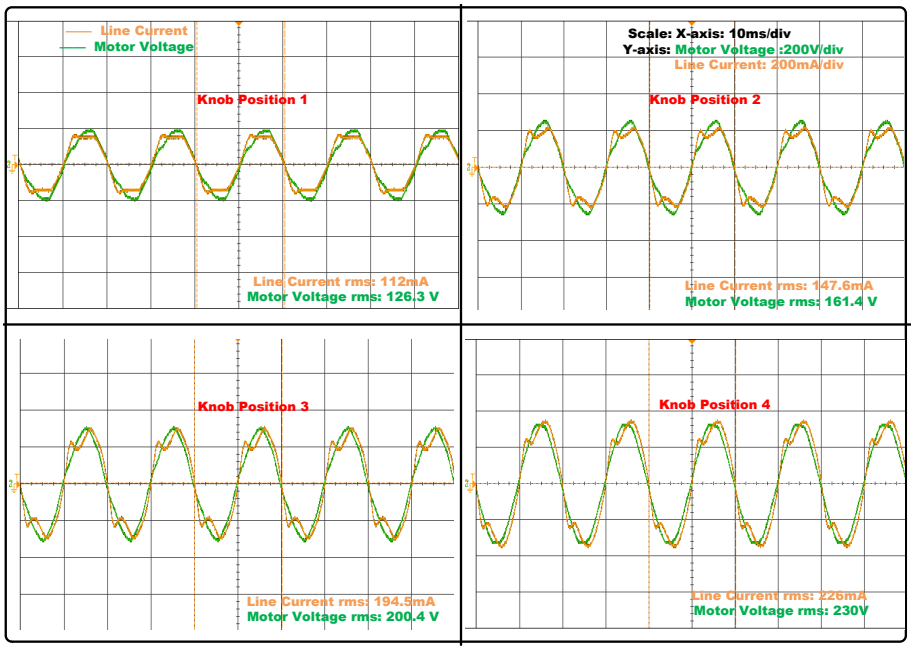

Figure 4.11: 4-step Capacitive Regulator: Line Current and Motor Voltage Waveforms

Figure 4.11 shows the line current and motor voltage waveforms for different knob position of a 4-step Capacitive regulator. Line current is found to be in phase with the motor voltage.

It can be observed that the line current leads the line voltage. This is due to the presence of capacitors inside the capacitive speed regulator as there is no phase shift between motor voltage and motor current waveforms.

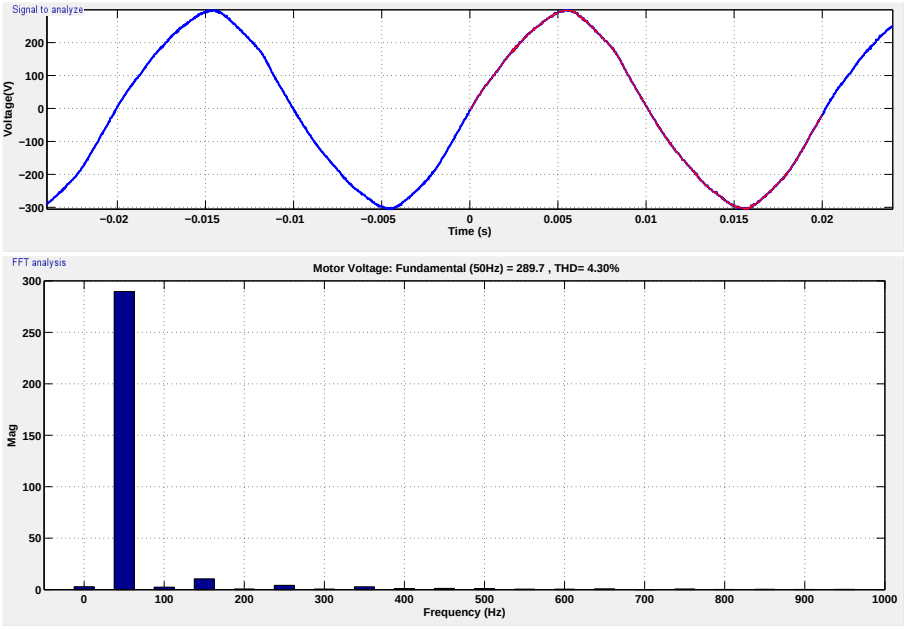

Figure 4.12: 4-step Capacitive Regulator: Motor Voltage Harmonic spectrum(Knob Position= 3

Figure 4.12 shows the harmonic spectrum of the motor voltage for a knob position of 3 of a 4-step Capacitive regulator. The $\%$ THD is found to be 4.3%. The fundamental motor voltage is found to have a peak of 290 V. The third harmonic is found to be of comparatively lesser magnitude, i.e. 15 V.

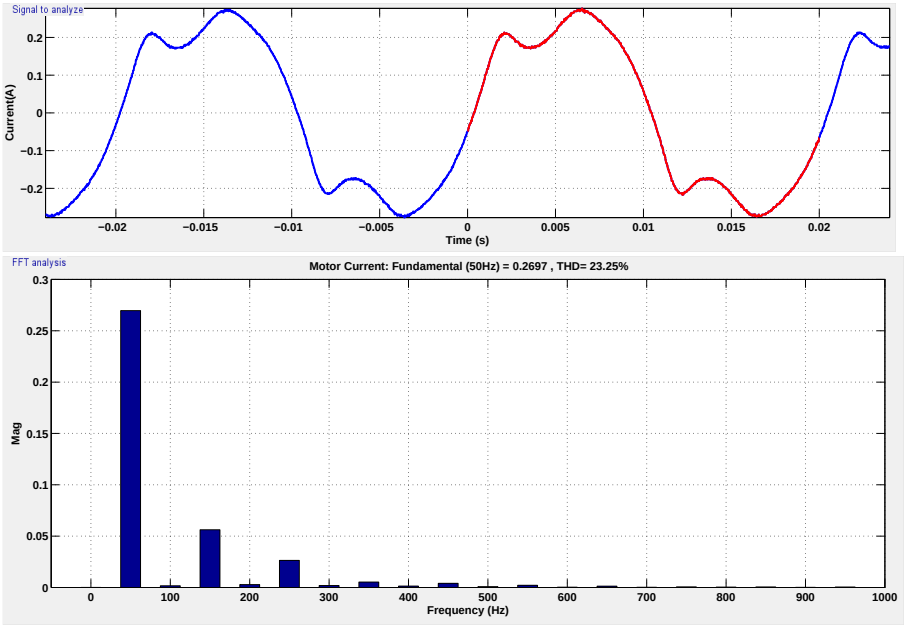

Figure 4.13: 4-step Capacitive Regulator: Motor Current Harmonic spectrum(Knob Position= 3)

Figure 4.13 shows the harmonic spectrum of the motor current for a knob position of 3 of a 4-step Capacitive regulator. The $\%$ THD is found to be 23.25%. The fundamental motor current is found to have a peak of $0.27A$. The third harmonic is of magnitude $\frac{1}{5}^{th}$ of fundamental peak. The performance is better compared to TRIAC regulator. The current THD is partly due to the saturation inside the fan.

4.4 PCB Design

The PCB design for the constant Volts/Hertz control scheme(with and without auxiliary winding capacitor) was done in Diptrace software. The layout of PCB is as given in figure 4.14

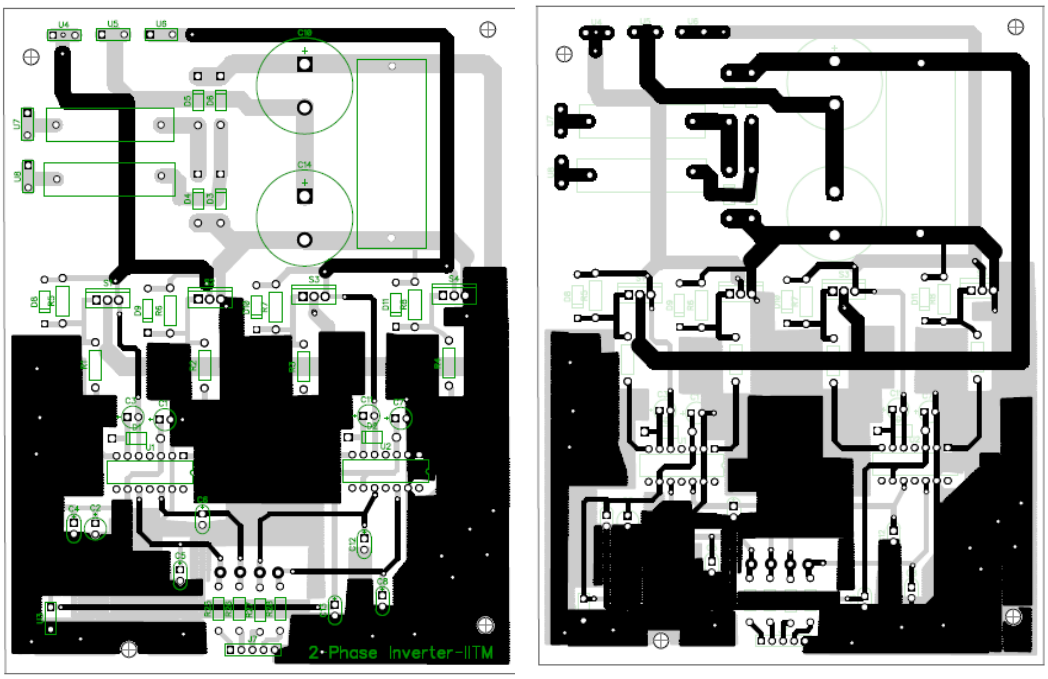

Figure 4.14: (a)PCB-top surface (b) PCB-bottom surface

4.5 Hardware Components

Diode Bridge Rectifier

The diode bridge rectifier was implemented using IN5408 diodes. The rating of the diode is:

Maximum RMS Voltage=700 V,

Maximum Average Forward Rectified Current=3 A

Snubber capacitor

The snubber capacitor used for the protection of switch is a 1000 V, 1 μF, polypropylene capacitor.

DC Bus Capacitor Selection

The fan load is approximated as a resistive load of $100W$. The allowable ripple in the bus voltage is 10%. So, the average voltage across the load is $0.95 * V_p$, where V_p is the

sine wave peak . Equating the power across the load,

$$\frac{(0.95 * V_p)^2}{R} = 100 \tag{4.1}$$

$$Here, V_p = 230 * \sqrt{2} \tag{4.2}$$

$$= 325.26 \tag{4.3}$$

$$\Rightarrow R = 954.8\Omega \tag{4.4}$$

Capacitor discharges from V_p to $0.9V_p$ in a time of $\frac{T}{2}$ approximately.
At $t = \frac{T}{2}$, capacitor voltage $V_c = 0.9 * V_p$

$$0.9 * V_p = V_p * [e^{-\frac{T}{2RC}}] \tag{4.5}$$

From this, we get C=99 μF.
A bus capacitance of $165\mu F$ is used in the PCB. Two $330\mu F$ capacitors are put in series as dc bus capacitor.

Switching Devices

The switching devices used for inverter are IGBT devices. The device used in the circuitry is **STGF7NC60HD**.The device ratings are V_{CES}=600V, I_C=6 A, freq= 70 kHz. The device has an inbuilt anti-parallel diode.

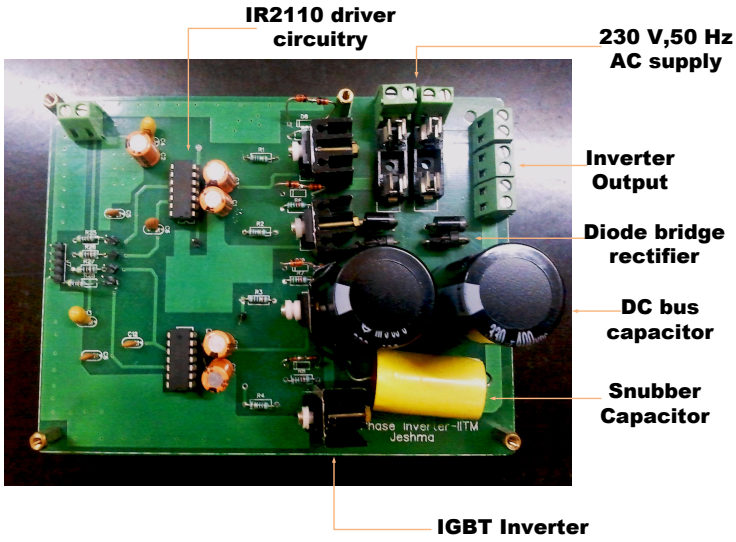

Figure 4.15: Hardware Implementation: PCB Board

4.6 Driver Circuit

The driver circuit for the IGBT switches was implemented in analog domain. The switching frequency for the sine PWM employed was 7.5 kHz. The triangular wave generated at 7.5 kHz was used to compare with the sine wave given from a signal generator to generate sine PWM waves. The triangular wave generator used was implemented as shown in figure 4.16. The integrator used in the circuit was LM318 opamp IC. The comparator used was LM339 comparator IC.

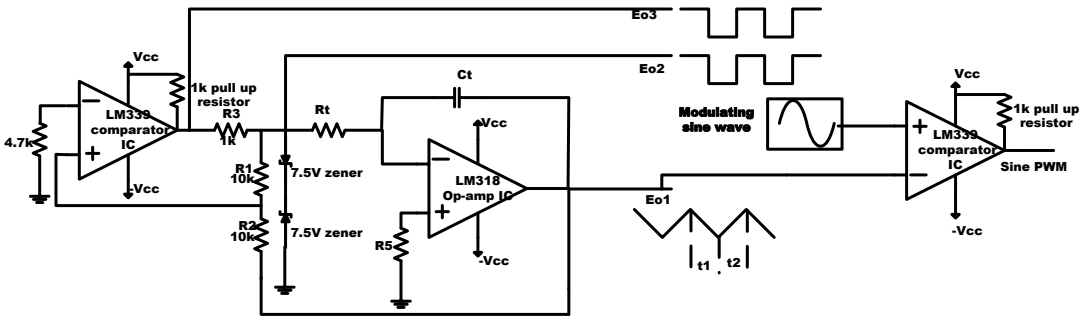

Figure 4.16: Triangular Wave generator

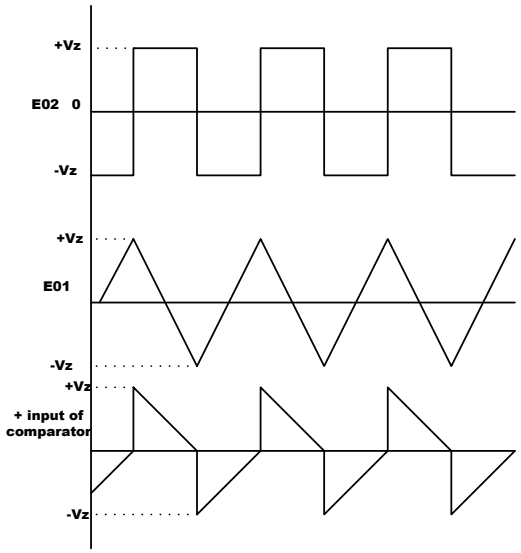

Figure 4.17: Triangular Wave generator: Waveforms

Assume that the output of the comparator has switched to high state and E_{02} is at V_z which is the input to the integrator. The integrator which follows integrates this voltage at a rate of $\frac{V_z}{R_t C_t} V/s$. This makes the voltage E_{01} ramp negative. The comparator IC

compares $E_{01} + E_{02}$ against ground reference on its negative input. When E_{01} crosses $-V_z$, it becomes equal and opposite to E_{02}. The voltage at positive input of comparator crosses zero and comparator changes state rapidly, aided by positive feedback. E_{02} becomes $-V_z$ now and integrator starts integrating positive towards $+V_z$. When E_{01} crosses $+V_z$, comparator switches back to high state and this cycle repeats.

$$\frac{dE_{01}}{dt} = \frac{V_z}{R_t C_t} \tag{4.6}$$

$$Here, E_{01peak} = \pm V_z * \frac{R_2}{R_1} \tag{4.7}$$

$$\Rightarrow t_1 = 2 * V_z * \frac{R_2 R_t C_t}{R_1 V_z} \tag{4.8}$$

$$\tag{4.9}$$

A zener diode of breakdown voltage 7.5 V was used and $R_1 = R_2 = 10k\Omega$. So, the triangular output generated is $15V$ peak-to-peak.

So, $t_1 = 2 * R_t * C_t$

Similarly, $t_2 = 2 * R_t * C_t$

Triangular wave time period, $T = 4 * R_t * C_t$

Triangular wave frequency, $f = \frac{1}{4 * R_t * C_t}$

A triangular wave of frequency $7.5kHz$ was generated using this circuit. The components used are R_t=3.3 kΩ, C_t= $0.01\mu F$.

The triangular wave generated is used to generate sine PWM wave by comparing it with a sine wave of required frequency. The comparator used for this is LM 339. The complimentary sine PWM wave is also generated.

4.6.1 Sine to Cosine Wave Converter

To implement constant volts per hertz scheme, a frequency independant sine wave to cosine wave converter to get 90° phase shifted modulating waves, is required. This was implemented in analog domain using a RC network arranged as shown in figure 4.18

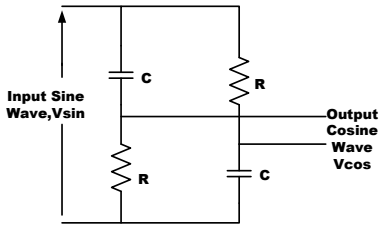

Figure 4.18: Sine wave to Cosine Converter

The transfer function of this network is

$$V_{cos} = V_{sin} * \frac{RCj\omega - 1}{RCj\omega + 1} \tag{4.10}$$

In this transfer function the phase angle shift of output from input is, $\phi = -2tan^{-1}(\omega RC)$. The phase shifted needed for all the frequencies operated in constant volts per hertz scheme is $90°(\omega RC = 1)$. The value of C is fixed at $0.1\mu F$. For this capacitor, the value of resistor required to give a phase shift of $90°$ is calculated for all the frequencies of operation. Two pots of suitable value are used as R in the circuit and varied according to the frequency of operation to get the required phase shift of $90°$. The value of resistance for different frequencies is tabulated in table 4.7

Table 4.7: Resistor Values for different Frequencies

Frequency(Hz)	R($k\Omega$)
50	31.8
40	39.8
30	53
20	79.6
10	159

4.6.2 Protection of the circuit

The IGBT switches used in the inverter legs will have a definite rise and fall times. Because of this, the two switches in the same leg will be on at the same time for a brief time which shorts the dc bus. This causes a huge current flow through the switches

which will destroy the switches permanently. So, a blanking period should be provided for the switches on the same leg so that both switches are off during the turn-on and turn-off periods of the switches. The blanking period provided is $2\mu s$.

In figure 4.19, A and B are the complimentary sine PWM waves generated from the comparator. A' and B' are the delay signals to be generated to drive the top and bottom switches of the inverter leg. By giving A' and B' as the gate pulses to the inverter module, the circuit can be protected.

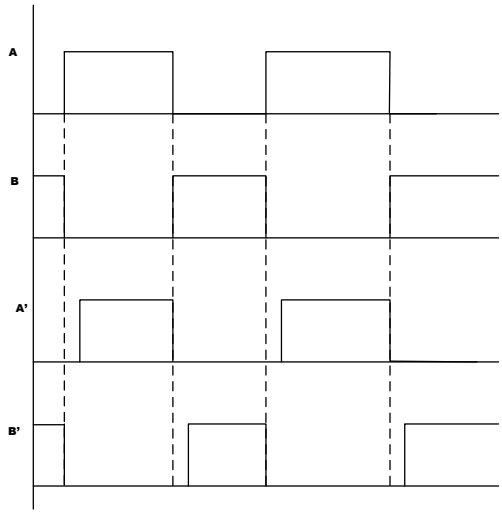

Figure 4.19: Gate pulses with blanking period

For this, a delay circuit was built in analog domain using $74LS123$ retriggerable monostable multi-vibrator and $74LS86$ XOR gate. $74LS123$ detects rising edge and generates impulse Q at rising edge for the required delay duration. The XOR function of original signal and impulse generated is done using $74LS86$. This generates delay in rising edge. Similarly, for the complimentary signal, we can give same operation.

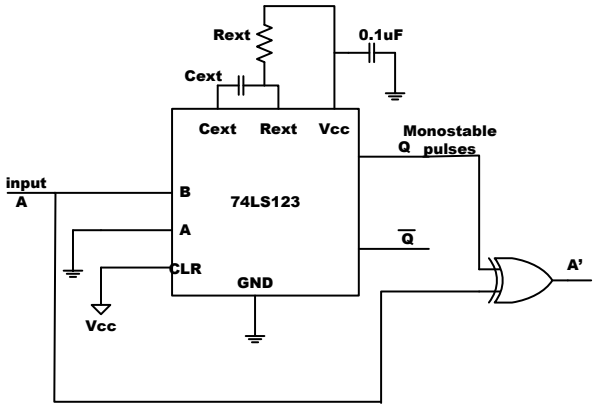

Figure 4.20: Delay Circuit

The delay period can be calculated by the formula:

$t_w = K_w * C_{ext} * R_t$

where, R_t is in kΩ, C_{ext} is in pF and t_w is in ns.

For $C \leq 1\mu F$,K_w=0.55.

For t_w= 2 μs, C_{ext}=100 pF, R_t=40$k\Omega$

4.7 Driver circuit:Hardware Results

The driver circuit was implemented in hardware using the circuit described above. The triangular wave generated was of frequency 7.5 kHz. The delay circuit was designed to provide a delay of $2\mu s$

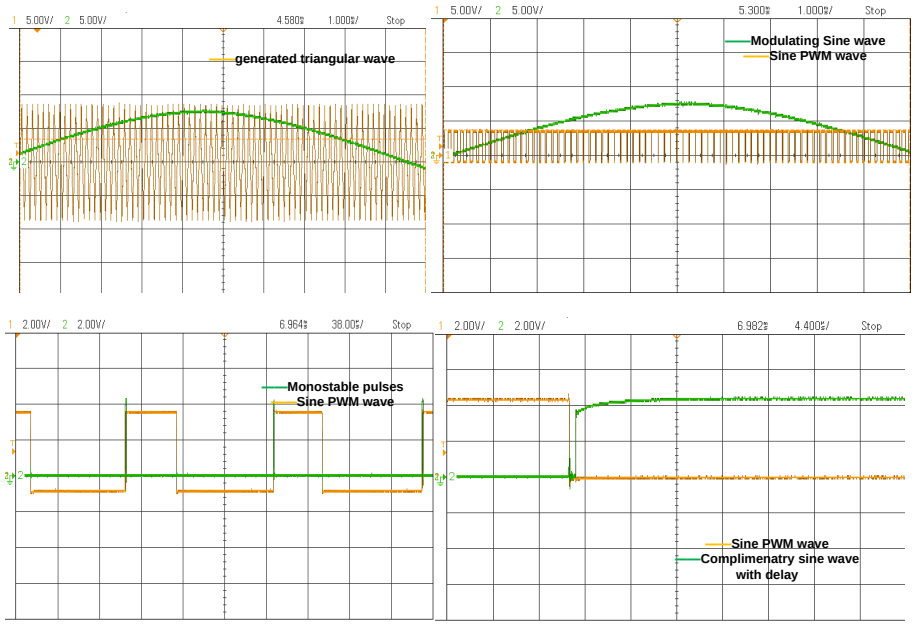

Figure 4.21: Driver Circuit Waveforms: (a) triangular Wave(b) Sine PWM pulses (c)Monostable Pulse generated (d)Complimentary pulses with delay

Figure 4.21 shows the driver circuit waveforms. The switching frequency of the sine PWM generated is 7.5 kHz. The delay provided is $2\mu s$ The speed response characteristics of the contemporary fan regulators were analysed. The motor voltage and current variation w.r.t knob position was studied for each regulator. The hardware implementation of simulated topologies for better speed control was tried out. The driver circuit in analog domain for the inverter circuit was built and tested. The PCB board for the inverter was designed and populated. The implementation of the topology has to be redesigned in a more economical way.

CHAPTER 5

CONCLUSION

In this project, the speed control techniques on single phase induction motor was studied. The single phase induction motors used in ceiling fans which was used for the study, generally have non identical stator windings. These types of motors are called unsymmetrical single phase induction motors. For simulation studies, the fan motor was modelled as a 2 phase induction motor. Modelling was done so that the simulations could be done in both SIMULINK and ORCAD. A brief study on some of the present day fan regulators was carried out. The following fan regulators were studied.

- Rheostatic Controller
- Phase Angle(TRIAC) Controller
- Capacitive Regulator

All these regulators are based on stator voltage control. Hence the speed control range achievable is small. The main disadvantage with the present day regulators is the non linearity in the speed range achievable. The TRIAC regulators had the worst performance compared to the other two. The rheostatic regulators consume a lot a power and the regulator gets heated up due to dissipation. The capacitive regulators are better in terms of speed control and also the input power consumed is less.

The following topologies were designed for betterment in speed control of SPIM and simulated in MATLAB.

- Bidirectional Switch Stator Voltage Controller
- SPWM Inverter based Speed Controller(without auxiliary winding capacitor)
- SPWM Inverter based Constant V/f Control(without auxiliary winding capacitance)
- SPWM Inverter based Stator Voltage Control(with auxiliary winding capacitance)
- SPWM Inverter based Constant V/f Control(with auxiliary winding capacitance)

5.1 Comparison of effectiveness in speed control

The bidirectional switch stator voltage control scheme is basically stator voltage control scheme and hence the range of speed control achievable is small. The SPWM based stator voltage scheme(with and without auxiliary winding capacitor) is better compared to bidirectional switch stator voltage control scheme in terms of the speed range achievable.

The constant volts per hertz (with and without auxiliary winding capacitor) is the best compared to all the topologies mentioned. The speed control has better linearity in comparison with the other voltage control schemes discussed. In this, Constant V/f Control without auxiliary winding capacitance is better compared to the Constant V/f Control with auxiliary winding capacitance when we compare the active power input taken by the motor.

5.2 Hardware Implementation

The PCB designing for the implementation of the constant volts per hertz scheme was done in diptrace software and the board was populated. The driver circuit was implemented in analog domain. The driver circuit results were taken.

5.3 Future scope of Work

Simulation results for the newly designed topologies for achieving a linear fan speed control show a satisfactory performance. The hardware implementation of the same was tried out. PCB board designing for the inverter board was completed. The PCB layout of the board can be improvised .The driver circuit for the inverter switches was implemented in analog domain.

A more economical realization of the desired topologies can be undertaken for future work.

REFERENCES

[1] Paul C. Krause, Oleg Wasynczuk, Scott D. Sudhoff. *Analysis of Electric Machinery and Drive Systems,* IEEE Power Engineering Society, second edition,2002

[2] P.C.Krause, "Simulation of Unsymmetrical 2-phase Induction Machines", IEEE Transactions on Power Apparatus and Systems, Vol. 84, November 1965,pp. 1025-1037.

[3] R. Krishnan. *Electric Motor drives: Modelling, Analysis and Control,* Prentice Hall, Upper Saddle River, New Jersey, Third Edition, 2002.

[4] Schiop.A, "Simulation of Induction Motor Drives in ORCAD Environment", Journal of Electrical and Electronics Engineering,Vol.2 Issue 2, p195, Dec 2009.

[5] D.P Kothari, I.J Nagrath. *Electric Machines,* Tata McGraw-Hill Publishing Company Limited, Third Edition,2008.

[6] R.K. Rajput. *Electrical Machines,* Laxmi Publications (P) Limited, Third Edition, 2002.

[7] A. S. Bu-Thunya , R. Khopkar , K. Wei and H. A. Toliyat, "Single phase Induction Motor Drives—A literature survey", Proc. IEEE Int. Electr. Mach. Drive

[8] Drawing Tool: Microsoft Visio 2007